THE CALCULATION OF THE THERMAL DEPENDENCY OF THE MAGNETIC SUSCEPTIBILITY IN EXTENDED SYSTEMS WITH AB INITIO ELECTRONIC STRUCTURE PARAMETERS

Igor Negodaev

ISBN: 978-84-694-2171-0
Dipòsit Legal: T. 1032-2011

UNIVERSITAT ROVIRA I VIRGILI
THE CALCULATION OF THE THERMAL DEPENDENCY OF THE MAGNETIC SUSCEPTIBILITY
IN EXTENDED SYSTEMS WITH AB INITIO ELECTRONIC STRUCTURE PARAMETERS
Igor Negodaev
ISBN:978-84-694-2171-0/DL:T. 1032-2011

Igor Vasilyevich Negodaev

The calculation of the thermal dependency of the magnetic susceptibility in extended systems with *ab initio* electronic structure parameters

Doctoral thesis

Supervised by

Dr. Rosa Caballol Lorenzo and Dr. Coen de Graaf

Department of Physical and Inorganic Chemistry

UNIVERSITAT ROVIRA I VIRGILI

Tarragona

February 2011

UNIVERSITAT ROVIRA I VIRGILI
THE CALCULATION OF THE THERMAL DEPENDENCY OF THE MAGNETIC SUSCEPTIBILITY
IN EXTENDED SYSTEMS WITH AB INITIO ELECTRONIC STRUCTURE PARAMETERS
Igor Negodaev
ISBN:978-84-694-2171-0/DL:T. 1032-2011

UNIVERSITAT ROVIRA I VIRGILI
THE CALCULATION OF THE THERMAL DEPENDENCY OF THE MAGNETIC SUSCEPTIBILITY
IN EXTENDED SYSTEMS WITH AB INITIO ELECTRONIC STRUCTURE PARAMETERS
Igor Negodaev
ISBN:978-84-694-2171-0/DL:T. 1032-2011

UNIVERSITAT ROVIRA I VIRGILI

Rosa Caballol Lorenzo, catedràtica de Química Física, i Coen de Graaf, investigador ICREA, del Departament de Química Física i Inorgànica de la Universitat Rovira i Virgili,

Fem constar que la present memòria, que porta per títol:

"The calculation of the thermal dependency of the magnetic susceptibility in extended systems with *ab initio* electronic structure parameters"

ha estat realitzada sota la nostra direcció al Departament de Química Física i Inorgànica de la Universitat Rovira i Virgili per Igor Vasilyevich Negodaev per a obtenir el Grau de Doctor en Química.

Tarragona, febrer de 2011

Rosa Caballol Lorenzo Coen de Graaf

UNIVERSITAT ROVIRA I VIRGILI
THE CALCULATION OF THE THERMAL DEPENDENCY OF THE MAGNETIC SUSCEPTIBILITY
IN EXTENDED SYSTEMS WITH AB INITIO ELECTRONIC STRUCTURE PARAMETERS
Igor Negodaev
ISBN:978-84-694-2171-0/DL:T. 1032-2011

UNIVERSITAT ROVIRA I VIRGILI
THE CALCULATION OF THE THERMAL DEPENDENCY OF THE MAGNETIC SUSCEPTIBILITY
IN EXTENDED SYSTEMS WITH AB INITIO ELECTRONIC STRUCTURE PARAMETERS
Igor Negodaev
ISBN:978-84-694-2171-0/DL:T. 1032-2011

Acknowledgements

I am very grateful to all people who taught me, helped me, assisted me, supported me and, one way or another, participated in this thesis.

First of all, I thank my supervisors, Dr. Rosa Caballol and Dr. Coen de Graaf. Their wise guidance and comprehensive assistance is impossible to overestimate. I will never forget the years of collaborations and I was honoured and pleased to work in their group.

I would like to thank Dr. Jordi Carbó, who introduced me to teaching Quantum Chemistry. That experience was very interesting and useful.

I also thank all the professors of Department, for their really useful advices and suggestions: Dr. Mar Reguero, Dr. Josep Maria Poblet, Dr. Antoni Rodríguez Fortea, Dr. Maria Angels Carvajal, Dr. Anna M. Clotet, Dr. Xavier López, Dr. Carles Bo, Dr. Joan Igual, Dr. Josep Manel Ricart.

I am indebted to the people responsible for the normal functioning of the complex organism of the department: José Ortiz, Elisenda Mas, Moises Álvarez Moreno, Yolanda Albero, Cristina Rodríguez, Anna Benages Maturana and other members of the staff.

Finally, I would like to thank all my colleagues who helped me with the really wide range of problems, from Quantum Chemistry to Catalan, and with searching for accommodation in Tarragona: Laia Vilà Nadal, Alberto Roldán, Alex Domingo, Rémi Maurice, Yannick Mercier, David Taratiel, Mireia Segado, Zahra Tabookht, Dr. Susana Romo, Nadya Antonova, John Zapata, Ramón Valencia, Xavier Aparicio, Benjamí Martorell, Sonia Aguado, Núria Alegret.

UNIVERSITAT ROVIRA I VIRGILI
THE CALCULATION OF THE THERMAL DEPENDENCY OF THE MAGNETIC SUSCEPTIBILITY
IN EXTENDED SYSTEMS WITH AB INITIO ELECTRONIC STRUCTURE PARAMETERS
Igor Negodaev
ISBN:978-84-694-2171-0/DL:T. 1032-2011

This work would not be possible without the support and encouragement of my beloved parents, family and friends. Дорогие мои мама и папа, спасибо вам! Я вас очень-очень люблю!!! Many thanks to my nearest and dearest sister Irina and niece Anastassia, to my granny, and to the best friend of mine, Alexey Umanskiy. Also, I thank Nadiya Dariyenko, whose warmth and care assisted me very much. Спасибо!

Thanks to Dr. Dmitry Kosynkin for checking and correcting errors in parts of the text.

Finally, I thank Tarragona, the pearl of Spain, definitely one of the most amazing and beautiful places of our planet. Thanks for four years of my life spent here, for your fantastic sea, for your deep blue sky and bright sun! Thank you... And see you! Moltes gràcies i ens veiem!!!

UNIVERSITAT ROVIRA I VIRGILI
THE CALCULATION OF THE THERMAL DEPENDENCY OF THE MAGNETIC SUSCEPTIBILITY
IN EXTENDED SYSTEMS WITH AB INITIO ELECTRONIC STRUCTURE PARAMETERS
Igor Negodaev
ISBN:978-84-694-2171-0/DL:T. 1032-2011

To my nearest and dearest

UNIVERSITAT ROVIRA I VIRGILI
THE CALCULATION OF THE THERMAL DEPENDENCY OF THE MAGNETIC SUSCEPTIBILITY
IN EXTENDED SYSTEMS WITH AB INITIO ELECTRONIC STRUCTURE PARAMETERS
Igor Negodaev
ISBN:978-84-694-2171-0/DL:T. 1032-2011

UNIVERSITAT ROVIRA I VIRGILI
THE CALCULATION OF THE THERMAL DEPENDENCY OF THE MAGNETIC SUSCEPTIBILITY
IN EXTENDED SYSTEMS WITH AB INITIO ELECTRONIC STRUCTURE PARAMETERS
Igor Negodaev
ISBN:978-84-694-2171-0/DL:T. 1032-2011

Index

UNIVERSITAT ROVIRA I VIRGILI
THE CALCULATION OF THE THERMAL DEPENDENCY OF THE MAGNETIC SUSCEPTIBILITY
IN EXTENDED SYSTEMS WITH AB INITIO ELECTRONIC STRUCTURE PARAMETERS
Igor Negodaev
ISBN:978-84-694-2171-0/DL:T. 1032-2011

UNIVERSITAT ROVIRA I VIRGILI
THE CALCULATION OF THE THERMAL DEPENDENCY OF THE MAGNETIC SUSCEPTIBILITY
IN EXTENDED SYSTEMS WITH AB INITIO ELECTRONIC STRUCTURE PARAMETERS
Igor Negodaev
ISBN:978-84-694-2171-0/DL:T. 1032-2011

UNIVERSITAT ROVIRA I VIRGILI
THE CALCULATION OF THE THERMAL DEPENDENCY OF THE MAGNETIC SUSCEPTIBILITY
IN EXTENDED SYSTEMS WITH AB INITIO ELECTRONIC STRUCTURE PARAMETERS
Igor Negodaev
ISBN:978-84-694-2171-0/DL:T. 1032-2011

UNIVERSITAT ROVIRA I VIRGILI
THE CALCULATION OF THE THERMAL DEPENDENCY OF THE MAGNETIC SUSCEPTIBILITY
IN EXTENDED SYSTEMS WITH AB INITIO ELECTRONIC STRUCTURE PARAMETERS
Igor Negodaev
ISBN:978-84-694-2171-0/DL:T. 1032-2011

Chapter 1

Introduction

UNIVERSITAT ROVIRA I VIRGILI
THE CALCULATION OF THE THERMAL DEPENDENCY OF THE MAGNETIC SUSCEPTIBILITY
IN EXTENDED SYSTEMS WITH AB INITIO ELECTRONIC STRUCTURE PARAMETERS
Igor Negodaev
ISBN:978-84-694-2171-0/DL:T. 1032-2011

ISBN:978-84-694-2171-0/DL:T. 1032-2011

The study of magnetism is one of the important fields of nowadays science. The achievements of investigators in this field are successfully applied in many areas of human activity, and materials with different magnetic properties are widely used in science and industry.

The magnetic molecule-based materials are usually formed with molecular complexes or extended structures of different dimensionality, and often have transition metal (TM) atoms as magnetic sites. One of the key factors to understand magnetic properties is the exchange interaction between paramagnetic ions intermediated by bridging ligands of diamagnetic nature. From a scientific point of view, the relations of the shown magnetism and different characteristics such as types and amounts of ligands, geometric parameters and coordination characteristics among others, are interesting to study, both within experimental techniques and theoretical approaches to clarify the relations between them.

Among the different multidentate ligand types, the oxalate ion, $[C_2O_4]^{2-}$ is frequently used to build magnetic TM-based structures. This ligand possesses good coordination properties and mediates reasonably well the magnetic coupling between TM sites.[1,2,3] Depending on the orientation of the ligands, the oxalate bridge gives rise to a magnetic coupling that ranges from weakly ferromagnetic to moderately strong antiferromagnetic.[4,5,6,7,8] Another factor that modulates the magnetic properties of a material is the nature of the TM. The homo-metallic Cu(II)-based systems were the very first of the studied materials. More recently the hetero-bimetallic structures were described in the literature, where two different paramagnetic ions are bridged with ligands. This latter class of materials gives an opportunity to design the magnetic systems with ferromagnetic and ferrimagnetic properties.

For the theoretical research, the dinuclear Cu(II) complexes

ISBN:978-84-694-2171-0/DL:T. 1032-2011

can be considered as ideal model systems to gain insight in the mechanism of the coupling. First of all, there exists an enormous library of synthesized complexes with two Cu(II) ions coupled through a diamagnetic bridge. The majority of these complexes are magnetically characterized, mostly by magnetic susceptibility measurements. Moreover, the electronic structure of dinuclear Cu(II) complexes is also simple: the Cu(II) – $3d^9$ electronic configuration has only one unpaired electron, which effectively simplifies the theoretical treatment.[9,10,11] However, computation is not restricted to Cu(II) dinuclear complexes. Recent developments cleared the way to extend the applicability of *ab initio* computational strategies to complexes with more complicated TM ions.[12,13]

The molecule-based magnetic materials can be subdivided into two groups. The low-dimensional cases represent so-called single-molecule magnets and single-chain magnets. Alternatively, the traditional magnetic systems have a spatial 1D-, 2D or 3D-structure. A special subgroup is constituted by the two-dimensional oxalato-bridged networks of TMs, where the magnetic centres form a hexagonal lattice.[14,15,16] These structures can be found in bifunctional materials. The countercations included to compensate the negative charge of magnetic layers may have complementary properties such as electronic conductivity,[17] optical chirality,[18] photoactivity,[19] proton conduction[20] or spin-crossover.[21] In such a way, different properties can be combined in the same material.

The magnetic properties of the oxalato-based hexagonal structures are normally derived from the temperature dependence of the magnetic susceptibility and the magnetization measurements. High temperature magnetic susceptibility ($\chi(T)$) data are fitted with the Curie-Weiss expression to determine the nature of the dominant magnetic interaction between the TM sites. The magnetization measurements give information about

the critical temperature for long-range (anti-)ferromagnetic ordering. But there is no easy way to determine the precise magnitude of the magnetic coupling from experiment, unlike simpler structures, where $\chi(T)$ is fitted to an analytical expression that depends on this coupling. Based on this observation, one of our main purposes is to obtain macroscopic properties such as $\chi(T)$ with the microscopic parameters such as magnetic coupling constant J, which can be calculated theoretically through the modern computational chemistry methods.

The thesis is organized as follows: the first part of chapter 2 describes the computational approaches applied in the scope of this thesis. Being focused on systems with important electron correlation and often characterized by electronic structures that cannot be described with a single electronic configuration, the computations are based on a wave function approach to find the best approximation to the Schrödinger equation. The chapter shortly discusses typical methodologies for these cases such as the Complete Active Space SCF (CASSCF), the CAS Perturbative Theory up to 2nd order (CASPT2) and Difference-Dedicated Configuration Interaction (DDCI). Some extensions to CASSCF, for instance, the Restricted Active Space SCF (RASSCF) and RAS State Interaction (RASSI) are also denoted. The overview of the methods is ended with a description of the Extended CAS + DDCI2 approach, which is a good compromise between the accuracy of the DDCI calculations and the required computational time. In addition, the essentials of the single reference the Coupled Cluster Singles Doubles (Triples) method (CCSD(T)) are outlined since this method has been used to obtain a reference curve of the dissociation of Mn_2.

The second section of chapter 2 is dedicated to obtain macroscopic properties such as the magnetic susceptibility from microscopic parameters like the magnetic coupling between localized spin moments. The section starts with a discussion of the

different model Hamiltonians that can be used to describe the magnetic coupling. More specifically, we compare the well-known Ising and Heisenberg Hamiltonians. Since the magnetic coupling parameter J is directly related to differences in the energy expectation values of the exact (non-relativistic) Hamiltonian, the Heisenberg model is widely applied to interpret magnetic data. Nevertheless, the simpler Ising model could be adequate for systems with high spin angular momenta and/or systems with large magnetic anisotropy. Therefore the comparison of Heisenberg and Ising models seems to be interesting and useful.

After that a link is made between these models and the electronic structure calculations on the one hand, and the simulation of the macroscopic properties on the other. Here the exact diagonalization of the Heisenberg Hamiltonian will be contrasted against the Ising model. The renormalization techniques such as REM (renormalization excitonic method) have also been explored.

After this general introduction and overview of the computational schemes, the results of the thesis will be discussed in the second part. Chapter 3 starts with the description of the Mn dimer. This system shows a weak van der Waals type of bond and a magnetic coupling of the 5/2 spin moments which is subject of controversy. Through the application of the high level *ab initio* methods described in chapter 2, we clarify the electronic structure and magnetic behaviour of this at first sight simple, but actually rather complicated system. A second group of molecular systems that will be described in this chapter concerns the Cu(II) dinuclear complexes with two asymmetrical bridges. Experimentally a series of compounds was synthesized by Lukov and co-workers[22] changing the original substituent in one of the bridges by more electronegative species. In contrast to the expected lowering of the magnetic coupling (due to electron withdrawal from the magnetic exchange path by the more

electronegative substituents) an increase was observed. Our theoretical analysis addresses this apparent contradiction and provides an alternative explanation for the experimental data.

Thereafter, chapter 4 treats systems where the transition metals are bridged by oxalato ligands. Firstly, the materials of low dimensionality (0D and 1D), observing different coupling from weak ferro- to strong antiferromagnetic, have been studied. Here the range of methods and techniques has been applied to develop a strategy which allows to combine accuracy and low computational cost. Secondly, the magnetic structure of the first synthesized 3D oxalato-based Cu(II) system will be determined. The crystal structure of this material is rather complicated and the magnetic topology is not easily derived from the geometry. Hence, we adopt a cluster model approach to calculate the magnetic interactions and construct a magnetic unit cell. Thirdly, the magnetic lattices of the bifunctional materials are treated. These composite systems combine properties that are not easily joined in standard materials. However, the magnetic coupling strength in the hexagonal magnetic layers is difficult to derive from experiment. Our approach of combining *ab initio* calculation and diagonalization of the Heisenberg Hamiltonian provides an alternative for the cumbersome analytical expression present in the literature to relate the magnetic susceptibility with the magnetic coupling strength.

In chapter 5, attention will be focused on a hexagonal lattices containing V(II) and V(III) ions. In addition to the isotropic magnetic coupling shared with the previous described system, this lattice presents magnetic anisotropy. The V(II) ions with a $3d^2$ electronic configuration shows a zero-field splitting. We propose a simple scheme to take into account this effect in the simulation of the magnetic susceptibility.

Finally, the last part contains the summary and conclusions of this thesis.

ISBN:978-84-694-2171-0/DL:T. 1032-2011

1.1 References

1 Kahn, O. Molecular Magnetism, VCH Publishers, 1993.

2 Kahn, O.; Jay Martinez, C. Science 1998, 279, 44.

3 Pilkington, M.; Decurtins, S. Oxalate-based 2D and 3D Magnets. In Magnetism: Molecules to Materials II; Miller, J. S., Drillon, M., Eds.; Wiley-VCH, 2001; chapter 10, 339.

4 Hall, G. R.; Duggan, M.; Hendrickson, D. N. Inorg. Chem. 1975, 14, 1956.

5 Julve, M.; Verdaguer, M.; Gleizes, A.; Philoche-Levisalles, M.; Kahn, O. Inorg. Chem. 1984, 23, 3808.

6 Willett, R. Magneto-structural correlations in Copper(II) compounds. In Magneto-structural correlations in exchange coupled systems; Willet, R. D., Ed.; Reidel Publishing Company, 1985; 389.

7 Cano, J.; Alemany, P.; Alvarez, S.; Verdaguer, M.; Ruiz, E. Chem. Eur. J. 1998, 4, 476.

8 Cabrero, J.; Ben Amor, N.; de Graaf, C.; Illas, F.; Caballol, R. J. Phys. Chem. A 2000, 104, 9983.

9 Hay, P. J.; Thibeault, J, C.; Hoffmann, R. J. J. Am. Chem. Soc. 1975, 97, 4884.

10 Kahn, O.; Briat, B. J. Chem. Soc.: Faraday Trans. 1976, 72, 268.

11 Anderson, P. W. Phys. Rev. 1959, 115, 2.

12 Bordas, E.; Caballol, R.; de Graaf, C. J. Mol. Struct. (THEOCHEM) 2005, 727, 173.

13 Negodaev, I.; de Graaf, C.; Caballol, R. J. Phys. Chem. A, 2010, 114 (28), 7553.

14 Pellaux, R.; Schmalle, H. W.; Huber, R.; Fischer, P.; Hauss, T.; Ouladdiaf, B.; Decurtins, S. Inorg. Chem. 1997, 36, 2301.

15 Andres, R.; Gruselle, M.; Malezieux, B.; Verdaguer, M.; Vaissermann, J. Inorg. Chem. 1999, 38, 4637.

16 Alberola, A.; Coronado, E.; Galán-Mascarós, J. R.; Giménez-Saiz, C.; Gómez-Garcia, C. J. J. Am. Chem. Soc. 2003, 125, 10774.

17 Coronado, E.; Galán-Mascarós, J. R.; Gómez-Garcia, C. J.; Laukhin, V. Nature 2000, 408, 447.

18 Train, C.; Gheorghe, R.; Krstic, V.; Chamoreau, L. M.; Ovanesyan, N. S.; Rikken, G. L. J. A.; Gruselle, M.; Verdaguer, M. Nature Mater. 2008, 7, 729.

ISBN:978-84-694-2171-0/DL:T. 1032-2011

19 Bénard, S.; Rivière, E.; Yu, P.; Nakatani, K.; Delouis, J. F. Chem. Mater. 2001, 13, 159.

20 Okawa, H.; Shigematsu, A.; Sadakiyo, M.; Miyagawa, T.; Yoneda, K.; Ohba, M.; Kitagawa, H. J. Am. Chem. Soc. 2009, 131, 13516.

21 Clemente-León, M.; Coronado, E.; López-Jordà, M.; Mínguez Espallargas, G.; Soriano-Portillo, A.; Warenborgh, J. C. Chem. Eur. J. 2010, 16, 7, 2207.

22 Kogan, V. A.; Lukov, V. V.; Novotortsev, V. M.; Eremenko, I. L.; Aleksandrov, G. G. Russ. Chem. Bull., Int. Ed. 2005, 54, 3, 600.

UNIVERSITAT ROVIRA I VIRGILI
THE CALCULATION OF THE THERMAL DEPENDENCY OF THE MAGNETIC SUSCEPTIBILITY
IN EXTENDED SYSTEMS WITH AB INITIO ELECTRONIC STRUCTURE PARAMETERS
Igor Negodaev
ISBN:978-84-694-2171-0/DL:T. 1032-2011

UNIVERSITAT ROVIRA I VIRGILI
THE CALCULATION OF THE THERMAL DEPENDENCY OF THE MAGNETIC SUSCEPTIBILITY
IN EXTENDED SYSTEMS WITH AB INITIO ELECTRONIC STRUCTURE PARAMETERS
Igor Negodaev
ISBN:978-84-694-2171-0/DL:T. 1032-2011

Chapter 2

Methods of calculation

UNIVERSITAT ROVIRA I VIRGILI
THE CALCULATION OF THE THERMAL DEPENDENCY OF THE MAGNETIC SUSCEPTIBILITY
IN EXTENDED SYSTEMS WITH AB INITIO ELECTRONIC STRUCTURE PARAMETERS
Igor Negodaev
ISBN:978-84-694-2171-0/DL:T. 1032-2011

2.1.1 The Complete Active Space SCF method

One of the most widely used MCSCF method defines the multiconfigurational space as the Complete Active Space (CAS).[1,2] This active space is generated by defining three subsets of orbitals: the inactive orbitals are doubly occupied orbitals in all the configurations of the multiconfigurational wave-function; the orbitals that remain unoccupied in all the CAS configurations are known as virtual or secondary orbitals; finally, from the set of active orbitals and the corresponding number of electrons all the possible configurations are generated that are compatible with the spin multiplicity and the spatial symmetry of the electronic state being studied. The widespread popularity of the CASSCF methods is partly due to the advantages of the CAS, which ensures properties of invariance to active orbital rotations. The CAS also has technical advantages because the completeness of the space can be exploited to construct algorithms of considerable computational efficacy. These methods also enable the user to straightforwardly define the MC function, merely by stating the active orbitals and the number of electrons involved.

The choice of the active space requires a good chemical knowledge of the system so that a rational choice can be made. It also depends on the demands of the problem being studied, which can fluctuate from merely qualitative interpretations to quantitative determinations. The common description of used CAS is CAS (n_e, n_a), where n_e is the number of electrons and n_a is the number of active orbitals.

In many systems, the multiconfigurational nature is associated with the chemical bond and its evolution, and this involves non-dynamic correlation contributions. Although in

ISBN:978-84-694-2171-0/DL:T. 1032-2011

excited state systems, the multireference character may have other origins such as the considerable weight of excited and Rydberg-type configurations. The well chosen CAS ensures a good dissociation and it can therefore be deduced that the choice of an appropriate CAS takes into account a sufficient electronic correlation. Indeed, this treatment may be sufficient to qualitatively explain the behaviour of some systems but although the contribution of the non-dynamic correlation is essential in all systems with near degeneracies, it is only a small part of the total correlation energy. For instance, for singlet-triplet excitation energies in magnetic binuclear complexes, the CASSCF estimation is typically 25% of the experimental value. This means that the inactive electrons play a key role in the accurate evaluation of the energy difference in such cases. Solving that, the size of the CAS in the CASSCF calculation may be increased, but it is not easy to select rationally the enlargement of the CAS, and its dimension will most probably become prohibitively large before giving an accurate value of the transition energy. Therefore, an other solution which can help to estimate the energy difference accurately should be applied. In other words, the dynamic electronic correlation has to be included in the computational scheme with an alternative computational technique taking CASSCF as reference.

A bond breaking process defines a minimal valence CAS, concerning the electrons of the bond as active electrons (two for a single bond, four for a double bond, *etc*.), and the bonding and antibonding valence MOs as active MOs. On the other hand, the electronic transitions are usually described as promotions of one or two electrons from the highest occupied MOs to low lying valence or Rydberg diffuse MOs. In both cases, one can expect from the long experience of quantum chemistry and the efficiency of such models that the zeroth-order description may be obtained

by considering an appropriate CAS of moderate dimension, involving a small number of active electrons and active MOs.

The magnetic interaction is a consequence of the coupling of spin moments, in systems with unpaired electrons in different centres. Therefore, the unpaired electrons of magnetically active sites with the corresponding number of orbitals (magnetic orbitals) will define the minimal CAS. Thus, CAS (2, 2) will be a minimal CAS to describe magnetic interactions between two sites with S = 1/2 (*i.e.* one unpaired electron on each centre, which corresponds to a Cu(II) dimer system), for the Ni(II) dimer the minimal CAS will be CAS (4, 4), *etc*. Due to the limited description of the instantaneous electron correlation effects in the CASSCF wave-function, post CASSCF calculations are needed to include relevant contributions of electron correlation, either from perturbation theory or from configuration interaction calculations. The CAS defined by the magnetic orbitals and the unpaired electrons is the minimal reference space in those calculations.

An extension to the CASSCF method exists whose possibilities are being explored[3,4,5,6,7] nowadays: the RASSCF method.[8] Here the active subspace is divided into three: RAS1, RAS2, and RAS3. The orbitals in RAS1 are doubly occupied but a limited number of holes is allowed. An arbitrary occupation is allowed in RAS2. A limited number of electrons is allowed to occupy the orbitals in RAS3. Many different types of RAS wave-functions can be constructed. Leaving RAS1 fully occupied and RAS3 empty, we retrieve the CAS wave-function. On the other hand, if we have no orbitals in RAS2 we obtain a wave-function that includes all single, double, *etc*. excitations out of a closed shell reference function (the SDTQ-CI wave-function). Maximizing the number of holes in RAS1 and restricting the number of electrons in RAS3 to two, we obtain what has been called a second order wave-function in the active space.

ISBN:978-84-694-2171-0/DL:T. 1032-2011

It is often convenient to compute matrix elements over a basis of wave-functions, each with its own optimized set of orbitals (*e.g.* different RASSCF wave-function) to obtain information about transition dipole moments and other properties. The RASSI method[9] was developed to handle this task effectively. Transformation to biorthonormal orbitals allows the use of simple formulae, just as if the orbitals were the same. When two (or several) wave-functions are expanded in a common set of Slater determinant functions or spin-coupled configuration functions, using orthonormal orbitals, the matrix elements of one- or two-body operators are easily computed. The Spin-Orbit interactions can be involved into this method giving rise to the SO-RASSI technique.[10] In this approach, spin-orbit coupling is introduced *a posteriori* by letting a set of CASSCF wave-functions mix under the influence of a spin-orbit Hamiltonian, which is approximated as an effective one-electron operator.

2.1.2 The CAS Perturbative Theory up to 2nd order

Based on the perturbation theory up to 2nd order, this method[11,12] is one of the simplest computational instruments to include the dynamic electronic correlation in the scheme of calculation. In multiconfigurational approaches, it is normally combined with the CASSCF method, where the reference functions are taken from. The results obtained with CASSCF/CASPT2 calculations are often reasonably accurate. Since the machine requirements of CASPT2 are modest, this scheme is widely applied in many theoretical researches.

ISBN:978-84-694-2171-0/DL:T. 1032-2011

Perturbative methods introduce a partitioning of the Hamiltonian $\hat{H}$ into a zeroth-order part $\hat{H}_0$ and the perturbation $\hat{V}$:

$$\hat{H}=\hat{H}_0+\hat{V} \qquad 2.1$$

The CASPT2 zeroth-order Hamiltonian[13] $\hat{H}_0$ is defined as

$$\hat{H}_0=\hat{P}_0\hat{F}\hat{P}_0+\hat{P}\hat{F}\hat{P} \qquad 2.2$$

Here $\hat{F}$ is Fock operator, expressed as

$$\hat{F}=\sum_{p,q,\sigma} f_{pq\sigma}\hat{E}_{pq} \qquad 2.3$$

where $\hat{E}_{pq}$ is the excitation operator defined as

$$\hat{E}_{pq}=a_q^{\dagger}a_p \qquad 2.4$$

and the matrix elements of $\hat{F}$ as

$$f_{pq\sigma}=-\langle\Psi^{(0)}|[[\hat{H},\hat{a}_{q\sigma}^{\dagger}],\hat{a}_{p\sigma}]_+|\Psi^{(0)}\rangle \qquad 2.5$$

The $\hat{P}_0$ and $\hat{P}$ in equation 2.2 are the projection operators onto the reference function $|\Psi^{(0)}\rangle$ and the first-order interacting space $|\mu\rangle$, respectively:

$$\hat{P}_0=|\Psi^{(0)}\rangle\langle\Psi^{(0)}| \quad \text{and} \quad \hat{P}=\sum_{\mu}|\mu\rangle\langle\mu| \qquad 2.6$$

The first-order wave-function is expanded as a linear combination of internally contracted excited configurations:

$$|\Psi^{(1)}\rangle=\sum_{pqrs} c_{pqrs}|pqrs\rangle \qquad 2.7$$

$$|pqrs\rangle=\hat{E}_{pq}\hat{E}_{rs}|\Psi^{(0)}\rangle \qquad 2.8$$

The one-electron nature of zeroth-order Hamiltonian can give rise to artificial degeneracies with $E^{(0)}$ of states external to the CAS, which makes the perturbation treatment divergent. This can be solved in a pragmatic way by applying a level shift.[14] The contracted nature of the first-order wave-function avoids the modification of the ratio of the configurations present in the CAS under the influence of dynamical electron correlation. This is partially remedied with the multi-state CASPT2 approach,[15] in

which an effective Hamiltonian is constructed to take into account the interaction of the different states caused by the dynamical electron correlation.

2.1.3 Configuration Interaction methods

Conceptually, the Configuration Interaction (CI) methods are the simplest to include electron correlation effects, because they are variational. In a compact way, the CI wave-function can be expressed as

$$\Phi = c_0 \Psi^{(0)} + c_M M + c_D D + c_T T + \ldots \qquad 2.9$$

where $\Psi^{(0)}$ is the reference or zeroth-order wave-function, and M, D, T,... symbolize the sets of single, double, triple,... excited Slater determinants. The Hamiltonian is expressed in the basis of Slater determinants.

In single reference methods, $\Psi^{(0)}$ is the Hartree-Fock determinant. In multiconfigurational methods, the zeroth-order wave-function is chosen according to the physics of the problem. Usually Ψ_{CAS} is taken as the reference.

The energy and the correlated wave-function of one or several states are obtained by diagonalizing the Hamiltonian matrix.

Difference-Dedicated Configuration Interaction method

Starting from CASSCF (or MCSCF) multiconfigurational wave-functions, excitations can be added to the previously obtained multiconfigurational space up to a particular degree of excitation, thus generating a Multireference Configuration Interaction space.

ISBN:978-84-694-2171-0/DL:T. 1032-2011

Among the MR CI methods, the DDCI has been developed to give accurate energy differences.[16,17] The method assumes that a zeroth-order description of the bond-breaking or excitation process may be obtained through a preliminary CI approach with a complete active space (CAS) of small size concerning a small number of electrons in a limited set of active molecular orbitals (MOs). Then using arguments based on quasi degenerate perturbation theory, it is assumed that in singles and doubles CI from the CAS, the purely inactive double excitations can be omitted without affecting the energy differences between the electronic states of interest. The resulting CI space remains of moderate size. The method avoids intruder states problems and numerical instabilities. Moreover, the size inconsistency defects are less severe than in the full MR-SDCI. Hence the DDCI space is defined by the CAS and all the determinants obtained by single (S) and double semi-active (D_{sa}) substitutions, involving at least one active MO. A schematic definition of the space may be written as

$$DDCI = CAS * (1 + S + D_{sa}) \qquad 2.10$$

DDCI is invariant under rotations of the MOs in their subset, *i.e.* among core MOs, among active MOs and among virtual MOs. Furthermore, the solutions are eigenfunctions of $\hat{S}^2$.

Considering the reference space constructed only with the magnetic orbitals, those determinants which are external to the CAS can be classified according to the number n of excited electrons from the inactive orbitals, nh (h = holes), and the number of electrons promoted to the virtual space m, mp (p = particles), as illustrated in Figure 2.1.

Many applications have established the precision of DDCI in the calculation of magnetic coupling constants as well in molecules[18,19] as in solids.[20,21] There are several variants of DDCI to reduce the computational cost of the full DDCI calculation. The DDCI2 space is spanned by all singles and doubles with at least

two replacements in the active orbitals. This level is useful in magnetic systems if the ligand does not play an important role in the superexchange mechanism. DDCI1 expands the wave-function in the subspace defined by all single excitations on top of the CAS space. In this thesis, the three levels were used for different purposes, depending on the accuracy required.

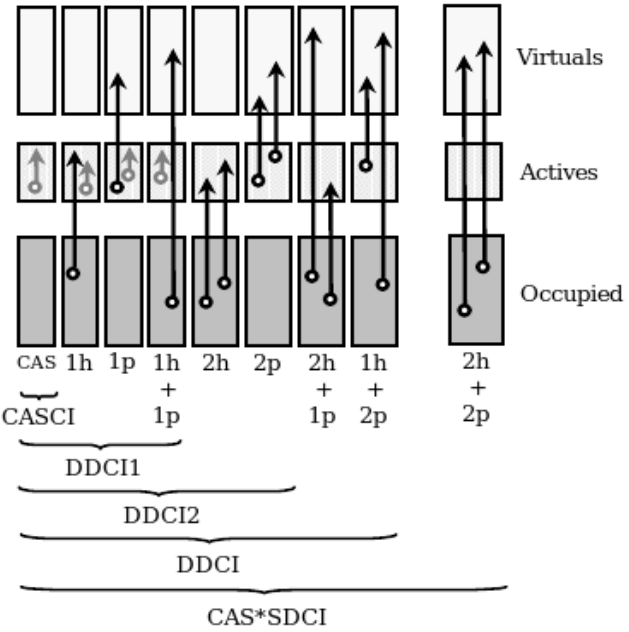

Figure 2.1. Schematic representation of the different excitations of CI space.[22]

If one is interested in a comparison of energies for two different conformations of the molecule (binding energies, activation barriers, adiabatic excitations or ionization energies), the changes in the correlation energy due to the inactive 2h-2p excitations should be added to the DDCI energies. Alternatively, the absolute energy of one of the involved states can be calculated

ISBN:978-84-694-2171-0/DL:T. 1032-2011

in a precise way (or extracted from experimental information)[23] and the energy difference(s) can be added vertically. This procedure is used in manganese dimer calculation (chapter 3).

The size of the DDCI increases as $N_{CAS}(n_c n_a n_v^2 + n_c^2 n_a n_v)$ where N_{CAS} is the number of determinants of the CAS and n_a, n_c, and n_v are respectively the number of inactive, active and virtual MOs, while the size of the CAS-SDCI is approximately

$$N_{CAS}(n_i+n_a)^2+(n_a+n_v)^2 \qquad 2.11$$

The energy obtained from DDCI essentially scales as the number of active electrons and size consistency errors should therefore be negligible. Nevertheless, since DDCI is a truncated CI method, the size-consistency problem can appear in the calculations especially for a large number of active electrons. There are several methods for solving the size-consistency problem, the most common of which is Davidson's[24] correction extended to MR-systems:

$$E_{DAV}=E^{(0)}+\frac{E_{corr}}{C_0^2} \qquad 2.12$$

where $E^{(0)}$ is the energy of the reference wave-function, E_{corr} is the calculated correlation energy associated to Φ and $C_0^2=\langle \Psi_0|\Phi\rangle$.

The Extended CAS (CAS_{ext}) approximation

Normally the DDCI calculations lead to accurate estimates of the energy splitting. Unfortunately, this family of methods requires huge amounts of computational resources for medium-sized systems or reference wave-function with an elevated number of configurations. A good compromise between accuracy and CPU-time is given by the extended CAS followed by DDCI1 or DDCI2 approximation.[25,26,27,28] The basic idea of this approximation

is to include important ligand-to-metal charge transfer configurations in the zeroth-order wave-function by extending the active space (CAS_{ext}) with orbitals of the bridge and the subsequent treatment of remaining electron correlation with DDCI1 or DDCI2 (see Figure 2.2). By introducing the LMCT determinants in the CAS, the excitations that account for the polarization (*i.e.* 2h-1p determinants) already appear at the CAS_{ext}/DDCI1 level which provide a possibility to reduce the computational cost of the variational determination of the energy splitting. However, it has also been shown[29] that important ferromagnetic contributions (1h-2p) are missing, leading to an overestimation of the energy difference for antiferromagnetic systems. This is partially corrected by the CAS_{ext}/DDCI2 approach.

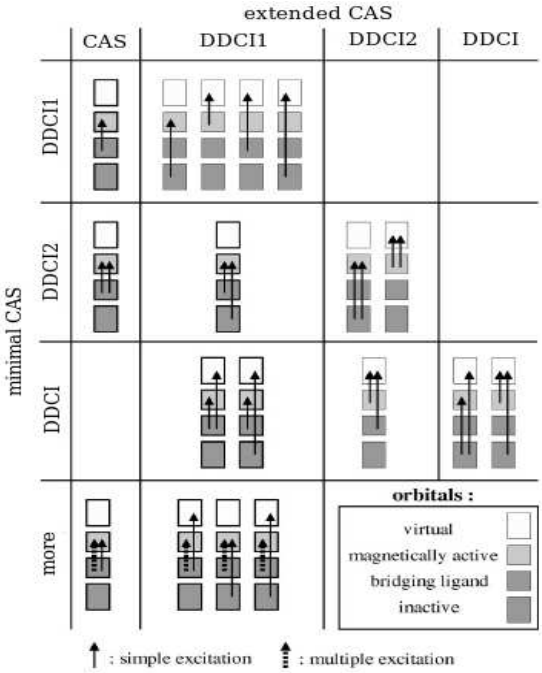

Figure 2.2. Schematic representation of the excitations of CI space at CAS_{ext}/DDCI1, CAS_{ext}/DDCI2 and CAS_{ext}/DDCI on their minimal CAS counterparts.[27]

ISBN:978-84-694-2171-0/DL:T. 1032-2011

2.1.4 The Coupled Cluster Singles Doubles (Triples) method

The Coupled Cluster (CC) approach goes back to the 1950s and is closely connected to developments in Many Body Perturbation Theory. At the beginning of the 1960s, Sinanoğlu introduced the cluster expansion of the wave-function for molecular systems and Čížek formulated the corresponding equations. The form of the wave-function, which is no longer a linear expansion but an exponential one, ensures a correct separability of the fragments and that the N-dependence (size consistency) is also correct. At present, CC methods have different levels of approximation. The most commonly-used ones are the single reference methods: the CCSD method, which includes up to double excitation operators, and several approaches that take into account triple excitation effects (CCSD(T)).

Let us use the definitions of the wave operator $\hat{\Omega}$ as the operator that transforms the reference wave-function into the exact one,

$$\Phi=\hat{\Omega}\Psi_0 \qquad 2.13$$

This definition is flexible, depending on the type of expansion that is used to define the wave-function. Thus, in the linear expansion of the Configuration Interaction, the exact wave-function can be written as

$$\Phi=(\hat{1}+\hat{C}_1+\hat{C}_2+\ldots)\Psi_0 \qquad 2.14$$

and the wave operator is given by

$$\hat{\Omega}=\hat{1}+\hat{C}_1+\hat{C}_2+\ldots \qquad 2.15$$

where $\hat{C}_1$, $\hat{C}_2$ are the single, double, *etc*., excitation operators. In the CC theory, an exponential expression of the wave-function is proposed:

$$\Phi = e^{\hat{T}}\Psi_0 \text{ with } \hat{\Omega} = e^{\hat{T}} \qquad 2.16$$

ISBN:978-84-694-2171-0/DL:T. 1032-2011

Here $\hat{T}$ is the cluster operator, which can be expanded as a sum of cluster operators for each excitation degree:

$$\hat{T}=\hat{T}_1+\hat{T}_2+\hat{T}_3+... \qquad 2.17$$

where $\hat{T}_1=\sum_{pq} t_{pq}\hat{a}_q^+\hat{a}_p$, *etc.*, and t_{pq} are the cluster amplitude. The first level of CCSD approximation consists of truncating the cluster expansion at the double excitations:

$$\hat{T}=\hat{T}_1+\hat{T}_2 \qquad 2.18$$

Expanding the exponential in a Taylor series:

$$e^{\hat{T}}=\hat{\Omega}=\hat{1}+\hat{T}+\frac{1}{2!}\hat{T}^2+\frac{1}{3!}\hat{T}^3+... \qquad 2.19$$

the following expression of the wave-function is obtained:

$$\Phi^{CCSD}=e^{(\hat{T}_1+\hat{T}_2)}\Psi_0=(\hat{1}+\hat{T}_1+\hat{T}_2+\frac{1}{2}(\hat{T}_1+\hat{T}_2)^2+\frac{1}{3!}(\hat{T}_1+\hat{T}_2)^3+...)\Psi_0 \qquad 2.20$$

This shows that at any level of truncation of the Taylor expansion, excitation levels higher than double appear. The inclusion of these higher level completely solves the size-consistency problems exhibited by truncated CI methods. The drawback of this method is that the equation system to solve is no longer a linear system: algorithms able to solve non-linear equations are required to obtain the amplitudes and finally determine the correlation energy.

There are at present different methods that go beyond double excitations and include the effect of the triple excitations, in the exact or approximate form through a perturbation theory estimation. The CC methods have the undoubted advantage that they lead to correct fragment separability. But, like the configuration interaction and the perturbative methods, they need the reference wave-function to give a qualitatively correct description of the system. Therefore, even if single reference CC methods such as CCSD include triple excitations, they cannot give correct descriptions for systems that at zeroth-order have a strong multireference character.

ISBN:978-84-694-2171-0/DL:T. 1032-2011

The determination of the electronic structure based on the exact Hamiltonian may lead to very accurate approximations to the exact N-electron eigenfunction following one of the previously described methodologies, but does not necessarily lead to the desired understanding of the intrinsically complex electronic structure of strongly correlated materials described in this thesis. Therefore, it is common practice to capture the essentials of the electronic structure in a simpler model Hamiltonian. This section describes three model Hamiltonians and the strategy that has been followed to extract the respective parameters from the *ab initio* results.

2.2.1 Magnetic Interactions

The coupling of localized spin moments in extended structures can be determined with the following model Hamiltonian:

$$\hat{H} = \sum_{i<j} -J_{ij}^{x}\hat{S}_i^{x}\cdot\hat{S}_j^{x} - J_{ij}^{y}\hat{S}_i^{y}\cdot\hat{S}_j^{y} - J_{ij}^{z}\hat{S}_i^{z}\cdot\hat{S}_j^{z} \qquad 2.21$$

This general formulation, which accounts for both isotropic and anisotropic coupling, is usually simplified assuming different relations between J^x, J^y and J^z. When pure isotropic coupling is considered ($J^x = J^y = J^z = J$), the well known Heisenberg Hamiltonian is obtained:

$$\hat{H} = \sum_{i<j} -J_{ij}\hat{S}_i\cdot\hat{S}_j \qquad 2.22$$

where $\hat{S}_i$ and $\hat{S}_j$ are the total spin operators on sites i and j. The Heisenberg model considers the spin as a classical vector without preferential orientation in the three-dimensional space.

ISBN:978-84-694-2171-0/DL:T. 1032-2011

On the other extreme, one can define the Ising Hamiltonian by imposing $J^x = J^y = 0$, $J^z = J$,

$$\hat{H} = \sum_{i<j} -J_{ij} \hat{S}_i^z \cdot \hat{S}_j^z \qquad 2.23$$

The spin moment in the Ising model is represented as a classical vector with just one component, always directed along the z-axis. Although there are more model Hamiltonians in the literature (XY model with $J^z = 0$; general model with $J^x = J^y = \xi J^z$), we consider only the Heisenberg and Ising Hamiltonians being the most relevant to non-relativistic Quantum Chemistry calculations.

The magnitude of the coupling of two spin moments decays very rapidly with the distance between the magnetic centres and usually only neighbouring centres are considered. Moreover, the coupling between neighbouring sites i and j is a basically local property, which is hardly affected by the presence of other spin moments in the neighbourhood of i and j. These properties make possible to study the magnetic coupling in extended systems in a pairwise manner in which the Heisenberg Hamiltonian is reduced to

$$\hat{H} = -J \hat{S}_i \cdot \hat{S}_j \qquad 2.24$$

In this specific case the eigenfunctions of the $\hat{S}^2$ operator are also eigenfunctions of the Heisenberg Hamiltonian. This is in general no longer the case when systems with more than two magnetic centres are considered, as will be illustrated in section 4.2.1. In the case of two S = 1/2 magnetic moments, the eigenvalues of the Heisenberg Hamiltonian are $\varepsilon = (-1/4)J$ for the triplet coupled spin eigenfunctions

$$\Psi(T) = \alpha(1)\alpha(2); \alpha(1)\beta(2) + \beta(1)\alpha(2); \beta(1)\beta(2) \qquad 2.25$$

and $\varepsilon = (3/4)J$ for singlet function

$$\Psi(S) = \alpha(1)\beta(2) - \beta(1)\alpha(2) \qquad 2.26$$

Hence, the difference is precisely J. The differences between the eigenvalues of the Heisenberg Hamiltonian for two centres with $S_1 \geq S_2$ follow a regular pattern characterized by:

$$E(S-1)-E(S) = S\,J \qquad 2.27$$

with $S_1 - S_2 \leq S \leq S_1 + S_2$.

Under the assumption of a common orbital part, the eigenfunctions of the electronic Hamiltonian are the same as those of the Heisenberg Hamiltonian considered in equation 2.24. Therefore, the energy eigenvalues can be matched directly with the Heisenberg eigenvalues and a strategy can be designed to determine J from the difference of energy eigenvalues of the N-electron eigenstates of the full Hamiltonian calculated with any standard Quantum Chemical methodology that conserves the spin symmetry.

The same reasoning can be followed to relate the eigenvalues of the Ising Hamiltonian with energy eigenvalues. However, in this case the spin part of the wave-function is not necessarily an eigenfunction of the $\hat{S}^2$ operator, and hence spin unrestricted methods can be used to calculate the energy eigenvalues. The use of the Ising Hamiltonian to relate J with calculated energy eigenvalues is especially useful for Density Functional Theory (DFT), which relies on a single determinant approach implying spin functions of broken symmetry for low spin states.[30,31,32]

2.2.2 Double-exchange Interactions

In the first exchange-coupled compounds that formed the basis of modern magnetochemistry, the spin carriers were completely localized on the magnetic sites. A new field of research was opened when electron delocalization was introduced in the

exchange-coupled molecular systems. In these mixed-valence (MV), itinerant electrons and localized magnetic moment can coexist, interact and show highly interesting properties.

The coupling of two localized magnetic moments of spin S_0, through an itinerant extra electron which can travel back and forth between the two magnetic centres can be described by the so-called double-exchange (DE) interaction proposed by Zener.[33] The mobility of the itinerant electron is largely hindered when the magnetic moments S_0 of the two sites are antiferromagnetically coupled as can be seen in Figure 2.3.

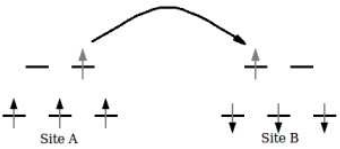

Figure 2.3. A scheme of itinerant electron hopping.

In the initial situation, all the electrons on site A are high spin coupled as expected from Hund's rule. When the itinerant electron hops to site B, a non-Hund state arises on this site due to the antiferromagnetic coupling of the S_0 spin moments. In the case of ferromagnetic coupling, there are always local Hund states, which is energetically more favourable.

The simplest case presents one d-electron moving between two spinless equivalent sites A and B. In other words, the two orbitals (a and b) are allowed to interact. The transfer process of the electron is ruled by the lowering of the kinetic energy

and the Coulomb attraction of the more positive charged neighbouring site, and is parametrized with the rate t associated with the transfer integrals:

$$t_{a\to b} = t_{b\to a} \qquad 2.28$$

The transfer integral for a one-electron MV dimer is defined as the matrix element of the monoelectronic part $\hat{h}$ of the Hamiltonian

$$t = \langle a|\hat{h}|b\rangle \qquad 2.29$$

The transfer process splits the energy level, and the two resulting delocalized functions are:

$$\psi_g = \frac{a+b}{\sqrt{2}} \text{ and } \psi_u = \frac{a-b}{\sqrt{2}} \qquad 2.30$$

with an energy difference of 2t.

In the most common case the TM ions are bridged by a ligand, and the electron transfer must occur through the orbitals of the ligand atoms. The following two-step exchange process is proposed by Zener. Firstly, one p-electron of the ligand jumps to one of TM sites occupying an empty orbital and keeping its spin orientation. Secondly, an electron jumps into the p-orbital of the ligand from the other TM site, restoring the ligand closed shell configuration.

Considering the dimer systems d^n – d^{n+1} with one itinerant electron, there are three different cases. The electron can be fully delocalized and hop without energy barrier, or the electron has to overcome a moderate barrier to move to the neighbouring site, or the electron stays completely localized on one of the TM ions. The energy levels for the first case can be expressed as

$$E(S) = \pm t\frac{(S+\frac{1}{2})}{2S_0+1} \qquad 2.31$$

where S_0 is the value of the spin core (*i.e.* the itinerant electron is not taken into account) and t is the one-electron transfer parameter associated with the hopping process of the extra

particle. Combining the effect of DE with magnetic exchange, the following expression for the energies arises:

$$E_{\pm}(S) = -JS(S+1) \pm t\frac{(S+\frac{1}{2})}{2S_0+1} \qquad 2.32$$

where J is the magnetic coupling constant.

In the second case, the extra electron might get trapped temporarily due to geometrical distortions (*e.g.* vibrational motions that make that the two TM-sites are no longer identical). Such trapping reduces the DE effect, eventually making the (anti)ferromagnetic exchange the dominant effect. Defining the energy difference between the left- and right-localized situation as $\Delta = E_A - E_B$, the energy levels of the intermediate hopping regime are determined as :

$$E_{\pm}(S) = -JS(S+1) \pm \sqrt{\Delta^2 + t^2\frac{(S+\frac{1}{2})^2}{(2S_0+1)^2}} \qquad 2.33$$

The last case, characterized by the strong localization, is naturally derived from this equation by taking the limit $t \to 0$. When Δ is large compared with t, the geometrical distortion eliminates the DE effect restoring the Heisenberg-type pattern of spin levels.[34]

In this thesis we study a material that belongs to the last class of mixed valence compounds, namely a V(II)V(III) oxalato-bridged lattice, where the magnetic anisotropy of the V(III) site is the main interest.

2.2.3 Effective Hamiltonian

In general, the parameters of the above described Hamiltonians can be determined from experiment. The magnetic coupling parameter J of the Heisenberg and Ising Hamiltonians

ISBN:978-84-694-2171-0/DL:T. 1032-2011

can be extracted from magnetic susceptibility measurements and subsequent fitting to analytical expressions of χ(T). However, there are many cases where a reliable parametrization is difficult to obtain. To give one example, the hopping parameter t in copper oxide materials is very hard to determine experimentally.[35] A versatile and (in principle) general applicable approach to extract detailed information about the electronic structure of strongly correlated materials from *ab initio* calculations proceeds through the determination of so-called effective Hamiltonians.[36,37]

The first step in the procedure is the definition of a model space that should contain all the essential physics of the property under study. If we take the magnetic coupling between two localized S = 1/2 spin moments as an example, the model space should at least contain the neutral ($|a\bar{b}\rangle$ and $|b\bar{a}\rangle$) and ionic ($|a\bar{a}\rangle$ and $|b\bar{b}\rangle$) determinants. The second step is the selection of the eigenstates of the exact Hamiltonians with the largest projection on the model space. In the present example, this implies the electronic states that are dominated by the neutral and/or ionic determinants. Subsequently, these states are projected onto the model space and orthonormalized. There are several methods to reach orthonormal expressions for the projected wave-functions. The original proposal of Bloch[36] involves biorthogonal vectors and leads to a non-Hermitian Hamiltonian with all kind of complications in the interpretation of the results.[38] Alternatively, the Löwdin orthogonalization can be followed as first suggested by des Cloizeaux.[39] This option is at present the preferred one and gave interesting results in double exchange systems[40] and magnetic anisotropy.[41] Finally, we mention the Gramm-Schmidt orthogonalization and the intermediate effective Hamiltonians.[37] The first procedure, only uses the energies of the higher lying states while the wave-function is imposed by the orthogonality condition with the lower lying states.[38] The

intermediate effective Hamiltonian is less ambitious and does not aim at a full determination of the states that span the model space, but only the lower roots of the matrix, and hence, a less complete picture of the physics is obtained. The final step consists in the application of the Bloch formula. The matrix elements of the effective Hamiltonian are defined as:

$$\hat{H}_{eff} = \sum_k \left| P\Psi_k \right\rangle E_k \left\langle P\Psi_k \right| \qquad 2.34$$

where $\left| P\Psi_k \right\rangle$ are the orthogonalized projections in Hermitian effective Hamiltonians onto the model space of the *ab initio* vectors and E_k are the corresponding eigenvalues. This effective Hamiltonian of reduced dimensions reproduces by definition the *ab initio* energies obtained in a much larger configuration space, and hence, opens a way to interpret the electronic structure.

2.3 Calculation of magnetic susceptibility

In order to continue the discussion, some words about magnetic susceptibility have to be written. The molar magnetic susceptibility is defined as:

$$\chi = \frac{\partial \vec{M}}{\partial \vec{H}} \qquad 2.35$$

where H is the magnetic field applied on a sample of 1 mol, and M is the acquired magnetic moment. If the applied magnetic field is weak, the susceptibility is independent of the field, and expression 2.35 can be simplified in this particular case to

$$\vec{M} = \chi \vec{H} \qquad 2.36$$

The magnetic susceptibility can be considered as a sum of two opposite contributions, the diamagnetic and the paramagnetic susceptibility, which are, respectively, negative and positive:

$$\chi = \chi^D + \chi^P \qquad 2.37$$

ISBN:978-84-694-2171-0/DL:T. 1032-2011

If χ^D dominates, the sample will be repelled by the applied magnetic field. In case where χ^P is the leading contribution, the sample is attracted. The diamagnetic nature of a substance is an intrinsic property of matter, independent of temperature. In the case of paramagnetic compounds of low molecular weight, the diamagnetic contribution to susceptibility is small and negligible at low temperatures.

The magnetic moment of the sample in a magnetic field is related to its energy as:

$$\vec{M} = -\frac{\partial E}{\partial \vec{H}} \qquad 2.38$$

In quantum mechanics the range of possible energies E_n (n = 1, 2, ..., n) is discrete. We can define a microscopic magnetic moment μ for each energy level n:

$$\vec{\mu_n} = -\frac{\partial E_n}{\partial \vec{H}} \qquad 2.39$$

The connection between microscopic and macroscopic properties can be achieved within Boltzmann statistical thermodynamics, where the macroscopic magnetic moment is derived as a sum of microscopic magnetic moments μ considering their weight:

$$\vec{M} = \frac{N \sum_n (-\partial E_n / \partial \vec{H}) \exp(-E_n / kT)}{\sum_n \exp(-E_n / kT)} \qquad 2.40$$

where N is Avogadro's number, T is temperature and k is Boltzmann constant. The application of equation 2.40 is difficult, and in order to relate the energy of electronic states and magnetic susceptibility, two approximations were proposed by Van Vleck.[42] Firstly, the energy can be expanded in the following sum:

$$E_n = E_n^{(0)} + E_n^{(1)} \vec{H} + E_n^{(2)} \vec{H}^2 + \ldots \qquad 2.41$$

where $E_n^{(0)}$ is the energy of level n in the absence of external magnetic field, and $E_n^{(1)}$ and $E_n^{(2)}$ are the first- and second-order corrections correspondingly (Zeeman coefficients). Using equation

ISBN:978-84-694-2171-0/DL:T. 1032-2011

2.39 we obtain the microscopic magnetic moment depending on the Zeeman coefficients and the applied magnetic field:

$$\vec{\mu}_n = -E_n^{(1)} - 2E_n^{(2)}\vec{H} + \ldots \qquad 2.42$$

The second approximation proposes to consider that $\vec{H}/(kT) \ll 1$, *i.e.* the applied magnetic field is weak and the temperature is not extremely small. Therefore the ratio E_n/kT is negligible comparing to unit, and the exponent from equation 2.40 can be expanded as:

$$\exp(-E_n/kT) = (1 - E_n^{(1)}\vec{H}/kT)\exp(-E_n^{(0)}\vec{H}/kT) \qquad 2.43$$

If the magnetic field is sufficiently weak, equation 2.41 can be cut after the first term and consider that the energies have a linear behaviour with respect to the magnetic field H (quadratic terms are therefore neglected):

$$E_n = E_n^{(0)} + E_n^{(1)}\vec{H} \qquad 2.44$$

Assuming these two approximations, the macroscopic magnetic moment can be expressed in terms of the energies as follows:

$$\vec{M} = \frac{N\vec{H}}{kT}\frac{\sum_n (E_n^{(1)})^2 \exp(-E_n^{(0)}/kT)}{\sum_n \exp(-E_n^{(0)}/kT)} \qquad 2.45$$

Therefore, using equation 2.35 the magnetic susceptibility can be expressed as:

$$\chi = \frac{N}{kT}\frac{\sum_n (E_n^{(1)})^2 \exp(-E_n^{(0)}/kT)}{\sum_n \exp(-E_n^{(0)}/kT)} \qquad 2.46$$

which is Van Vleck's formula. To apply it, only two things are required: the energy in absence of magnetic field $E_n^{(0)}$, and first-order correction $E_n^{(1)}$. Taking the energy of the lowest state as zero level of energy and taking into account Zeeman splitting effect, the following expression for magnetic susceptibility can be achieved:

$$\chi = \frac{Ng^2\beta^2}{kT}\frac{\sum_S \sum_{M_S=-S}^{+S} M_S^2 \exp(-E(S)/kT)}{\sum_S (2S+1)\exp(-E(S)/kT)} \qquad 2.47$$

where g is gyromagnetic factor and β is the Bohr magneton. Now only the energies of states with different multiplicities are needed to express the susceptibility. The models that relate the different energies with a single parameter (magnetic coupling constant J) are described above. This relation for dinuclear systems is given in equation 2.27.

Having the calculated or fixed at a certain value (for model aims) J, the thermal dependency of magnetic susceptibility can be achieved. We base our strategy of calculating the magnetic susceptibility on the procedure outlined by Novoa and co-workers.[43,44,45] The Heisenberg Hamiltonian for a large model can be built from J, and the spectrum will be calculated. The most straightforward way is to fully diagonalize the interaction matrix. This puts a limit on the size of the model of approximately 16 S = 1/2 centres and less for materials with higher spin moments. Other techniques as renormalization approaches[46,47] (see below) and Monte Carlo simulations[48,49] can be used to deal with large spin models, but for the systems treated in this thesis, the finite size effects are small and 16 centres is sufficient. With the obtained spectrum of Heisenberg Hamiltonian, the thermal dependency of χ can be achieved with equation 2.47, which has been coded.

2.4 The embedded cluster model

Extended structures cannot be treated directly but need some level of modeling. There are basically two approaches; on the one hand, the periodic approach and on the other the embedded cluster method. Within the latter model a small but relevant part of the structure is treated with high level *ab initio* computational schemes. The effect of the rest of the structure on

this cluster is taken into account in a more approximate way. The cluster method can be applied when certain local properties of crystalline solids are studied. Among others, these are effects connected with the existence of isolated defects and impurities in an otherwise perfect infinite lattice, core level excitations, localized electronic states in transition metal and rare earth materials, and molecule-surface interactions.

The other choice is the periodic approach in which a unit cell is defined and repeated periodically, so that band structure calculations can be applied to determine properties specific for the extended nature of the compound. However, in describing defects or impurities, the mutual interaction of ”defect” sites in neighbouring cells limits the accuracy of the results in a periodic approach.[50] Enlarging the cell will reduce such artefacts, but the increase in the computational effort could make the problem intractable. Moreover, the periodic approach relies primarily on DFT approaches to treat electronic correlation. The monoconfigurational nature implies that the broken symmetry approximation should be imposed to treat magnetic systems, and that many properties depend on the exact details of the functional applied without a clear hierarchy in the precision. On the other hand, when combined with advanced quantum chemical wave-function based calculations, the cluster model enables a systematic study of local correlation and a rigorous way to describe all possible spin couplings of the electrons. An accurate treatment of electron correlation effects is important in 3d systems which is exactly one of the objectives of this thesis.

To insure the proper connection with the rest of the solid various embedding schemes have been developed, whose description is somewhat outside of the thesis. More detailed approaches are described in literature.[51,52,53,54,55] In the present work, the cluster model is applied in a simple way. The relevant part of the extended structure has one or two transition metals

(depending on the property) and the atoms or groups of atoms in the direct surrounding. The atoms around the cluster are represented by pseudo-potentials, while point charges are used for atoms still further away from the cluster.

2.5 Comparison of the Ising *vs* Heisenberg Hamiltonian

In the largest part of the systems studied in this thesis, the magnetic properties are accurately described with the Heisenberg Hamiltonian introduced before. However, in some cases, we have to deal with magnetic anisotropy or the simulation of macroscopic properties requires the use of simpler Hamiltonians. Here we explore the possibility of the Ising Hamiltonian to provide a spectrum of eigenvalues that lead to an accurate estimate of the temperature dependence of the magnetic susceptibility. To this end, Table 2.1 compares several properties of the model spectrum of the two Hamiltonians for a dimer with $S_1 = S_2 = (1/2, 1, 3/2, 2, 5/2)$, assuming an interaction of J = -1 K. Figure 2.4 defines two of the parameters that are compared. Δ is the energy difference between the two lowest energy levels and W is the total width of the spectrum, *i.e.* the energy difference between the state with S = 0 and $S = S_{max}$ for the Heisenberg Hamiltonian and between the broken symmetry (BS; $M_s = 0$) and the high spin (HS; $M_s = \pm S_{max}$) state for the Ising Hamiltonian. Finally, the Table 2.1 also includes the degeneracy (d) of the first excited state with S different from zero for the Heisenberg Hamiltonian and M_s different from zero for the Ising Hamiltonian.

Table 2.1. Comparison of several properties of spectra of dimers obtained within Heisenberg and Ising models. d is the degeneracy of the first excited state with S ≠ 0 (Heisenberg) or M_s ≠ 0 (Ising).

$S_1 = S_2$	Ising			Heisenberg		
	Δ	d	width	Δ	d	width
1/2	1/2 J	2	1/2 J	1 J	3	1 J
1	1 J	4	2 J	1 J	3	3 J
3/2	3/2 J	4	5 J	1 J	3	6 J
2	2 J	4	8 J	1 J	3	10 J
5/2	5/2 J	4	13 J	1 J	3	15 J

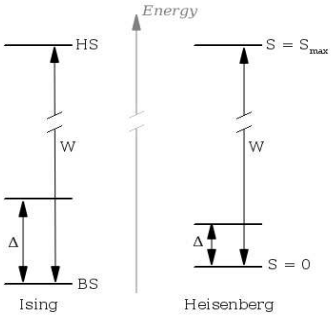

Figure 2.4. Definition of width and energy difference Δ of spectra obtained within Heisenberg and Ising models.

The magnetic susceptibilities calculated for the five different dimers are depicted in Figure 2.5, where the red curves are obtained from the Ising spectrum and the blue ones from the Heisenberg spectrum. It is readily seen that the smaller Δ (energy difference between the ground and first excited state) in the Ising spectrum for the dimer with S1 = S2 = 1/2 leads to a faster increase of the magnetic susceptibility at lower temperatures and χ(T) reaches its maximum at lower temperature, see Table 2.2.

Table 2.2. Characteristics of the thermal dependency of the magnetic susceptibility for dimers obtained within Heisenberg and Ising models. T is given in K, χ in emu/mol.

$S_1=S_2$	Ising			Heisenberg		
	T_{max}	$\chi(T_{max})$	$\chi(T=inf)$	T_{max}	$\chi(T_{max})$	$\chi(T=inf)$
1/2	0.4	0.835	0.001	0.6	0.603	0.001
1	0.9	0.943	0.002	1.0	0.787	0.002
3/2	1.5	0.979	0.004	1.5	0.865	0.004
2	2.4	0.996	0.006	2.2	0.907	0.006
5/2	3.4	1.005	0.009	2.9	0.931	0.009

The agreement between Ising and Heisenberg results is better for the dimer with S = 1 spin moments. Δ is identical for both Hamiltonians, which results in a T_{max} in the Ising curve that is only slightly smaller than for the Heisenberg curve. The Ising curve reaches slightly higher values due to the higher degeneracy of the first excited state. The comparison between the two curves for the dimer with S = 3/2 spin moments is even more favourable. T_{max} is almost identical and the maximum value of χ is also comparable. However, the two curves start to deviate at lower temperature, which can be related to the larger Δ in the Ising spectrum with respect to the Heisenberg spectrum. The effects of this larger energy difference between ground and first excited state becomes more obvious for the dimers with S = 2 and S = 5/2.

While Δ in the Heisenberg spectrum remains constant, it continuously increases for the Ising Hamiltonian (see Table 2.1). Then, the Ising curve rises less steep at low temperatures and reaches a maximum at higher temperatures. The maximum value of χ remains slightly larger due to the higher number of states in the vicinity of the first excited state.

ISBN:978-84-694-2171-0/DL:T. 1032-2011

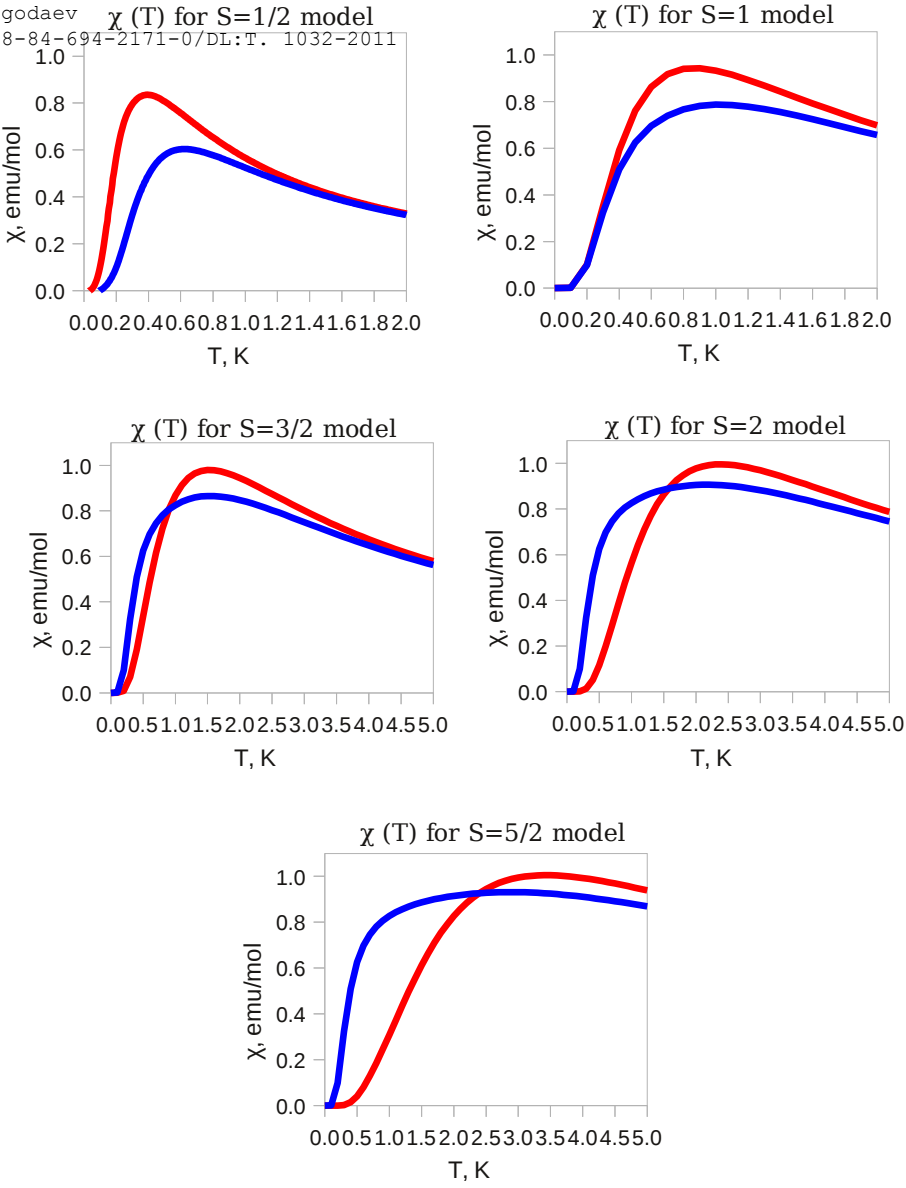

Figure 2.5. Thermal dependency of the magnetic susceptibility of dimers obtained within Heisenberg and Ising models. Red curves correspond to Ising model, blue curves correspond to Heisenberg model. J = -1K.

ISBN:978-84-694-2171-0/DL:T. 1032-2011

Secondly, we studied the behaviour of the two models for one-dimensional chains of connected spin moments. Starting with a uniform chain of S = 1/2 spin moments coupled with J = -1 K, we obtain the χ(T) curves. Two of them (for smallest 6- and largest 16-centres model) are shown in Figure 2.6. The models were used applying periodic boundary conditions. The same strategy was used to calculate χ(T) for the alternating chain with J_1 = -1 K and J_2 = -0.5 K (Figure 2.7). As can be seen in Tables 2.3 – 2.4, the finite size effects are small for both Hamiltonians.

Table 2.3. Characteristics of the χ(T) for 1D uniform chains. S = 1/2, T is given in K, χ in emu/mol.

N	Ising				Heisenberg			
	Δ	T_{max}	$\chi_{(T_{max})}$	$\chi_{(T=inf)}$	Δ	T_{max}	$\chi_{(T_{max})}$	$\chi_{(T=inf)}$
6	1	0.54	0.541	0.001	0.685	0.68	0.438	0.001
8	1	0.51	0.550	0.001	0.523	0.65	0.439	0.001
10	1	0.50	0.552	0.001	0.423	0.64	0.440	0.001
12	1	0.50	0.552	0.001	0.356	0.64	0.440	0.001
14	1	0.50	0.552	0.001	0.307	0.64	0.440	0.001
16	1	0.50	0.552	0.001	0.270	0.64	0.440	0.001

Table 2.4. Characteristics of the χ(T) for 1D alternating chains. S = 1/2, T is given in K, χ in emu/mol.

N	Ising				Heisenberg			
	Δ	T_{max}	$\chi_{(T_{max})}$	$\chi_{(T=inf)}$	Δ	T_{max}	$\chi_{(T_{max})}$	$\chi_{(T=inf)}$
6	0.75	0.43	0.693	0.001	0.726	0.68	0.437	0.001
8	0.75	0.42	0.699	0.001	0.682	0.61	0.535	0.001
10	0.75	0.41	0.699	0.001	0.666	0.61	0.535	0.001
12	0.75	0.41	0.700	0.001	0.661	0.61	0.535	0.001
14	0.75	0.41	0.700	0.001	0.659	0.61	0.535	0.001
16	0.75	0.41	0.700	0.001	0.658	0.61	0.535	0.001

ISBN:978-84-694-2171-0/DL:T. 1032-2011

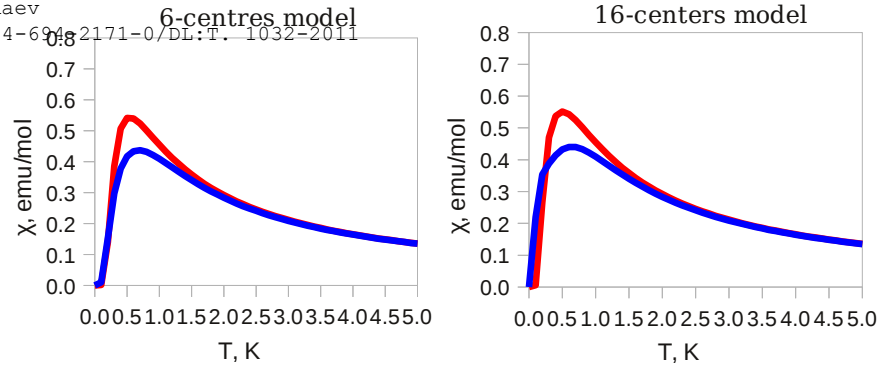

Figure 2.6. χ(T) for uniform S = 1/2 1D-chains. Left: 6-centres model. Right: 16-centres model. Red curves correspond to Ising model, blue curves correspond to Heisenberg model. J = -1K.

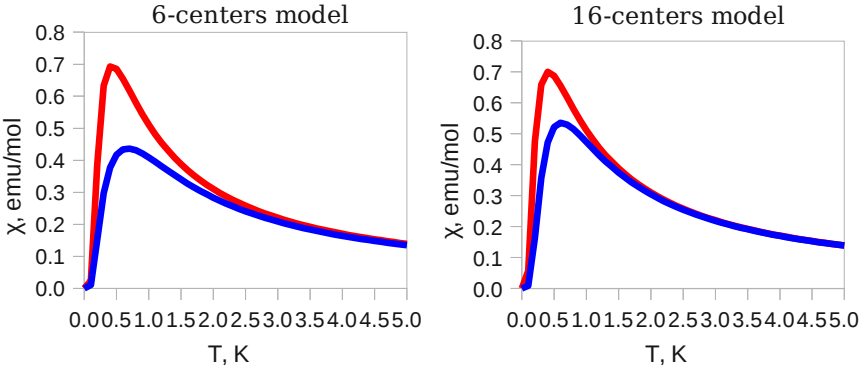

Figure 2.7. χ(T) for alternating S = 1/2 1D-chains. Left: 6-centres model. Right: 16-centres model. Red curves correspond to Ising model, blue curves correspond to Heisenberg model. J_1 = -1K, J_2 = -0.5K.

ISBN:978-84-694-2171-0/DL:T. 1032-2011

For the alternating chain (see Table 2.4), Δ is independent of the length of the chains within the Ising model, and slightly decreases, when the Heisenberg model is applied. Hence, the shape of the magnetic susceptibility curve is practically the same for all lengths considered here. In the uniform chain, Δ(Ising) is larger than Δ(Heisenberg). This causes a slower raise of χ(T) when the Ising spectrum is used. However, there are many more states close to this first excited state than in the Heisenberg spectrum, resulting in a larger χ value at T_{max}. The spectra of the two Hamiltonians are even more similar for the alternating chains. The main difference is the number of low-lying states, which is significantly larger for the Ising model leading again to a larger value of χ at T_{max}.

The next step concerns the comparison of the curves for the uniform chain with estimates of the exact susceptibility that have been published in the literature. The most famous estimate of χ(T) for the uniform S = 1/2 magnetic chain is the one published in 1964 by Bonner and Fisher[56] (BF), shown as green curve in Figure 2.8. The finite susceptibility at T = 0 is in line with the exact solution based on the Bethe Ansatz[57] and indicates that there is no finite gap between the ground state singlet and the first excited triplet state. More recently modifications of the BF estimate have been published[58] that concentrate on the very low temperature regime, but are not very relevant here.

We see how simple estimates are in good agreement for not too low temperatures but go to zero due to the finite gap in the calculated spectrum. The temperature for which χ reaches its maximum is nicely reproduced with the procedure based on the Heisenberg Hamiltonian and less accurately for the Ising spectrum. In chapter 4, we will compare to experimental data to further establish the validity of the outlined procedure.

ISBN:978-84-694-2171-0/DL:T. 1032-2011

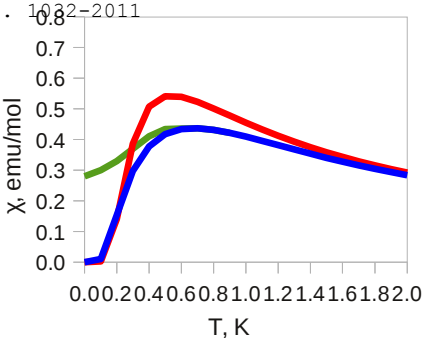

Figure 2.8. χ(T) for alternating S = 1/2 6-centres chain. Red curve corresponds to Ising model, blue curve corresponds to Heisenberg model, green curve is a result of applying BF expression. J = -1K.

Finally we compare the two model Hamiltonians for the 1D chains with elevated spin moments. The χ(T) curves are depicted in Figure 2.9 and show a similar behaviour as for the dimers: χ(T) with Ising spectrum rises too fast for S = 1/2 chains, then gives nearly identical results for S = 1, and gradually slower and slower rise of Ising in comparison to Heisenberg due to the increasing difference in Δ in the two models.

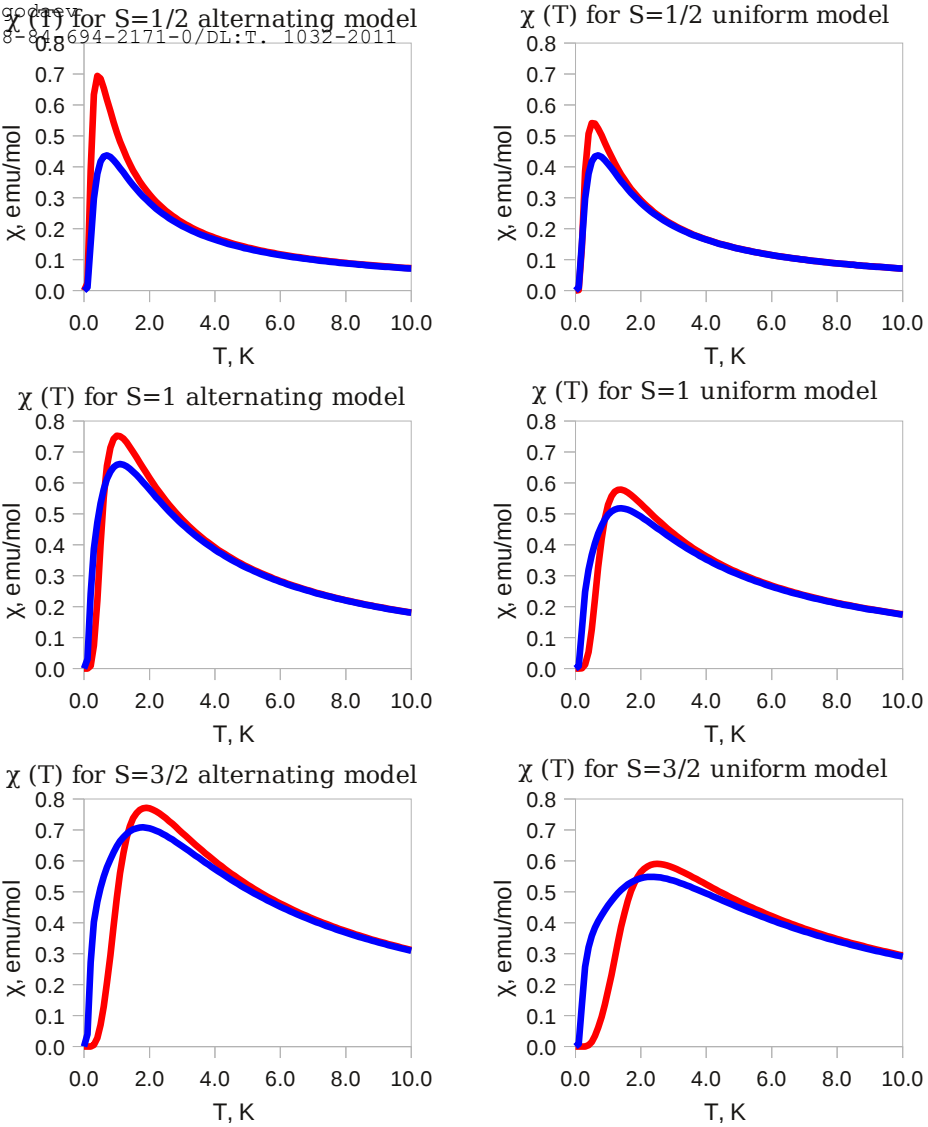

Figure 2.9. χ(T) for 6-centres chain systems. Red curves correspond to Ising model, blue curves correspond to Heisenberg model. Left: The alternating chains, J_1 = -1K, J_2 = -0.5K. Right: The uniform chains, J = -1K.

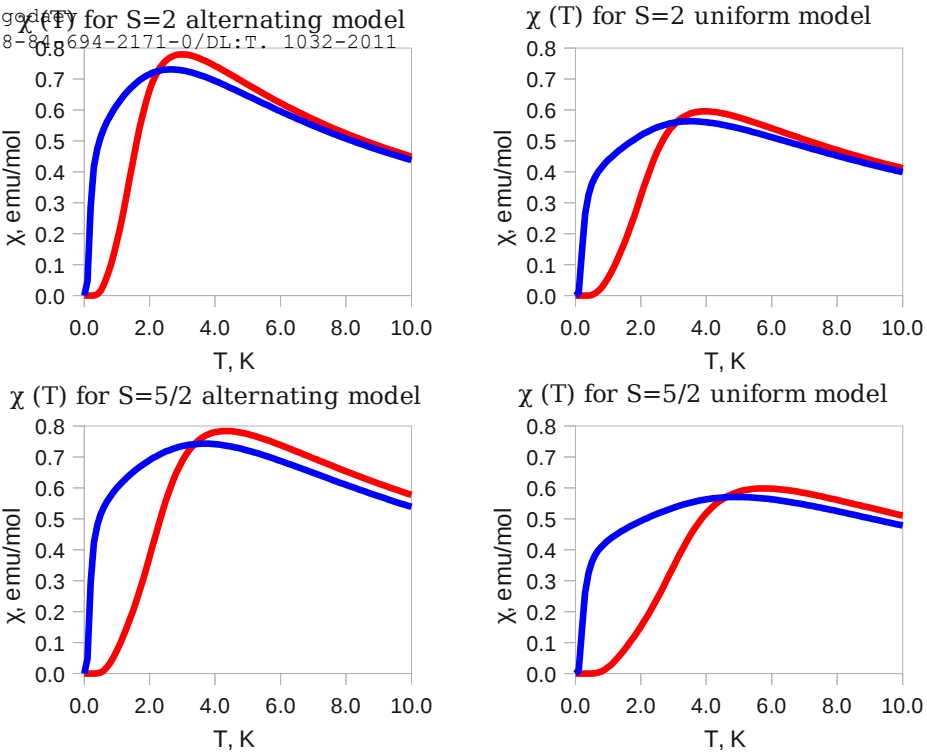

Figure 2.9. Continuation.

As a general conclusion, we observed that the Ising model does not reproduce the magnetic susceptibility extracted from the Heisenberg spectrum and deviates more strongly for systems with elevated spins. One may naively think that the Ising model is more appropriate for larger spin moments, being closer to the classical spin regime. However, at least for the systems tested here, we cannot support this assumption.

ISBN:978-84-694-2171-0/DL:T. 1032-2011

2.6 Renormalized excitonic method (REM)

The exact diagonalization applied above is not the only solution to obtain macroscopic properties *via* microscopic calculated parameters. The Monte-Carlo simulations (MCS)[48,49] or Real Space Renormalization Group (RSRG) methods[59,60] could be alternative options. Among the strategies to deal with extended systems, RSRG methods depart from the assumption that periodic lattices can be constructed from blocks of centres instead of the centres themselves. This viewpoint represents a change of scale because the interactions to be accounted for are those between the different blocks instead of the interactions between the centres that constitute a block. This approach can be especially adequate for systems with local interactions like the magnetic coupling between paramagnetic TMs. A relevant point of RSRG is that effective interactions between blocks can be determined by means of the effective Hamiltonian theory. The method consists in the definition of the building blocks for which the low energy spectrum is calculated as accurately as possible. A variant of this method developed by Malrieu and co-workers[47,61] is based on the supposition that the ground state of the extended system is composed by blocks in their respective ground state and that the lowest excited states arise from local excitations in one block maintaining all other blocks in their ground state. Since the method is based on the propagation of this local excitations (excitons) through the lattice, it has been called the Renormalized Excitonic Method (REM). The method has been applied to S = 1/2 systems and collective properties such as phase transitions have been successfully determined.[47,61]

The method starts with the accurate determination of the low energy spectrum of one block including the effects of the dynamical electron correlation. If no Heisenberg spectrum

ISBN:978-84-694-2171-0/DL:T. 1032-2011

deviations are expected in the magnetic system, this point can be limited to determine a very accurate value of J. After this, the effective interaction between blocks is calculated by the explicit evaluation of the electronic states of two blocks simultaneously, by using the results of Heisenberg Hamiltonian of a two-block system. This gives expressions of the energies of this dimer in terms of block energies and an inter-block interaction that can simply be derived from the Heisenberg Hamiltonian calculation. At this point, the calculation of the macroscopic properties is rather straightforward and only depends on the topology of the lattice. Different choices of building blocks are possible, but the results for the whole lattice should converge to the same results.

The hypothesis can be extended *a priori* to other collective properties as magnetic susceptibility, as well as to higher spin centres. Some tentative calculations on models have been made to investigate the applicability of the method, by supposing that a Heisenberg Hamiltonian gives a good description of the system. The preliminary results on S = 1/2 linear chains are reported below.

2.6.1 Building blocks, topology and interactions

An extended system can be built from 4-site blocks of S = 1/2 in each site:

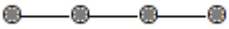

The extended system is built taking into account its topology in different nets, as shown in Figure 2.10.

UNIVERSITAT ROVIRA I VIRGILI
THE CALCULATION OF THE THERMAL DEPENDENCY OF THE MAGNETIC SUSCEPTIBILITY
IN EXTENDED SYSTEMS WITH AB INITIO ELECTRONIC STRUCTURE PARAMETERS
Igor Negodaev
ISBN:978-84-694-2171-0/DL:T. 1032-2011

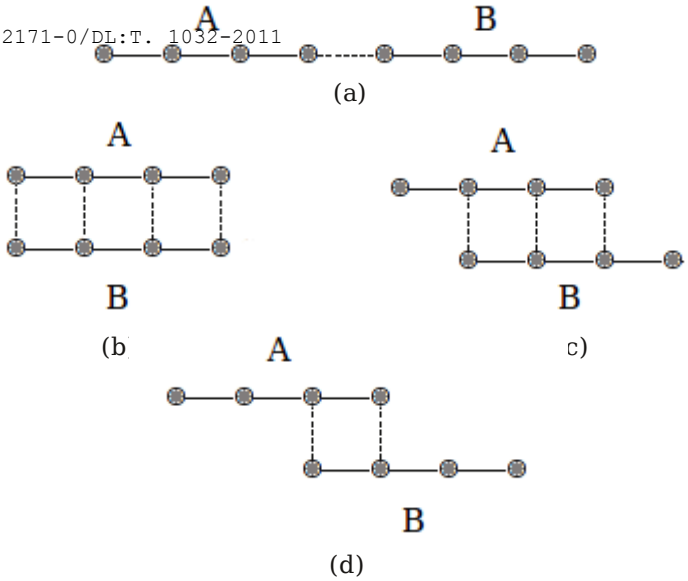

Figure 2.10. Different schemes of extended system construction from 4-site blocks A and B.

The unitary blocks interact differently depending on the topology. We will concentrate on linear chains (a), showing only an interaction between two blocks A and B, V_{AB}. The next step in increasing the chain includes 3 building blocks:

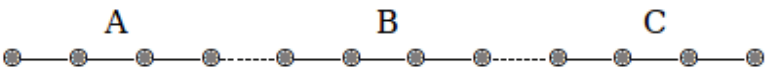

Blocks A and C have only an interaction with one neighbour block, while block B presents two interactions, and so on.

As in the previous models, we take an AF interaction with J = -1 K. We need the exact spectrum (assumed as the Heisenberg spectrum) of one building block (4 sites) and of a dimer (8 sites) to extract the interaction. The corresponding eigenvalues and multiplicities are reported in Annex 1.

ISBN:978-84-694-2171-0/DL:T. 1032-2011

The first step in the REM procedure is to find the interaction between two blocks both in the ground state, as well as the interaction of a block on the ground state and a singly excited block. Let us use the symbols A_0 and A^* (respectively B_0 and B^*) for ground state and first triplet state of blocks A and B, and A_0B_0, A^*B_0 and A_0B^* for the ground state and locally excited dimers:

$$\begin{aligned} &\text{Ground state } A_0B_0\text{: } E_{A_0B_0}=E_{A_0}+E_{B_0}+V_{A_0B_0} \\ &\text{Local excitation on A, } A^*B_0\text{: } E_{A^*B_0} \\ &\text{Local excitation on B, } A_0B^*\text{: } E_{A_0B^*} \end{aligned} \qquad 2.48$$

Since the system is antiferromagnetic, the ground state is a singlet, and the first excited state in a block is a triplet:

$$\begin{aligned} &A_0 \rightarrow S \\ &A^* \rightarrow T \\ &\text{and } E_{A^*}-E_{A_0}=\Delta E>0 \end{aligned} \qquad 2.49$$

According to the Heisenberg exact energy (see Annex 1), the first excited state in each 4-sites block has relative energy 0.659 K, *i.e.* $\Delta E = 0.659$ K. A^*B_0 and A_0B^* are local singly excited triplets in the dimer AB, which energy is to be determined, since the 8-sites linear model gives the exact values in the delocalized system. In particular, the first excited states in the exact 8-sites model are two single excitations on AB, the lowest triplet states, T_1 and T_2. The interaction diagram shows the energies of these two delocalized triplets from the local ones:

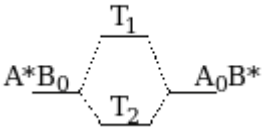

The energy of the local triplets A^*B_0 and A_0B^* can be found from the eigenvalues equation:

ISBN:978-84-694-2171-0/DL:T. 1032-2011

$$\mathbb{H}\left|T_1\right\rangle = E_{T_1}\left|T_1\right\rangle \text{ and } \mathbb{H}\left|T_2\right\rangle = E_{T_2}\left|T_2\right\rangle \qquad 2.50$$

where $\mathbb{H}$ is the 2x2 Hamiltonian matrix in the basis of the two local triplets:

$$\begin{array}{c|cc} & A^*B_0 & A_0B^* \\ \hline A^*B_0 & E_{A^*B_0}-E_{A_0B_0} & h \\ A_0B^* & h & E_{A_0B^*}-E_{A_0B_0} \end{array} \qquad 2.51$$

Here h is the interaction matrix element:

$$h=\left\langle A^*B_0\middle|\hat{H}\middle|A_0B^*\right\rangle \qquad 2.52$$

Since blocks A and B are identical, $E_{A^*B_0}=E_{A_0B^*}$, the diagonal elements give the local triplets excitation energy

$$E_{A^*B_0}-E_{A_0B_0}=E_{A_0B^*}-E_{A_0B_0} \qquad 2.53$$

The relative energies E_{T_1} and E_{T_2} are reported in Annex 1 (8 sites):

$$E_{T_1}-E_{A_0B_0}=0.393\,K \text{ and } E_{T_2}-E_{A_0B_0}=0.871\,K \qquad 2.54$$

The secular equation gives:

$$(E_{A^*B_0}-E_{A_0B_0}-x)^2-h^2=0 \text{ and } x=(E_{A^*B_0}-E_{A_0B_0})\pm h \qquad 2.55$$

$$\begin{aligned} E_{T_1}-E_{A_0B_0}&=(E_{A^*B_0}-E_{A_0B_0})+h \\ E_{T_2}-E_{A_0B_0}&=(E_{A^*B_0}-E_{A_0B_0})-h \end{aligned} \qquad 2.56$$

$$\text{and } h=(E_{T_1}-E_{T_2})/2$$

From the calculated 8-sites values, $E_{T_1}=0.393\,K$ and $E_{T_2}=0.871\,K$, hence h = -0.239 K, which gives for the local triplet energy the mean value of delocalized ones:

$$E_{A^*B_0}-E_{A_0B_0}=([E_{T_1}-E_{A_0B_0}]+[E_{T_2}-E_{A_0B_0}])/2=0.632\,K \qquad 2.57$$

Let us now consider the energy of the ground state and of the local triplet as the sum of fragment energies, plus an interaction:

$$\begin{aligned} E_{A_0B_0}&=E_{A_0}+E_{B_0}+V_{A_0B_0} \\ E_{A^*B_0}&=E_{A^*}+E_{B_0}+V_{A^*B_0} \end{aligned} \qquad 2.58$$

$$\text{and } E_{A^*B_0}-E_{A_0B_0}=E_{A^*}-E_{A_0}+V_{A^*B_0}-V_{A_0B_0}=\Delta E+V_{A^*B_0}-V_{A_0B_0}$$

Since the 4-site block excitation energy is ΔE = 0.659 K,

$$V_{A^*B_0} - V_{A_0B_0} = E_{A^*B_0} - E_{A_0B_0} - \Delta E \qquad 2.59$$

$$V_{A^*B_0} - V_{A_0B_0} = 0.632 - 0.659 = -0.027 K$$

From this information, we will build up singly excited triplet states of larger systems.

2.6.2 Singly excited states of 3-block systems

The next step in the enlargement of the chain is a 12-sites chain, built from three 4-sites blocks, A, B, and C.

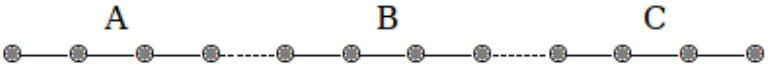

Taking only into account the interactions with nearest-neighbours, A presents one interaction with B, B has one interaction with A and one with C, and finally, C is involved in one interaction with B. The single excitations are generated from the interaction of locally excited blocks: $A^*B_0C_0$, $A_0B^*C_0$ and $A_0B_0C^*$. The matrix representation of the singly excited triplets in this basis is given in expression 2.60:

	$A^*B_0C_0$	$A_0B^*C_0$	$A_0B_0C^*$
$A^*B_0C_0$	$E_{A^*B_0C_0} - E_0$	h	0
$A_0B^*C_0$	h	$E_{A_0B^*C_0} - E_0$	h
$A_0B_0C^*$	0	h	$E_{A_0B_0C^*} - E_0$

2.60

where only the interaction between near-neighbours is taken into account, and

$$E_0 = E_{A_0B_0C_0} = 3E_{A_0} + 2V_{A_0B_0} \qquad 2.61$$

The diagonal elements can be calculated, referred to $A_0B_0C_0$ ground state:

ISBN:978-84-694-2171-0/DL.T. 1032-2011

$$E_{A^*B_0C_0} = E_{A^*} + E_{B_0} + E_{C_0} + V_{A^*B_0} + V_{B_0C_0}$$
$$E_{A_0B_0C_0} = E_{A_0} + E_{B_0} + E_{C_0} + V_{A_0B_0} + V_{B_0C_0} \qquad 2.62$$

and $E_{A^*B_0C_0} - E_{A_0B_0C_0} = \Delta E + V_{A^*B_0} - V_{A_0B_0}$

$$E_{A_0B^*C_0} = E_{A_0} + E_{B^*} + E_{C_0} + V_{A_0B^*} + V_{B^*C_0}$$
$$E_{A_0B_0C_0} = E_{A_0} + E_{B_0} + E_{C_0} + V_{A_0B_0} + V_{B_0C_0} \qquad 2.63$$

and $E_{A_0B^*C_0} - E_{A_0B_0C_0} = \Delta E + 2(V_{A^*B_0} - V_{A_0B_0})$

$$E_{A_0B_0C^*} - E_{A_0B_0C_0} = E_{A^*B_0C_0} - E_{A_0B_0C_0} \qquad 2.64$$

From the dimer, we know

$\Delta E = 0.659$ K

h = -0.239 K

and $V_{A^*B_0} - V_{A_0B_0} = -0.027\,\mathrm{K}$.

Consequently, the diagonal elements are:

$$E_{A^*B_0C_0} - E_{A_0B_0C_0} = \Delta E + V_{A^*B_0} - V_{A_0B_0} =$$
$$E_{A^*B_0C_0} - E_{A_0B_0C_0} = 0.659 - 0.027 = 0.632\,\mathrm{K} \qquad 2.65$$

$$E_{A_0B^*C_0} - E_{A_0B_0C_0} = \Delta E + 2(V_{A^*B_0} - V_{A_0B_0}) =$$
$$E_{A_0B^*C_0} - E_{A_0B_0C_0} = 0.659 - 2*0.027 = 0.605\,\mathrm{K} \qquad 2.66$$

Therefore the Hamiltonian matrix representation on the basis of the three local excited triplets is:

	$A^*B_0C_0$	$A_0B^*C_0$	$A_0B_0C^*$
$A^*B_0C_0$	0.632	−0.239	0
$A_0B^*C_0$	−0.239	0.605	−0.239
$A_0B_0C^*$	0	−0.239	0.632

2.67

The diagonalization of this 3-block matrix gives three triplets, whose relative energies (to the ground $A_0B_0C_0$ state) are shown in Table 2.5 and can be compared with the exact values given by a 12-sites linear chain. The agreement seems really good for the 3-block triplet energy. Following the same procedure, the REM results for a 4-block system, compared to a 16-sites chain gives the singly excited states whose energies are given in Table 2.6.

ISBN:978-84-694-2171-0/DL:T. 1032-2011

Table 2.5. Singly excited triplet states energies (in K) for a 3-block system from REM and from diagonalization of 12-sites Heisenberg Hamiltonian.

Triplet energies (K)	E_{T_1}	E_{T_2}	E_{T_3}
REM	0.280	0.632	0.957
Exact (12-sites)	0.281	0.629	0.950

Table 2.6. Singly excited triplet states energies (in K) for a 4-block system from REM and from diagonalization of 16-sites Heisenberg Hamiltonian.

Triplet energies (K)	E_{T_1}	E_{T_2}	E_{T_3}	E_{T_4}
REM	0.225	0.477	0.773	0.999
Exact (16-sites)	0.219	0.491	0.746 0.752	0.991 1.003

As can be seen in Table 2.6, two additional values appear in the same range in the exact spectrum. This suggests that these triplets are multiexcited states.

2.6.3 Multiexcited states energy

The next step in the REM method is to define how to obtain multiexcited states in the N-block system. For each multiplicity, singlet, triplet, quintet, ..., doubly excited states of the N blocks system will be $A^*B^*C_0D_0$...., $A^*B_0C^*D_0$...., $A_0B^*C^*D_0$...., *etc*. and so on for triply or highly excited states, $A^*B^*C^*D_0$..., $A^*B_0C^*D^*$..., $A_0B^*C^*D^*$..., *etc*. A first simplistic supposition is to consider that the single excitations are independent one from another (because

supposed relatively localized) and therefore the energy of multiexcited states in the extended system can be calculated by adding singly excited energies of the N-block system. This crude supposition will be shown incorrect, but it is useful to start with this procedure since it illustrates how to build the spectrum of the N-block system. The energies of the different multiplicities are reached from a combination of single excitations, *i.e.* from a combination of triplets. Since they are considered independent, the energies can be considered additive and the different multiplets are degenerated. The different multiplets are obtained by adding the different M_s components, of the different blocks. For N blocks, N singly excited triplet states would be found, and different multiplets are accessible (see Table 2.7):

Table 2.7. Multiplets obtained for N blocks, as a function of the number of singly excited state. S, T, Q, H, N are singlet, triplet, quintet, septet, nonuplet correspondingly.

Number of singly excited states	Multiplets	Degeneracy
2	1S, 1T, 1Q	9
3	1S, 3T, 2Q, 1H	27
4	1S, 3T, 3Q, 2H, 1N	48
N	...	

From previous results, we have obtained three singly excited triplet states in the 3-block system, with energies: 0.280, 0.632 and 0.957 K. Let us build the spectrum of the 12-sites system by considering all possible combinations of ground state, T_1, T_2 and T_3 single excitations. This procedure implies that the resulting states give the lowest part of the spectrum and that states resulting from other type of excitations should be higher in

energy. Table 2.8 reports the energy values calculated from this procedure.

By comparing the energies reported in Table 2.8 with the exact values in Table 2.5 (12 sites) it is clear that $E(2T_1) = 0.56$ K does not match with any of the exact values of the 12-sites Heisenberg spectrum, since there is no singlet, triplet or quintet state with this energy. Therefore, a different strategy has to be used to estimate multiexcited energies, and the coupling of single excitations in two neighbour blocks will be considered explicitly, giving doubly excited singlet, triplet, quintet excited states.

Table 2.8. Energies of the different singly and multiexcited states (in K) in the 3-block model obtained by considering independent processes.

Single excitations	Energy	Multiplets	Degeneracy
T_1	0.280	T	3
$2T_1$	0.560	S, T, Q	9
T_2	0.632	T	3
$3T_1$	0.840	1S, 3T, 2Q, 1H	27
$T_1 + T_2$	0.912	S, T, Q	9
T_3	0.957	T	3
$2T_1 + T_2$	1.192	1S, 3T, 2Q, 1H	27
$T_1 + T_3$	1.237	S, T, Q	9
$2T_2$	1.264	S, T, Q	9
$2T_1 + T_3$	1.517	1S, 3T, 2Q, 1H	27
$2T_2 + T_1$	1.544	1S, 3T, 2Q, 1H	27
$T_3 + T_2$	1.589	S, T, Q	9
$2T_3$	1.914	S, T, Q	9
$2T_3 + T_1$	2.194	1S, 3T, 2Q, 1H	27
$2T_2 + T_3$	2.221	1S, 3T, 2Q, 1H	27
$2T_3 + T_2$	2.546	1S, 3T, 2Q, 1H	27
$3T_3$	2.871	1S, 3T, 2Q, 1H	27

ISBN:978-84-694-2171-0/DL:T. 1032-2011

If we consider the interaction of single excitations in neighbour blocks, the interaction between A^* and B^*, $V(A^*B^*)$, is different from the previously calculated one, $V(A^*B)$ and must be determined. Furthermore, it depends on the resulting state: singlet, triplet or quintet, and must be determined for each multiplicity. The procedure is similar to the extraction of singly excited triplet energies from the 2-block interaction.

Let us start with the singlet state resulting of two neighbour excitations. According to the exact 8-sites solution, the first singlet excited state has an energy: $E^S = 1.041\,K$. Considering that this state results from 2 single excitations, one in each 4-sites block,

$$E^S_{A^*B^*} - E_{A_0B_0} = 1.041 = 2\Delta E + (V^S_{A^*B^*} - V_{A_0B_0}) \qquad 2.68$$

Since $\Delta E = 0.659$ K,

$$V^S_{A^*B^*} - V_{A_0B_0} = -0.277\,K \qquad 2.69$$

where $V^S_{A^*B^*} - V_{A_0B_0}$ is the interaction giving a singlet state from two neighbour triplets.

Taking now 3 blocks including singlet diexcitations: $A^*B^*C_0$, $A^*B_0C^*$, $A_0B^*C^*$, the diagonal elements of the matrix representation become:

$$\begin{aligned} E^S_{A^*B^*C_0} &= E_{A^*} + E_{B^*} + E_{C_0} + V^S_{A^*B^*} + V_{B^*C_0} \\ E_{A_0B_0C_0} &= E_{A_0} + E_{B_0} + E_{C_0} + V_{A_0B_0} + V_{B_0C_0} \end{aligned} \qquad 2.70$$

$$\text{and } E^S_{A^*B^*C_0} - E_{A_0B_0C_0} = 2\Delta E + (V^S_{A^*B^*} - V_{A_0B_0}) + (V_{B^*C_0} - V_{B_0C_0})$$

Since $V_{B^*C_0} - V_{B_0C_0} = -0.027\,K$,

$$\begin{aligned} E^S_{A^*B^*C_0} - E_{A_0B_0C_0} &= 1.041 - 0.027 = 1.014\,K \\ E^S_{A^*B_0C^*} &= E_{A^*} + E_{B_0} + E_{C^*} + V^S_{A^*B_0} + V_{B_0C^*} \\ E_{A_0B_0C_0} &= E_{A_0} + E_{B_0} + E_{C_0} + V_{A_0B_0} + V_{B_0C_0} \end{aligned} \qquad 2.71$$

$$\text{and } E^S_{A^*B_0C^*} - E_{A_0B_0C_0} = 2\Delta E + 2(V_{A^*B_0} - V_{A_0B_0}) = 1.264\,K$$

By considering that the off-diagonal elements do not change:

$$\langle A^*B^*C_0|\hat{H}|A^*B_0C^*\rangle = \langle B^*C_0|\hat{H}|B_0C^*\rangle = h \qquad 2.72$$

the matrix representation for the excited singlets is:

ISBN:978-84-694-2171-0/DL.T. 1032-2011

$$\begin{array}{c|ccc} & A^*B^*C_0 & A^*B_0C^* & A_0B^*C^* \\ \hline A^*B^*C_0 & 1.014 & -0.239 & 0 \\ A^*B_0C^* & -0.239 & 1.264 & -0.239 \\ A_0B^*C^* & 0 & -0.239 & 1.014 \end{array} \qquad 2.73$$

The diagonalization of this 3-block matrix gives three singlets, whose relative energies (to the ground $A_0B_0C_0$ state) are compared in Table 2.9 with the exact values given by a 12-sites linear chain.

Table 2.9. Excited singlet states energies (in K) for a 3-block system from REM, taking into account two neighbour single excitations, compared to the exact eigenvalues of Heisenberg Hamiltonian.

Singlet energies (K)	E_{S_1}	E_{S_2}	E_{S_3}
REM	0.779	1.014	1.499
Exact (12-sites)	0.734	1.068	1.350

The third triplet of the 8-sites system can be considered as a diexcitation, as the first quintet:

$$\begin{aligned} E^T_{A^*B^*} - E_{A_0B_0} &= 1.267\,K \\ E^Q_{A^*B^*} - E_{A_0B_0} &= 1.543\,K \end{aligned} \qquad 2.74$$

Since $E^T_{A^*B^*} - E_{A_0B_0} = 2\Delta E + (V^T_{A^*B^*} - V_{A_0B_0})$ and $V^T_{A^*B^*} - V_{A_0B_0} = -0.051\,K$,

$$\begin{aligned} E^Q_{A^*B^*} - E_{A_0B_0} &= 2\Delta E + (V^Q_{A^*B^*} - V_{A_0B_0}) \\ V^Q_{A^*B^*} - V_{A_0B_0} &= 0.225\,K \end{aligned} \qquad 2.75$$

Therefore, the diagonal elements for the diexcited local triplets are:

$$\begin{aligned} E^T_{A^*B^*C_0} - E_{A_0B_0C_0} &= 2\Delta E + (V^T_{A^*B^*} - V_{A_0B_0}) + (V_{B^*C_0} - V_{B_0C_0}) = 1.240\,K \\ E^T_{A^*B_0C^*} - E_{A_0B_0C_0} &= 2\Delta E + 2(V_{A^*B_0} - V_{A_0B_0}) = 1.264\,K \end{aligned} \qquad 2.76$$

and those of the quintets

$$\begin{aligned} E^Q_{A^*B^*C_0} - E_{A_0B_0C_0} &= 2\Delta E + (V^Q_{A^*B^*} - V_{A_0B_0}) + (V_{B^*C_0} - V_{B_0C_0}) = 1.516\,K \\ E^Q_{A^*B_0C^*} - E_{A_0B_0C_0} &= 2\Delta E + 2(V_{A^*B_0} - V_{A_0B_0}) = 1.264\,K \end{aligned} \qquad 2.77$$

ISBN:978-84-694-2171-0/DL:T. 1032-2011

These expressions show that for non-neighbour diexcitations

$$E^{S}_{A^*B_0C^*} = E^{T}_{A^*B_0C^*} = E^{Q}_{A^*B_0C^*} \qquad 2.78$$

Therefore, the matrix representation for triplets and quintets can be expressed as 2.81 and 2.82 correspondingly.

	$A^*B^*C_0$	$A^*B_0C^*$	$A_0B^*C^*$
$A^*B^*C_0$	1.240	−0.239	0
$A^*B_0C^*$	−0.239	1.264	−0.239
$A_0B^*C^*$	0	−0.239	1.240

2.79

	$A^*B^*C_0$	$A^*B_0C^*$	$A_0B^*C^*$
$A^*B^*C_0$	1.516	−0.239	0
$A^*B_0C^*$	−0.239	1.264	−0.239
$A_0B^*C^*$	0	−0.239	1.516

2.80

The REM spectra for diexcited triplets and quintets, referred to the ground singlet, compared with exact 12-sites values are shown in Table 2.10. The order of magnitude is similar, although the agreement is less good than for singly excited triplets. From the previously reported values, we can compare both spectra, see Table 2.11. The attribution of the singly or doubly excited character in the exact spectrum is of course arbitrary.

Table 2.10. Doubly excited triplet and quintet states energies (in K) for a 3-blocks system from REM, taking into account two neighbour single excitations, compared to the exact eigenvalues of Heisenberg Hamiltonian.

	Triplet		Quintet	
	REM	Exact	REM	Exact
E_1	0.914	0.954	1.029	1.132
E_2	1.240	1.224	1.516	1.438
E_3	1.590	1.269	1.751	1.699

Table 2.11. Energies (in K) of the low singlet, triplet and quintet states from REM procedure in a 3-blocks system taking into account two neighbour single excitations, compared to the exact 12-sites Heisenberg energies.

State	Excitation[a)]	REM	Exact	Additive energies (see Table 2.8)
T	s	0.280	0.281	
T	s	0.632	0.629	
S	d	0.779	0.734	0.560
T	s	0.957	0.950	
T	d	0.914	0.954	0.560
S	d	1.014	1.068	0.912
Q	d	1.029	1.132	0.560
T	d	1.240	1.224	0.912
T	d	1.590	1.269	1.237
S	d	1.499	1.350	1.237
Q	d	1.516	1.438	0.912
Q	d	1.751	1.699	1.237

a) s: single excitation; d: double excitation

The additive energies (see Table 2.8) are also reported for double excitations for an easier comparison. It can be concluded that considering independent single excitations leads to too low energies. The consequence is particularly dramatic for triple excitations, since the energy of triplets, quintets and heptets is severely underestimated, with very high degeneracy degrees. Procedures to estimate the energy of these excited states with high excitation degree can be derived but the level of complexity increases dramatically.

ISBN:978-84-694-2171-0/DL:T. 1032-2011

2.6.4 Influence on magnetic susceptibility curves

To conclude this section, it is interesting to check how the precedent conclusion affects the magnetic susceptibility curves. Figure 2.11 shows the shapes obtained with the different energies previously discussed of the 3-block REM system, compared with the previously described 12-sites linear Heisenberg model (blue curve). The crude additive model gives the sharpest curve (pink curve), with the susceptibility maximum strongly overestimated and T_{max} severely underestimated (0.24K in front of 0.56 K). This is obviously due to the presence of very low energies with a high degeneracy, giving a high number of populated states at low temperatures. This incorrect behaviour is slightly corrected when explicitly taking into account double excitations (green curve), since T_{max} increases to 0.28 K, and the maximum χ slightly decreases. However, the effect is not very important because in the spectrum triple excitations have not been corrected and many underestimated values with high degeneracy remain. To verify the potential effect of including further corrections, the two lowest triple excitations have been suppressed in the azure curve, which is still incorrect but with an important reduction of χ and an important increase of T_{max} to 0.39 K. This suggests that in order to apply the REM method to collective effects that are very sensitive to a correct description of the spectrum in a range of energies of at least twice the value of J, efforts have to be done to better describe multiexcited processes.

UNIVERSITAT ROVIRA I VIRGILI
THE CALCULATION OF THE THERMAL DEPENDENCY OF THE MAGNETIC SUSCEPTIBILITY
IN EXTENDED SYSTEMS WITH AB INITIO ELECTRONIC STRUCTURE PARAMETERS
Igor Negodaev
ISBN:978-84-694-2171-0/DL:T. 1432-2011

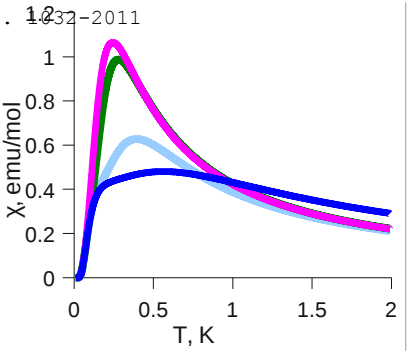

Figure 2.11. χ(T) curves given by the 3-block REM system compared with the exact 12 sites Heisenberg model. J = -1K. Blue: 12-sites linear Heisenberg model. Pink: additive single excitations model. Green: model including low double excitations. Azure: model without first two triple excitations.

ISBN:978-84-694-2032-2011

2.7 References

1 Roos, B.; Taylor, P.; Siegbahn, P.Chem. Phys. 1980, 48, 157.

2 Siegbahn, P.; Heiberg, A.; Roos, B.; Levy, B. Phys. Scr. 1980, 21, 323.

3 Tokmachev, A.; Boggio-Pasqua, M.; Mendive-Tapia, D.; Bearpark, M.; Robb, M. A. J. Chem. Phys. 2010, 132, 044306.

4 Shahi, A. R. M.; Cramer, C. J.; Gagliardi, L. Phys. Chem. Chem. Phys. 2009, 11, 10964.

5 Cauët, E.; Liévin, J. J. Phys. Chem. A 2009, 113 (36), 9881.

6 Malmqvist, P.-Å.; Pierloot, K.; Shahi, A. R. M.; Cramer, C. J.; Gagliardi, L. J. Chem. Phys. 2008, 128, 204109.

7 Bearpark, M.; Ogliaro, F.; Vreven, T.; Boggio-Pasqua, M.; Frisch, M.;, Larkin, S. M.; Morrison, M.; Robb, M. A. J. Photochem. Photobiol. A, 2007, 190, 207.

8 Malmqvist, P.-Å.; Rendell, A.; Roos, B. O. J. Phys. Chem. 1990, 94, 5477.

9 Malmqvist, P.-Å.; Roos, B. O. Chem. Phys. Lett. 1989, 155, 189.

10 Malmqvist, P.-Å.; Roos, B. O.; Schimmelpfennig, B. Chem. Phys. Lett. 2002, 357, 230.

11 Andersson, K.; Malmqvist, P.-Å.; Roos, B. O.; Sadlej, A. J.; Wolinski, K. J. Phys. Chem. 1990, 94, 5483.

12 Andersson, K.; Malmqvist, P.-Å.; Roos, B. O. J. Chem. Phys. 1992, 96, 1218.

13 Azizi, Z.; Roos, B. O.; Veryazov, V. Phys. Chem. Chem. Phys. 2006, 8, 2727.

14 Roos, B. O.; Anderson, R. Chem. Phys. Lett. 1995, 245, 215.

15 Finley, J.; Malmqvist, P.-Å.; Roos, B. O.; Serrano-Andrés, L. Chem. Phys. Lett. 1998, 288, 299.

16 Miralles, J.; Daudey, J.-P.; Caballol, R. Chem. Phys. Lett. 1992, 198, 555.

17 Miralles, J.; Castell, O.; Caballol, R.; Malrieu, J.-P. Chem. Phys. 1993, 172, 33.

18 Cabrero, J.; Ben Amor, N.; de Graaf, C.; Illas, F.; Caballol, R. J. Phys. Chem. A 2000, 104, 9983.

19 Cabrero, J.; de Graaf, C.; Bordas, E.; Caballol, R.; Malrieu, J.-P. Eur. J. Chem. 2003, 9, 2307.

ISBN:978-84-694-2171-0/DL:T. 1032-2011

20 de Graaf, C.; Sousa, C.; Moreira, I. de P.R.; Illas, F. J. Phys. Chem. A 2001, 105, 11371.

21 Bordas, E.; de Graaf, C.; Caballol, R.; Calzado, C. J. Phys. Rev. B 2005, 71, 045108.

22 Cabrero, J. in PhD thesis "Análisis de las contribuciones físicas al acoplamiento magnético en sistemas binucleares de CU (II)", ISBN 688 1094-0.

23 García, V. M.; Caballol, R.; Malrieu, J.-P.; J. Chem. Phys. 1998, 109, 504.

24 Langhoff, S. R.; Davidson, E. R. Int. J. Quant. Chem. 1974, 8, 61.

25 Calzado, C. J.; Malrieu, J.-P. Eur. Phys. J. 2001, 21, 375.

26 Calzado, C. J.; Malrieu, J.-P. Phys. Rev. B 2001, 63, 214520.

27 Gellé, A.; Munzarová, M. L.; Lepetit, M. B.; Illas, F. Phys. Rev. B 2003, 68, 125103.

28 Bordas, E.; Caballol, R.; de Graaf, C.; Malrieu, J.-P. Chem. Phys. 2005, 309 2-3, 259.

29 Bordas, E. in PhD thesis "Determinación ab initio de parámetros de estructura electrónica en óxidos de metales de transición".

30 Noodleman, L.; Davidson, E. R. Chem. Phys. 1986, 109, 131.

31 Illas, F.; de P. R. Moreira, I.; de Graaf, C.; Barone. V. Theor. Chem. Accounts 2000, 104, 265.

32 de P. R. Moreira, I.; Illas, F. Phys. Chem. Chem. Phys., 2006, 8, 1645.

33 Zener, C. Phys. Rev. 1951, 82, 403.

34 Borrás-Almenar, J. J.; Clemente-Juan, J. M.; Coronado, E.; Palii A.; Tsukerblat, B. S. in Magnetism: Molecules to Materials; WILEY-VCH (Weinheim, 2001).

35 Hozoi, L.; Nishimoto, de Graaf, C. Phys. Rev. B 2007, 75, 174505.

36 Bloch, C.; Horowitz, J. Nucl. Phys. 1958, 8, 91.

37 Malrieu, J.-P.; Guihéry, N. Phys. Rev. B, 2001, 63, 085110.

38 Calzado, C.; Cabrero, J.; Malrieu, J.-P.; Caballol, R. J. Chem. Phys. 2002, 116, 3985.

39 des Cloizeaux, J. Phys. Rev. 1963. 129, 554.

ISBN:978-84-694-2171-0/DL:T- 1032-2011

40 Bastardis, R.; Guihéry, N.; Suaud, N.; de Graaf C. J Chem Phys. 2006, 125 (19), 194708.

41 Maurice, R.; Guihéry, N.; Bastardis, R.; de Graaf, C. J. Chem. Theory Comput. 2010, 6, 55.

42 van Vleck, J. H. in The Theory of Electric and Magnetic Susceptibilities; Oxford University Press, (Oxford, 1932).

43 Deumal, M.; Bearpark, M. J.; Novoa, J. J.; Robb, M. A. J. Phys. Chem. A 2002, 106, 1299.

44 Jornet, J.; Deumal, M.; Ribas-Ariño, J.; Bearpark, M. J.; Robb, M. A.; Hicks, R. G.; Novoa, J. J. Chem. Eur. J. 2006, 12, 3995.

45 Jornet-Somoza, J.; Deumal, M.; Robb, M. A.; Landee, C. P.; Turnbull, M. M.; Feyerherm, R.; Novoa, J. J. Inorg. Chem. 2010, 49, 1750.

46 Al Hajj, M.; Guihéry, N.; Malrieu, J.-P.; Bocquillon, B. Eur. Phys. J. B 2004, 41, 11.

47 Al Hajj, M.; Malrieu, J.-P.; Guihéry, N. Phys. Rev. B 2005, 72, 224412.

48 Boullant, E.; Cano, J.; Journaux, Y.; Decurtins, S.; Gross, M.; Pilkington, M. Inorg. Chem. 2001, 40, 3900.

49 de Graaf, C.; de P. R. Moreira, I.; Illas, F.; Iglesias, Ò.; Labarta, A. Phys. Rev. B 2002, 66, 014448.

50 Hozoi, L. in PhD thesis “Localized states in transition metal oxides”, ISSN 1570.

51 Fisher, A. J. Rev. Solid State Sci. 1991, 5, 107.

52 Inglesfield, J. E. J. Phys. C: Solid State Phys. 1981, 14, 3795.

53 Baraff, G. A.; Schlüter, M. J. Phys. C: Solid State Phys. 1986, 19, 4383.

54 Fisher, A. J. J. Phys. C: Solid State Phys. 1988, 21, 3229.

55 Winter, N. W.; Pitzer, R. M.; Temple, D. K. J. Chem. Phys. 1987, 86, 3549.

56 Kahn, O. Molecular Magnetism; VCH Publishers, (New York, 1993).

57 Griffiths, R. B. Phys. Rev. 1964, 133, A768.

58 Eggert, S.; Affleck, I.; Takahashi, M. Phys. Rev. Lett. 1994, 73, 332.

59 Wilson, K. G. Rev. Mod. Phys. 1975, 47, 773.

60 Morningstar, C. J.; Weinstein, M. Phys. Rev. D 1996, 54, 4131.

61 Malrieu, J.-P.; Guihéry, N. Phys. Rev. B 2001, 63, 085110.

UNIVERSITAT ROVIRA I VIRGILI
THE CALCULATION OF THE THERMAL DEPENDENCY OF THE MAGNETIC SUSCEPTIBILITY
IN EXTENDED SYSTEMS WITH AB INITIO ELECTRONIC STRUCTURE PARAMETERS
Igor Negodaev
ISBN:978-84-694-2171-0/DL:T. 1032-2011

UNIVERSITAT ROVIRA I VIRGILI
THE CALCULATION OF THE THERMAL DEPENDENCY OF THE MAGNETIC SUSCEPTIBILITY
IN EXTENDED SYSTEMS WITH AB INITIO ELECTRONIC STRUCTURE PARAMETERS
Igor Negodaev
ISBN:978-84-694-2171-0/DL:T. 1032-2011

Chapter 3

Dinuclear systems

UNIVERSITAT ROVIRA I VIRGILI
THE CALCULATION OF THE THERMAL DEPENDENCY OF THE MAGNETIC SUSCEPTIBILITY
IN EXTENDED SYSTEMS WITH AB INITIO ELECTRONIC STRUCTURE PARAMETERS
Igor Negodaev
ISBN:978-84-694-2171-0/DL:T. 1032-2011

The theoretical modeling of the magnetic coupling in small complexes with two transition metal centres has a long-standing history and is well-established. In this chapter, we use these small systems as models to establish the validity of the computational schemes described in the previous chapter.

3.1 Manganese dimer

Although dinuclear systems can be considered as good starting points for studying the properties of larger clusters, in many cases both experiments and theoretical studies lead to disperse results. The manganese dimer can be considered to belong to this category. The adequacy of both theoretical models (*e.g.* Heisenberg Hamiltonian) can be proved on this structure as well as computational techniques (DDCI, CASPT2 *etc.*) without excessive expenses of CPU facilities. Dealing with simple dimers one can feel flexible to modify and adjust a methodology which is planned to be applied on the more complicated extended systems. The validity of the Heisenberg model discussed in chapter 2 is studied on the Mn dimer before starting with the more complicated extended systems.

3.1.1 A brief review

Much experimental work has been published on this molecule and, although there is experimental agreement in the weak nature of the bonding, different dissociation energies ranging up to 0.8 eV with large error bars and interatomic distances from 3.2 to 3.8 Å have been reported, depending on the

ISBN:978-84-694-2171-0/DL:T. 1032-2011

experimental technique used. By using both mass spectrometry and resonance Raman data, a more narrow range of dissociation energies, from 0.02 to 0.15 eV, has been determined by a variety of methods.[1] The electronic structure of Mn_2 has been analysed in rare-gas matrix isolation experiments, by using resonance Raman and ultraviolet–visible spectroscopy[2,3] as well as with electron spin resonance (ESR)[4,5] and an equilibrium distance of 3.4 Å has been estimated.[4] The experiments indicate a singlet ground state and weak antiferromagnetic coupling. From ESR,[4] Raman spectroscopy[3] and magnetic circular dichroism experiments[6] coincident estimates for the exchange coupling constant have been given, J = [-8, -11] cm^{-1}, depending on the experimental technique and on the rare-gas used in the matrix.

While most transition metal atoms belonging to the fourth row of the Periodic Table (the 3d elements) form stable dimers with dissociation energies higher than 1 eV and with rather short equilibrium distances, the atoms Mn and Zn stand out as an exception, giving rise to very weakly bound dimers. Whereas the closed shell electronic structure of Zn provides an immediate explanation for its inability to form a strong chemical bond, the situation is less evident for Mn. The ground state of the manganese atom is classified as ^6S with an electronic structure described by the configuration $[Ar]3d^54s^2$. The energy required to promote an electron from 4s to 3d, giving rise to a ^6D state ($3d^64s^1$), is known to be unusually high (2.14 eV).[7] Bringing together two Mn atoms gives rise to a strong repulsion due to the overlapping filled 4s orbitals before bond formation can arise in the half-filled 3d orbitals. Hence a weak interaction is expected and the lowest part of the spectrum can be associated to the different spin couplings between the singly occupied d orbitals of each atom. This leads to six molecular states giving the ground

ISBN:978-84-694-2171-0/DL:T. 1032-2011

state dissociation limit: $Mn_2 \longrightarrow 2Mn(^6S)$: $^{11}\Sigma_u^+$, $^9\Sigma_g^+$, $^7\Sigma_u^+$, $^5\Sigma_g^+$, $^3\Sigma_u^+$ and $^1\Sigma_g^+$.

In a pioneering paper, Nesbet[8] performed approximate Hartree-Fock calculations followed by perturbative estimations of the energy of the different multiplets giving ^6S ground state Mn atoms at dissociation. He predicted a multiconfigurational $^1\Sigma_g^+$ ground state, with a rather short equilibrium distance, 2.88 Å, a binding energy of 0.79 eV and an exchange coupling constant of -4cm^{-1} at R_e, rapidly decreasing with the distance.

After this work, many other calculations on Mn_2 have been reported, either using density functional theory (DFT) or wave-function based methods. A variety of functionals have been used but most of the DFT results[9,10,11,12,13] give an incorrect ground state multiplicity, conclude unbound character or lead to very different equilibrium distances, although a recent study[14] with hybrid DFT using a large percentage of Hartree-Fock exchange achieves concluding a singlet ground state. The origin of the discrepancies lie in part in the difficulty of DFT methods to describe Van der Waals interactions but also in the necessary use of broken symmetry approach to describe a system with a high number of unpaired electrons where the singlet state has a strong multiconfigurational character.

In the multiconfigurational (MR) wave-function methods framework, complete active space self consistent field (CASSCF) calculations were performed by Bauschlicher[15] on both the $^1\Sigma_g^+$ and the $^{11}\Sigma_u^+$ states. The $^1\Sigma_g^+$ potential energy curve was found repulsive at this level of theory since an extensive inclusion of electron correlation is needed to describe Van der Waals interactions. This state was however lower in energy than $^{11}\Sigma_u^+$ and antiferromagnetic coupling was concluded.

ISBN:978-84-694-2171-0/DL:T. 1032-2011

More recently, Wang and Chen[16] undertook CASPT2 calculations on the Σ states and found a minimum in all the potential energy curves, a singlet ground state with an equilibrium distance of 3.64 Å and a binding energy of 0.12 eV, in good agreement with experiment, although the basis set superposition error was not considered. As a relevant result, they observed strong deviations from the Landé interval rule, which gives the separation between two spin states of total spin S and S-1 as a multiple of the coupling J, as shown in equation 2.27. Wang and Chen found exchange coupling constants ranging from -17.5 to -4.5 cm^{-1}, depending on the pair of states used in the calculation. They attributed these deviations to the Heisenberg Hamiltonian expected value, to biquadratic spin-spin interactions.

Yamamoto et al.[17] investigated several states of Mn_2 with CASSCF calculations followed by quasi-degenerate perturbation theory up to second-order (MCQDPT2). They have provided a complete characterization of the potential energy for the ground state ($^1\Sigma_g^+$) and for two high spin states ($^{11}\Sigma_u^+$ and $^{11}\Pi_u$) and concluded that the ground state is the $^1\Sigma_g^+$ state and found an equilibrium distance, a binding energy and a vibrational constant in agreement with experiment.

Just after our results were published,[18] the ground state and a few excited states of the manganese dimer have been studied making use of a good basis set and of accurate CASSCF + NEVPT2 (NEVPT3 in one case) techniques in the paper of Angeli et al.[19], and a fairly good accordance with our results was noted. The study has been confined to some singlets and to some undecuplet states which were indicated as candidates for the ground state in previous DFT studies. The ground state has been predicted to be the $^1\Sigma_g^+$ singlet, dissociating to the ^6S + ^6S atomic limit, *viz.* the ground states of the separated atoms. Mn_2 is also shown to be a Van der Waals molecule with rather large an

equilibrium distance (3.7–3.8 Å), low dissociation energy (≈ 0.07 eV) and low harmonic frequency (41–43 cm^{-1}). The agreement with the experimental estimates in that research can be considered as fairly satisfactory, since the latter have been obtained in rare gas matrices where deviations from the isolated molecules are liable to occur. At short distances, where the conditions for the formation of a bond between a ^{6}D and a ^{6}S Mn atom are favourable, the calculations reveal the presence of an avoided crossing with the first $^1\Sigma_g^+$ excited state dissociating to the ^{6}S + ^{6}D atomic limit. At the equilibrium distance of the ground state, single point calculations carried out for all the other $^{2S+1}\Sigma_p^+$ states dissociating to the ^{6}S + ^{6}S asymptote (with S ranging from 1 to 5 and with the parity p being g (u) for even (odd) S) show that all such states lie in a tiny energy interval and can be fairly well described by diagonalization of an effective Heisenberg Hamiltonian. Among the excited states dissociating to ^{6}S + ^{6}D examined in that work, $^{11}\Pi_u$, which most DFT studies indicate as the ground state, stands out as the state with the shortest equilibrium distance (2.50 Å) and the lowest adiabatic excitation energy (0.45 eV).

From the previous results, it emerges that multireference calculations have proved to be necessary to give the correct $^1\Sigma_g^+$ ground state and to predict Van der Waals interactions as responsible of the weakly bound character of the molecule with rather flat potential energy curves for the Σ states. Whereas the correct order of magnitude of the magnetic coupling constant is found at the CASPT2 level, surprisingly strong deviations of the Heisenberg behaviour were reported. In a recent work[20] the same type of deviations in oxalato-bridged binuclear complexes when using CASPT2 has been discussed. The comparison with variational procedures has shown that this result is not related to

physical effects but to limitations of the CASPT2 method leading to an artificial stabilization of the higher states. We analyse here the magnetic coupling of Mn_2 by using CASPT2 and CI methods to elucidate this aspect to get more insight in the electronic structure of this molecule.

3.1.2 Computational details

Potential energy curves of the six Σ states of the molecule resulting from the spin coupling of Mn (^{6}S) ground state, $^{11}\Sigma_u^+$, $^9\Sigma_g^+$, $^7\Sigma_u^+$, $^5\Sigma_g^+$, $^3\Sigma_u^+$ and $^1\Sigma_g^+$ have been obtained, using CASPT2 method[21,22] and ANO-RCC 6s5p4d3f2g1h basis set. Starting with a CASSCF[23] zeroth-order wave-function, the second-order energy correction was determined using the original definition of H_0 Hamiltonian. The definition of the zeroth-order CASPT2 Hamiltonian has been modified a few years ago with the introduction of the IPEA shift.[24] This modification repairs the systematic error in the dissociation energies using the original zeroth-order Hamiltonian. The modification has in principle no effect on the magnetic coupling parameter but was shown to introduce extra numerical noise in comparison to the old Hamiltonian.[19] The active space included the five 3d orbitals of each manganese centre and 10 electrons, giving a CAS (10, 10). Some CAS (14, 12) calculations including also the 4s orbitals were carried out to confirm that their role was not relevant in the electron correlation. The level-shift technique was used to remove some zeroth-order energy degeneracies.

As a second step, DDCI[25,26] calculations have been performed. The DDCI1 and DDCI2 variants (see chapter 2) were applied to this material. Due to the nature of the method, a unique set of molecular orbitals is used to perform DDCI calculation of

the different states. This unique set can be obtained from standard CAS average procedures or, when different spatial or spin symmetries are implied, through the Natural Orbitals of an average of the density matrices of the different states. DDCI therefore is adapted to evaluate vertical energy transitions but the differential effect of the neglected external double excitations has to be included to calculate adiabatic transitions or construct potential energy surfaces. There are several ways to solve this problem. The first one is to estimate by perturbation techniques the contribution of the external double excitations and to add it to the variational calculation.[27] An alternative way can be applied if the potential energy surface (or the surface portion of interest) of a given state A is known with high accuracy. The potential energy surfaces of other states B can be obtained by adding the DDCI vertical energy differences between A and B to the known surface of state A

$$E_B(\vec{r}) = E_A(\vec{r}) + \Delta E^{DDCI}_{B-A}(\vec{r}) \qquad 3.1$$

This procedure was successfully applied to the calculation of the lowest transitions in alkali diatomics[27] and to some reactivity problems[28] and is also used in the present study. Several strategies exist to obtain the reference energy surface. One possibility is to add the second-order perturbation estimates of the electron correlation contributions not included in DDCI, namely the inactive to virtual orbitals double excitations. These extra correlation terms include the dispersion interactions, which are responsible of the bond in Mn_2. However it is difficult to accurately estimate the dispersion contribution and localized orbitals are usually needed. Since the highest multiplet of Mn_2, $^{11}\Sigma_u^+$, can be correctly described through a single reference method, the CCSD(T) approach seems to be in the present case the best choice to obtain its potential energy curve with high precision and correct dissociation limit. The potential energy

curves of the remaining states are constructed by adding the corresponding DDCI energy difference. As an example, the $^9\Sigma_g^+$ energy curve is obtained by applying

$$^9E(\vec{r}) = {}^{11}E^{CCSD(T)}(\vec{r}) + \Delta E_{9-11}^{DDCI}(\vec{r}) \qquad 3.2$$

at different internuclear distances.

Potential energy curves and dissociation energies are subjected to the well known basis set superposition error (BSSE), although it is difficult to evaluate the exact size of it. In order to give an estimation, the counterpoise method[29] has been used to correct the shape of the curves as well as the spectroscopic constants. All calculations were performed with the MOLCAS 7.0 package[30], except the DDCI calculations which were performed with the CASDI program.[31]

3.1.3 Results and discussion

The potential energy curves of the six Σ states of Mn_2 were calculated at the CASPT2 level. Equilibrium distances, R_e, and dissociation energies, D_e, for the different states are reported in Table 3.1.

The $^1\Sigma_g^+$ state is the ground state, in agreement with the antiferromagnetic character found experimentally. The equilibrium distance for the ground state, 3.19 Å, is slightly shorter than the experimental value,[4] 3.4 Å, and the dissociation energy, is somewhat overestimated: 0.28 eV with respect to the reported values around 0.15 eV.[1] All these data suggest that the basis set superposition error, BSSE, can be relevant in our calculation, leading to an overestimation of the Mn–Mn interaction.

Table 3.1. CASPT2 equilibrium distance R_e (Å), and *dissociation energy D_e (eV) for the different spin couplings in Mn_2.*

State	CASPT2		CASPT2 + BSSE		CASPT2[16]		NEVPT2[19]	
	R_e	D_e	R_e	D_e	R_e	D_e	R_e	D_e
$^{11}\Sigma_u^+$	3.34	0.24	3.55	0.12	3.79	0.10	3.68	0.08
$^{9}\Sigma_g^+$	3.30	0.25	3.51	0.12				
$^{7}\Sigma_u^+$	3.26	0.26	3.46	0.13				
$^{5}\Sigma_g^+$	3.23	0.27	3.43	0.13				
$^{3}\Sigma_u^+$	3.21	0.27	3.41	0.14				
$^{1}\Sigma_g^+$	3.19	0.28	3.40	0.14	3.64	0.12	3.70	0.08

By using the counterpoise method, BSSE corrected CASPT2 potential energy curves have been obtained as plotted in Figure 3.1. Although this procedure gives an upper limit of this error, Table 3.1 shows that correcting the CASPT2 curves gives an equilibrium distance of 3.40 Å and a good dissociation energy estimate, 0.14 eV. Figure 3.1 and Table 3.1 also show that the equilibrium distance becomes longer for higher multiplicities, in agreement with experiment[5] and previous theoretical works.[16,17]

The magnetic coupling parameter J has been also calculated from the vertical energy differences at the equilibrium distance, and equation 2.27 using both the CASPT2 and the BSSE corrected CASPT2 potential energy curves. The values reported in Table 3.2 show very strong Heisenberg deviations, in coincidence with previous CASPT2 calculations.[16]

ISBN:978-84-694-2171-0/DL:T. 1032-2011

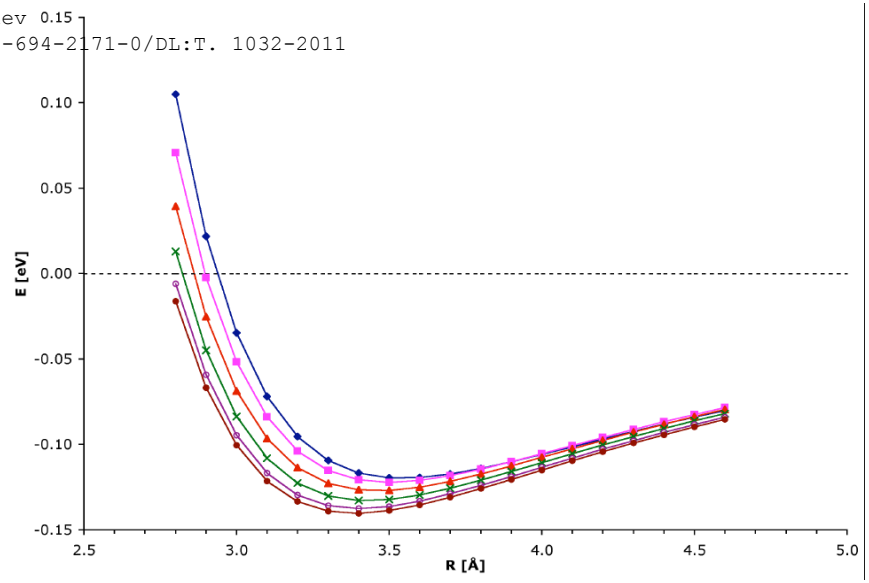

Figure 3.1. BSSE corrected CASPT2 potential energy surface for the different spin couplings of Mn_2. $^{11}\Sigma_u^+$ *diamonds,* $^{9}\Sigma_g^+$ *squares,* $^{7}\Sigma_u^+$ *triangles,* $^{5}\Sigma_g^+$ *crosses,* $^{3}\Sigma_u^+$ *open circles,* $^{1}\Sigma_g^+$ *filled circles .*

A previous study of oxalato-bridged binuclear complexes[20] has revealed that this type of deviations is not unusual in perturbative treatments, the coupling parameter calculated from the lowest two states being more negative, due to an artificial stabilization of the higher states induced by the second-order treatment. The largest deviations from the Heisenberg behaviour are also observed in this class of excitations.

Table 3.2. CASPT2 magnetic coupling parameters at the singlet experimental distance without BSSE correction (R_e = 3.2 Å) and with BSSE correction (R_e = 3.4 Å)

	J (cm^{-1})	J (cm^{-1}) with BSSE
$^9\Sigma_g^+ \rightarrow {}^{11}\Sigma_u^+$	-13.5	-6.5
$^7\Sigma_u^+ \rightarrow {}^9\Sigma_g^+$	-19.5	-11.9
$^5\Sigma_g^+ \rightarrow {}^7\Sigma_u^+$	-24.5	-16.5
$^3\Sigma_u^+ \rightarrow {}^5\Sigma_g^+$	-27.9	-19.5
$^1\Sigma_g^+ \rightarrow {}^3\Sigma_u^+$	-30.8	-22.2

To establish whether the deviations in Table 3.2 can be attributed to biquadratic spin–spin interactions or originate from numerical errors due to the very small energy differences, several levels of DDCI calculations have been performed at a series of interatomic distances. The calculations were performed by using a set of molecular orbitals obtained from the averaged density matrix over the six states at the CASSCF level. Table 3.3 reports the values of J calculated from $^{11}\Sigma_u^+$, $^9\Sigma_g^+$, $^7\Sigma_u^+$ and $^5\Sigma_g^+$ energies found at DDCI1 and DDCI2 levels on top of CAS (10,10), at four internuclear distances. As shown previously,[32] DDCI1 accounts for polarization effects, in particular polarization effects on the charge transfer configurations included in the CAS leading to ionic configurations, such as Mn^+-Mn^-, in the equivalent valence bond description.

Table 3.3. Magnetic coupling parameters (in cm^{-1}) at four internuclear distances for DDCI1, DDCI2 and DDCI2 + Davidson correction.

	DDCI1			DDCI2		DDCI2 + Davidson
R (Å)	$^9\Sigma_g^+ \rightarrow {}^{11}\Sigma_u^+$	$^7\Sigma_u^+ \rightarrow {}^9\Sigma_g^+$	$^5\Sigma_g^+ \rightarrow {}^7\Sigma_u^+$	$^9\Sigma_g^+ \rightarrow {}^{11}\Sigma_u^+$	$^7\Sigma_u^+ \rightarrow {}^9\Sigma_g^+$	$^9\Sigma_g^+ \rightarrow {}^{11}\Sigma_u^+$
3.2	-10.5	-10.5	-10.5	-8.5	-8.5	-12.4
3.4	-5.6	-5.6	-5.6	-4.2	-4.2	-6.9
3.7	-2.5	-2.5	-2.5	-1.5	-1.5	-3.2
4.0	-1.2	-1.2	-1.2	-0.6	-0.6	-1.6

DDCI2 accounts for all the second-order differential contributions in the Anderson model[33] of magnetic coupling. In the absence of a bridging ligand, this approximation is well suited for the evaluation of the magnetic coupling since all the additional second-order effects added in DDCI[32] account for an active role of the ligand in the superexchange phenomenon, which are, of course, absent in Mn_2. The results show that the variational inclusion of electron correlation effects does not break the strict Heisenberg spectrum along the potential energy curves. The expected Landé pattern in the energy spacing of the Σ states is maintained at all distances. It may be therefore concluded that the deviations found at the CASPT2 level are not attributable to physical factors, as biquadratic interactions, but have a numerical origin. This result is in agreement with the conclusions of ESR experiments in rare-gas matrices that indicate that small differences in the magnetic coupling parameter are within the experimental error.[4] Hence, the calculation of such small energy differences are at (or beyond) the limit of the applicability of perturbation theory as discussed previously.[20]

ISBN:978-84-694-2171-0/DL:T. 1032-2011

As observed for CASPT2 before, the value of the coupling depends on the Mn–Mn distance. At the experimental equilibrium distance, 3.4 Å, the magnetic coupling parameter is found -5.6 cm^{-1} at DDCI1 and -4.2 cm^{-1} at DDCI2 level. Given that the experimental value derived from ESR in rare-gas matrices[4] is -9 ± 3 cm^{-1}, the deviation from the experiment is small in both cases. It is, however, somewhat unexpected that DDCI2 predicts a smaller (less antiferromagnetic) coupling constant than DDCI1. The analysis of the magnetic coupling[27] shows that DDCI2 includes some additional antiferromagnetic effects at the second-order and therefore larger coupling is expected than in DDCI1. A common source of error in all truncated CI treatments is the lack of size-consistency. The fact that DDCI only includes differential effects of electron correlation and excludes the largest part of it (namely that brought by external double excitations, the vast majority of all possible double excitations), ensures that the size-consistency error is relatively small in this family of multireference CI methods. Nevertheless, dealing with small energy differences and a large number of unpaired electrons, we investigated the effect of the size-inconsistency by correcting the energies with the Davidson's correction.[34] According to equation 2.12, the corrected DDCI2 energy can be written as

$$E_{Dav.}^{DDCI2} = E_0 + \frac{E_{corr}^{DDCI2}}{C_0^2} \qquad 3.3$$

where E_0 is the energy of the reference wave-function, E_{corr}^{DDCI2} is the DDCI2 correlation energy and $C_0^2 = \langle \Phi_0 | \Phi_{DDCI2} \rangle^2$ is the norm of the reference function in the DDCI2 wave-function. The last column in Table 3.3 shows the effect of Davidson's correction on J and indicates that even if small, the size-consistency error seems to be at the origin of the trend shown by DDCI1 and DDCI2 results. The corrected value observed at the experimental

ISBN:978-84-694-2171-0/DL:T. 1032-2011

equilibrium distance, -6.9 cm^{-1}, is now within the experimental range.

As mentioned before, to obtain the potential energy curves at the DDCI (DDCI1, DDCI2) level, a previous accurate calculation of the absolute energy of one state is necessary. The $^{11}\Sigma_u^+$ state is well described at zeroth-order by a single configuration and therefore CCSD(T) calculations on this state have been taken as the energy reference. The CCSD(T) method ensures both the inclusion of dispersion contributions and a correct dissociation. The calculated $^{11}\Sigma_u^+$ equilibrium distance is 3.60 Å and the dissociation energy 0.13 eV. After BSSE correction, these values are R_e ($^{11}\Sigma_u^+$) = 3.99 Å and D_e = 0.04 eV. The effect of the correction on the dissociation energy is of the same order as at CASPT2 level, giving an extremely flat potential energy curve. The lengthening of the equilibrium distance is considerable, due to the same reason. It has been already written that the counterpoise procedure gives a BSSE overestimation and the correct parameters are expected to be found in an intermediate value within the range of both limits, without and with the BSSE correction. When compared to experimental values, the BSSE corrected equilibrium distance is too long ($R_{e,exp}$ = 3.4 Å)[2,3] and the dissociation energy probably too low although different values have been reported depending on origin of the experimental data and of the molecular parameters used in the evaluation: $D_{e,exp}$ = 0.02 eV,[1] 0.1 eV[35] or 0.15 eV.[1] Most of the reported values of R_e and D_e do not correspond to gas phase but to matrix isolation experiments. The influence of interactions with the matrix, although expected to have little influence, cannot be completely excluded in the tiny Van der Waals manganese dimer molecular parameters. The DDCI2 method was after used to obtain the $^9\Sigma_g^+$ and the $^7\Sigma_u^+$ states potential curves, by adding for each

Mn-Mn distance the $^{9}\Sigma_g^+$ - $^{11}\Sigma_u^+$ (or $^{7}\Sigma_u^+$ - $^{11}\Sigma_u^+$) energy difference to the $^{11}\Sigma_u^+$ CCSD(T) curve. Since it has been shown that Landé interval rule is hold, the singlet $^{1}\Sigma_g^+$ curve is also calculated. When DDCI2+Davidson correction is used, the equilibrium distance of the ground state $^{1}\Sigma_g^+$ is found shorter than the highest multiplet one by 0.1 Å, R_e = 3.5 Å, slightly longer than previous results and than experiment. The dissociation energy is D_e = 0.14 eV, in agreement with experimental results. The coupling constant at this distance, as shown in Table 3.3, is -5.3 cm^{-1} in good agreement with the experimental value, -9 ± 3 cm^{-1}.

3.1.4 Conclusion

Although the CASPT2 results for the equilibrium distance and the dissociation energy are in good agreement with experimental data, the results on the magnetic coupling in manganese dimer show that CASPT2 calculations lead to very large deviations in the values of the coupling parameter J depending on the states used in its calculation. The Heisenberg model is shown to be adequate to study the magnetic coupling of the Mn_2 dimer system. Variational schemes as DDCI perfectly fit the expected Heisenberg spectrum showing that the quantitative study of weakly coupled magnetic systems is at (or beyond) the limit of applicability of this perturbative approach. As shown previously,[20] perturbation treatments using a bielectronic zeroth-order Hamiltonian as NEVPT2[36,37] method can give a better description of the spectrum of the states of different multiplicity. The DDCI2 magnetic coupling parameter, J = -5.3 cm^{-1}, is in good agreement with experimental results.

ISBN:978-84-694-2171-0/DL:T. 1032-2011

3.2 Asymmetrically bridged Cu(II) dinuclear complexes

After the study of the magnetically coupled dinuclear Mn_2 system, our next step was to expand the obtained experience on systems where two TM atoms are coupled *via* a diamagnetic bridge. As mentioned in chapter 1, the Cu(II)-based systems can be considered as ideal for the theoretical research. From the other hand, taking into account that one of the goals of nowadays efforts of magnetochemistry is the development and synthesis of so-called molecule-based magnets as an alternative for the traditional magnetic systems, on this step we have concentrated on the Cu(II) isolated systems.

3.2.1 A brief review of carboxylato and alkoxo bridged Cu(II) dinuclear complexes

A really interesting class of such magnetic complexes is formed by the molecules in which the two Cu(II) ions are bridged by two different diamagnetic bridges. The combination of alkoxo- and carboxylato-groups as bridges can give rise to ferromagnetic, weakly antiferromagnetic or strongly antiferromagnetic behaviour.[38,39,40,41] Several structural factors have been suggested to determine the large interval of magnetic couplings in these compounds. Among these are the Cu–O–Cu angle; the dihedral angle formed by the two basal planes of the first coordination sphere of the Cu(II) ions; the Cu-Cu distance; and the influence of the R-group of the alkoxo bridge, either through covalency effects or the out-of-plane angle.

ISBN:978-84-694-2171-0/DL:T. 1032-2011

Recently, an interesting series of compounds has been synthesized by Lukov and co-workers in which different substituents on the carboxylato bridge were compared.[42,43] It was found that the magnetic coupling changes significantly when the OOC–CH_3 group is replaced by OOC–CH_2Cl, OOC–CCl_3 and OOC–CF_3. However, the observed tendency is contrary to what is expected *a priori*. Instead of a reduction of the magnetic coupling when the methyl group is replaced by a stronger electron withdrawal group, a slightly stronger antiferromagnetic coupling was observed in the complex with the OOC–CF3 group. On the other hand, the replacement of hydrogen atoms with Cl atoms leads to a reduction of the coupling. An overview of the experimental coupling constants are listed in Table 3.4. Thus, it seems to be interesting to analyse not only the magnetic coupling between two Cu atoms, but also the relations of coupling and substitutions in the carboxylato group, some magneto-structural correlations, and the relative importance of the two exchange paths at a high level of theoretical calculations.

Table 3.4. Experimental coupling constant for dinuclear Cu(II) complexes with asymmetric bridges (alkoxo- and carboxylato).

R	J (cm^{-1})
CH_3	-174
CH_2Cl	-134
CCl_3	-116
CF_3	-188

ISBN:978-84-694-2171-0/DL:T. 1032-2011

3.2.2 Computational details

Four different approximations to the exact N-electron wave-function were used to determine the singlet and triplet energies of the molecules considered. In the first place, a zeroth-order wave-function is constructed using the complete active space self-consistent field (CASSCF) approach.[23] Here, the active space contains the two magnetic orbitals (mainly Cu-3d_{xy}-like) and the two unpaired electrons, *i.e.* CAS (2, 2) was used. Using the CASSCF wave-function as zeroth-order description, CASPT2[21,22] method has been applied for series of brief calculations, where the tendencies of J due to geometry changes are more important than the accuracy of J-values themselves. A more accurate approximation of the wave-function is provided by the DDCI method[25,26] which normally gives very accurate magnetic coupling constants,[44,45] albeit at a higher computational cost than CASPT2. As a compromise between accuracy and CPU-time, the CAS_{ext}+DDCI2 approximation[46,47] has been used to get the J-values with a reasonable CPU-costs. The used ANO basis sets are presented in Table 3.5.

Table 3.5. Specification of the contracted ANO basis functions used in the calculations.

Atom	Basis set
Cu	6*s* 5*p* 4*d* 1*f*
C, O, N, F	3*s* 2*p* 1*d*
Cl	4*s* 3*p* 1*d*
H	2*s* 1*p*
C (external)	3*s* 2*p*
H (external)	2*s*

ISBN:978-84-694-2171-0/DL:T. 1032-2011

3.2.3 Results and discussion

In the first place, we determine how the rather large complex reported in the literature can be modelled in order to maintain the computational demand within reasonable limits. Although the calculations in the full molecule are not infeasible, it is important to find a model that correctly represents the coupling of the real molecule, since the computational experiments that we will perform involve a significant number of calculations. Table 3.6 reports the calculated coupling parameters for the models shown in Figure 3.2.

Table 3.6. CASSCF and CASPT2 magnetic coupling parameter J (cm^{-1}) of models of increasing size of the complex with the acetate bridge.

Model	CASSCF	CASPT2
Small	-50	-202
Intermediate I	-29	-122
Intermediate II	-26	-102
Intermediate III	-27	-122
Large I	-22	-98
Large II	-21	-93
Complete	-18	-82

UNIVERSITAT ROVIRA I VIRGILI
THE CALCULATION OF THE THERMAL DEPENDENCY OF THE MAGNETIC SUSCEPTIBILITY
IN EXTENDED SYSTEMS WITH AB INITIO ELECTRONIC STRUCTURE PARAMETERS
Igor Negodaev
ISBN:978-84-694-2171-0/DL:T. 1032-2011

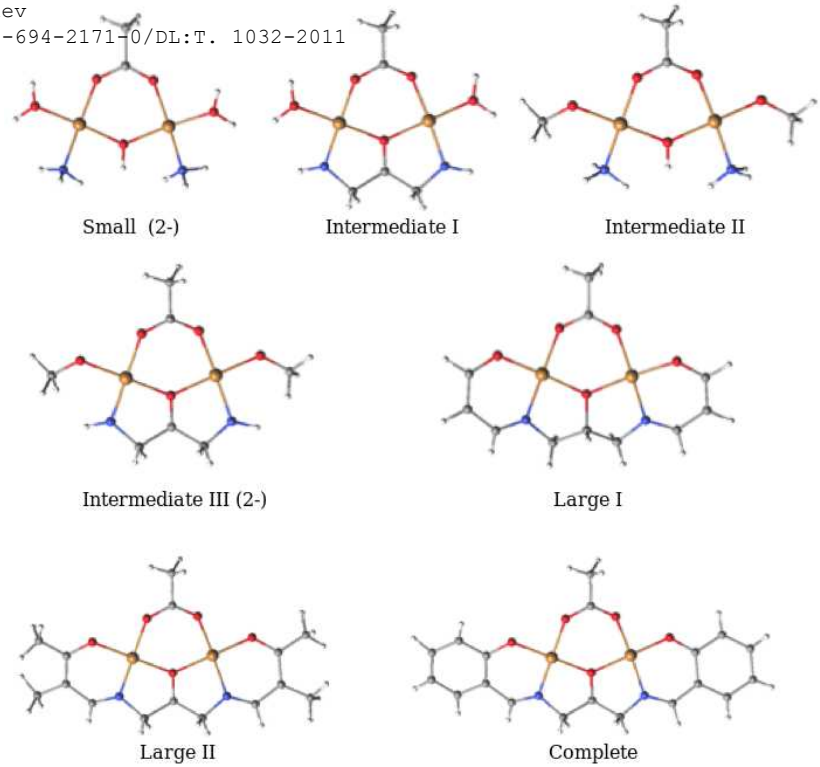

Figure 3.2. Graphical representation of the models of the acetate bridged complex used to determine the smallest yet relevant model. Orange is Cu; Red is O; Grey is C; Blue is N, and light grey is H.

It is obvious that the smallest representation of the complete structure is too approximate a model. The OH^- representation of the alkoxy group leads to an overestimate of the magnetic coupling as is also found in Intermediate II, although it cannot be excluded that the NH_3 group also influences J. Once the OH and NH_3 groups are replaced with a more correct representation in Intermediate I and III, the magnetic coupling stabilizes around 100 cm^{-1} at the CASPT2 level. A good candidate

ISBN:978-84-694-2171-0/DL:T. 1032-2011

to perform all the computational experiments seems to be the Intermediate III complex. It is still reasonably small in comparison to the real structure and the nearest atoms around the magnetic key-unit are all correctly represented. The comparison with experiment of the Large II and the Complete model show a rather large deviation. The final CASPT2 estimate is roughly 50% of the experimental value. This is a common phenomena for Cu(II) dinuclear complexes and can be (at least partially) repaired by improving the CASSCF wave-function that is used as reference function for the perturbative treatment of the electron correlation. However, for a complete accurate description of the coupling, we leave aside the perturbative description of the electron correlation and apply the CAS_{ext}/DDCI2 approach to show that experimental couplings can be reproduced with the here applied methodologies. However, it should be mentioned that these calculations are rather costly, and that all the relevant tendencies are already observed with CASPT2 on Intermediate III. Stretching the computational effort to the limit, we applied the CAS_{ext}/DDCI2 approach to the Large I and Large II models, the complete model becomes computationally too expensive. The extended CAS was constructed by adding two occupied ligand orbitals to the active space, one for the alkoxo bridge and the other localized on the carboxylato ligand. To maximize the effect of the ligand orbitals and in such a way ensure an optimal treatment of the ligand-to- metal charge transfer processes that play a key role in the magnetic coupling, we projected two model vectors in the doubly occupied orbital space as described in Ref. 47. The addition of the projected orbitals, shown in Figure 3.3, causes a moderate increase of the magnetic coupling. Only after treating the remaining electron correlation effects with DDCI2, we observe a large increase of the coupling and a nearly quantitative agreement with the experimental value. The CAS_{ext}/DDCI2 J-values are -198 cm^{-1} and -204 cm^{-1} for the Large I and Large II models,

respectively. As expected,[47,48,49,50] the antiferromagnetic contribution to the coupling is overestimated and we obtain couplings that are slightly too strong.

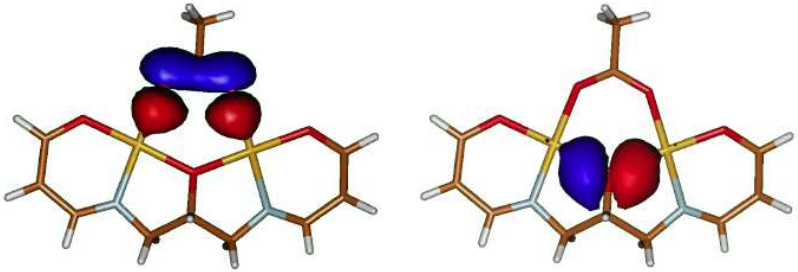

Figure 3.3. Projected ligand orbitals added to the CAS in the CAS_{ext}/DDCI2 calculations in the Large I model.

The substitutions on the methyl group of the acetato ligand not only induce a change in the electronegativity of the carboxylato bridge but also affect the overall crystal structure. The most obvious computational test to pinpoint the influence of the changes in the electronegativity on the magnetic coupling is to take Intermediate III (see Figure 3.2) and replace the CH_3 group by the other groups listed in Table 3.4 without applying any further geometry relaxation. As can be seen in Table 3.7, the influence of the substitutions in the carboxylato group are nearly negligible and cannot be at the origin of the variations in the magnetic coupling observed experimentally. A first straightforward explanation is that the substitutions are made on a position that is too far away from the carboxylate bridge and that the electron withdrawal by the more electronegative groups is too small to be of influence on the magnetic coupling. This is sustained by the calculated LoProp charges[51] on the atoms of the carboxylato group. These changes are small for the oxygens coordinated to the Cu^{2+}, and hence, the electron density in the

ISBN:978-84-694-2171-0/DL:T. 1032-2011

neighbourhood of the copper ions on the carboxylato bridge is not affected by the replacement of the H atoms in the R-group by halogens.

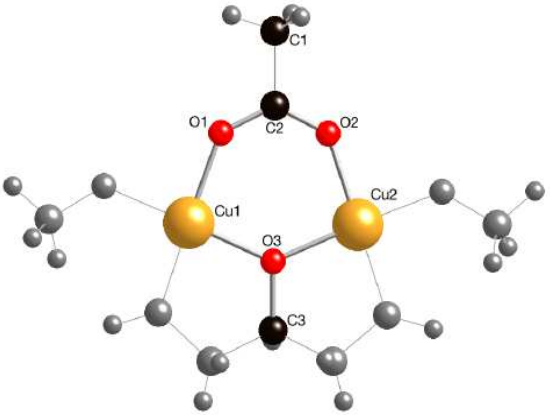

Figure 3.4. Labels of the central atoms of the complex.

Table 3.7. CASPT2 magnetic coupling parameter J (cm^{-1}) and LoProp charges on C and O of the carboxylato bridge. Lables of atoms are given in Figure 3.4.

R-group	J	q(C2)	q(O1/O2)
CH_3	-122	-0.47	-0.72
CH_2F	-114	0.08	-0.70
CH_2Cl	-125	-0.21	-0.70
CF_3	-126	0.86	-0.67
F	-192	0.88	-0.67

Even if we replace the whole CH_3 group by F, we do not observe important changes in the oxygen charges, even though the magnetic coupling is strongly enhanced. The origin of this larger J cannot be ascribed to electron withdrawal effects, since the calculated charges do not change significantly compared to the

other cases with weaker coupling. The origin of the difference lies in the complementary of the orbitals, as described in the literature[52,56,57] and will be discussed in detail below.

First, we focus on the relative importance of the alkoxo- and carboxylato bridge for the magnetic coupling. The carboxylato bridge is known to be an efficient antiferromagnetic coupler. In fact the binuclear Cu(II) acetate complex described by Bleaney and Bowers is one of the first examples of a polynuclear system with strong antiferromagnetic interactions ($J = -294 \pm 4$ cm^{-1}).[53] However, in the present complexes, there is a second bridge formed by an alkoxy (OR) group. The Cu–OR–Cu angle is close to 140 degrees, and hence, far away from the ferromagnetic regime around 95 degrees.[54,55] This fact may indicate that the alkoxo bridge is at least as important as the carboxylato bridge. To quantify the relative effectiveness of the two bridges to magnetically couple the copper ions, we perform a computational experiment in which J is calculated with one of the bridges completely deactivated. In the first step, the molecule is divided in two fragments, the carboxylato bridge (fragment A) and the rest of the model (fragment B). Subsequently, the charge distribution of the isolated fragments is calculated and superimposed to form the AB molecule. The charge distribution of fragment B is reoptimized in the presence of the frozen charge distribution of fragment A. In this way, all the covalent interactions between Cu and the carboxylato bridge are completely eliminated and the calculated singlet-triplet energy difference is solely due to the coupling over the alkoxy bridge. The same procedure is applied taking the OR group as frozen fragment and activating only the coupling through the carboxylato bridge. Results are listed in Table 3.8.

Table 3.8. Magnetic coupling parameter J (cm^{-1}) and Mulliken spin populations ρs on Cu, the oxygen atoms of the alkoxy group (O_a) and the carboxylato group (O_b) with different active bridges.

Active bridge	J	ρ_s (Cu)	ρ_s (O_a)	ρ_s (O_b)
Alkoxy	-158	0.932	0.034	0
Carboxylato	-28	0.938	0	0.011
Both	-122	0.924	0.031	0.010

The first obvious conclusion that can be extracted from Table 3.8 is that the alkoxo bridge is much more effective in the coupling of the magnetic moments of the Cu ions than the carboxylato bridge. This is not only reflected in the calculated J-values but also in the larger delocalization of the spin density from Cu onto the alkoxy-bridge (O3). Furthermore, we observe that the two bridges have an antisynergistic effect. The sum of the two individual couplings is larger than the coupling calculated without imposing any restrictions on the optimization of the electron distribution. This is readily explained with the theory of counter-complementarity of Nishida *et al*.[56] and McKee *et al*.[57] The explanation is based on the Hay-Thibeault-Hoffmann model,[58] which relates the energy gap of the magnetic orbital energies with the coupling parameter: the larger the separation, the larger the magnetic coupling. The first magnetic orbital φ_1 is dominated by the in-phase combination of the $3d_{xy}$ atomic orbitals of the two Cu ions and φ_2 is mainly formed by the out-of-phase combination of these atomic orbitals. As can be seen in the left column of Figure 3.5, the interaction with the O-2p orbitals lead to a larger destabilization of the out-of-phase combination (φ_2) due to the stronger antibonding interactions with the O-2p orbital oriented along the Cu–Cu axis than the interaction with the O-2p axis perpendicular to this axis, which contributes to φ_1. The energy gap

UNIVERSITAT ROVIRA I VIRGILI
THE CALCULATION OF THE THERMAL DEPENDENCY OF THE MAGNETIC SUSCEPTIBILITY
IN EXTENDED SYSTEMS WITH AB INITIO ELECTRONIC STRUCTURE PARAMETERS
Igor Negoda
ISBN:978-84-694-2171-0/DL:T. 1032-2011

($\Delta\varepsilon$) is equal to 0.0161 au. after taking into consideration this interaction.

However, the carboxylato group also makes a contribution to the magnetic orbitals. Because of symmetry, φ_3 mainly interacts with φ_2, while φ_4 can be combined with φ_1. Assuming that the overlap and interaction integrals involving these orbitals are similar, the net effect of the interaction is determined by the energy separation of the interacting orbitals. Since ε_1- ε_4 is slightly smaller than ε_2- ε_3, the interaction with the carboxylato group leads to a larger destabilization of φ_1 than of φ_2, and hence, a decrease of the energy gap that separate the two magnetic orbitals to $\Delta\varepsilon^* = 0.0145$ au. This is in line with the smaller J when the interaction with both bridges is considered in comparison to the alkoxo-bridge only calculation.

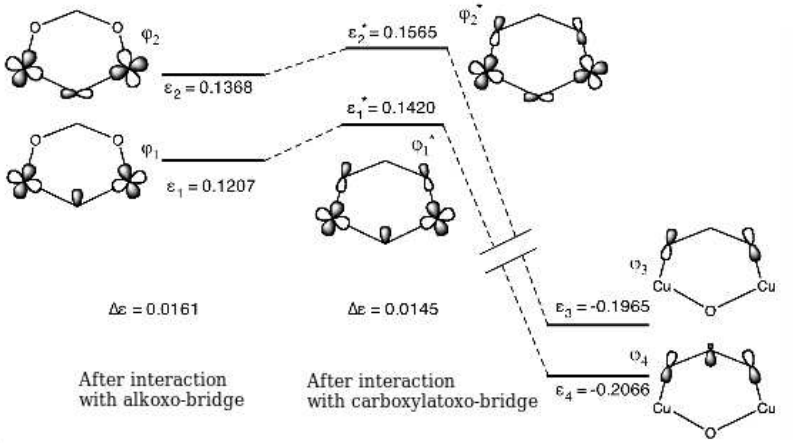

Figure 3.5. Schematic molecular orbital diagram of the interaction between the alkoxo-bridge dinuclear copper fragment and the carboxylato bridge. Orbital energies (ε) and energy gaps ($\Delta\varepsilon$) in au.

ISBN:978-84-694-2171-0/DL:T. 1032-2011

Having established that the electronegativity of the R-group in the carboxylato bridge is not determining and that the alkoxy bridge is the most efficient coupler, an apparently evident explanation for the differences in the magnetic coupling observed in the structures reported in Table 3.4 are the magneto-structural correlations, and Cu–O–Cu angle is the first candidate to study. In principle, larger angles should lead to stronger antiferromagnetic coupling. However, this angle probably is not the only geometrical parameter that influences the magnetic coupling. Therefore, we have summarized a series of geometrical parameters for the three compounds in Table 3.9 and compared them to the experimental J-values.

The small increase of the Cu-O3-Cu angle may contribute to the increase of J when comparing (1) to (2), but fails to explain the marked decrease observed for compound (3). None of the other distances or angles listed in Table 3.9 shows enough variation as to be determinant to explain the differences in J in the three compounds. The only significant variation is found for the O3-C3 distance, which is smaller in (2) than in the other two structures. However, a quick inspection of the magneto-structural correlation with CASPT2 shows that the J-value decreases with smaller O3-C3 distance, and hence, contrary to the observed behaviour.

To further explore the origin of the difference of the J-values in (1), (2) and (3), we determined the out-of-plane angle of C3 with respect to the Cu1-O3-Cu2 plane (θ), the degree of pyramidalization of O3, the dihedral angle of the Cu1-C3-Cu2 and Cu1-C2-Cu2 planes (δ_1), and the dihedral angle of the C2-Cu1-C3 and C2-Cu2-C3 planes (δ_2) in the three structures. The first two parameters have been explicitly mentioned before in the literature to be of influence on the magnetic properties in this type of

asymmetrically bridged systems,[59] while the latter two are more general for doubly bridged systems.

Table 3.9. Selected experimental bond distances and angles of the three Cu(II) dinuclear complexes with different R-groups on the carboxylato brdige.

Distance [Å]	Structure		
	1 (R = CH_3) J = -174 cm^{-1}	2 (R = CF_3) J = -188 cm^{-1}	3 (R = CH_2Cl) J = -134 cm^{-1}
Cu1-O3	1.91	1.93	1.91
Cu2-O3	1.91	1.91	1.93
O3-C3	1.43	1.35	1.41
Cu1-O1	1.93	1.98	1.95
Cu2-O2	1.94	1.96	1.96
C2-O1	1.25	1.23	1.24
C2-O2	1.24	1.25	1.24

Angle [degrees]	Structure		
	1 (R = CH_3) J = -174 cm^{-1}	2 (R = CF_3) J = -188 cm^{-1}	3 (R = CH_2Cl) J = -134 cm^{-1}
Cu1-O3-Cu2	132.8	133.6	132.7
O1-Cu1-O3	94.4	94.0	94.3
O2-Cu2-O3	94.4	94.2	94.6
O1-C2-O2	127.1	130.9	129.4
C2-O1-Cu1	135.9	132.9	134.7
C2-O2-Cu2	135.4	133.7	133.7

A fully planar conformation of the two bridges lead to an optimal orientation of the magnetic orbitals and in this way to maximum coupling of the spin moments localized on the Cu(II) ions. The pyramidalization of O3 is measured by h, the distance

from this atom to the Cu-C3-Cu plane. In Table 3.10 lists the values of these more complicated geometrical parameters for (1), (2) and (3) and relates them to the experimental J-value.

Again, it is readily seen that the pyramidalization and the C3 out-of-plane angle are similar in the three compounds and do not relate with the experimental J-values.

Table 3.10. C3 out-of-plane angle θ (in degrees), C3–Cu–Cu–C2 dihedral angle δ_1 (in degrees), Cu-C2-C3-Cu dihedral angle δ_2 (in degrees) and pyramidalization of O3 measured by h (Å) defined as the distance of O3 to the Cu-C3-Cu plane.

Parameter	Structure		
	1	2	3
	(R = CH_3)	(R = CF_3)	(R = CH_2Cl)
	J = -174 cm^{-1}	J = -188 cm^{-1}	J = -134 cm^{-1}
θ	13.1	6.5	8.2
δ_1	173.4	176.3	168.4
δ_2	171.4	175.3	165.1
h	0.110	0.067	0.042

However, there is a slightly larger variation in the dihedral angles and we observe that these variations correlate consistently with the tendency in J, for smaller δ, smaller J-values are observed. To establish the relative importance of the variations in δ_1 and δ_2 with respect to the changes in the magnetic coupling parameter, we performed a set of calculations on Intermediate III varying the two dihedrals independently. The variation of δ_1 between 180º and 160º result in a tiny variation of the CASPT2 estimate for J from -124.0 cm^{-1} for the planar structure to -121.8 cm^{-1} for δ_1=165º. For larger dihedrals, J increases again. On the other hand, the magnetic coupling is much more susceptible to changes in δ_2. Successively reducing this dihedral angle from 180º

to 160º in steps of 5 degrees shows a continuous decrease of the coupling from to -95 cm^{-1} to +3.9 cm^{-1}. The effect of this distortion is of course overestimated in the present model calculation since the real experimental structures show all kind of geometrical changes, but these model calculations reveal the correlation between δ_2 and the strength of the magnetic coupling in the structures studied here.

3.2.4 Conclusion

The electronic effects induced by the different substitutions due to its electronegative properties on the carboxylato bridge can be completely neglected when the magnetic coupling parameter is compared in the dinuclear copper complexes in which the metal ions are bridged by an alkoxo- and a carboxylato bridge. When all geometrical differences between the different structures are cleaned, the calculations firmly establish that replacing the CH_3 group of the acetato bridge with more electronegative groups does not affect the magnetic coupling.

The magnetic coupling in studied systems appears almost exclusively due to the alkoxo-bridge, and the carboxylato bridge plays unimportant role. The isolated action of the alkoxo bridge is more than 5 times larger than of the carboxylato brigde, illustrated by the -158 cm^{-1} and -28 cm^{-1} singlet-triplet gap in the intermediate III model freezing one of the bridges. The fact that the total coupling is smaller than the sum of two couplings allows to declare the counter-complementarity of the bridges. This effect can be understood in a one electron picture by considering the interaction of the in-phase and out-of-phase magnetic orbitals with the (mainly) O-$2p_x$ and O-$2p_y$ orbitals on the alkoxo bridge and the HOMO-1 and HOMO-2 of the carboxylato bridge.

ISBN:978-84-694-2171-0/DL:T. 1032-2011

The differences of J-values different in the complexes described in Ref. 42 and 43 is related to the crystal structure. The analysis of the geometrical data and the study of the magneto-structural correlations reveal that there is interesting dependency between δ_2 (Cu1-C2-C3-Cu2 dihedral angle) and the measured magnetic coupling constant. Other geometrical parameters are either too similar in the studied compound or do not significantly affect the J-value.

The obtained J-values are comparable with experimental, although the observed phenomenon of $J(2) > J(1)$ is not supported. This can be related to insufficient sensitivity of methods for the differences of such range. Also the experimental inaccuracy cannot be surely excluded.

ISBN:978-84-694-2171-0/DL:T. 1032-2011

3.3 References

1 Haslett, T. L.; Moskovits, M.; Weitzman, A. L. J. Mol. Spectrosc. 1988, 135, 259.

2 Bier, K. D.; Haslett, T. L.; Kirkwood, A. D.; Moskovits, M. J. Chem. Phys. 1988, 89, 6.

3 Kirkwood, A. D.; Bier, K. D.; Thompson, J. K.; Haslett, T. L.; Huber, A. S.; Moskovits, M. J. Phys. Chem. 1991, 95, 2644.

4 Baumann, C. A.; van Zee, R. J.; Bhat, S. V.; Weltner Jr., W. J. Chem. Phys. 1983, 78, 190.

5 Cheeseman, M.; van Zee, R. J.; Flanagan, H.L.; Weltner Jr., W. J. Chem. Phys. 1990, 92, 1553.

6 Rivoal, J. C.; Shakhs Emampour, J.; Zeringue, K. J.; Vala, M.; Chem. Phys. Lett. 1982, 92, 313.

7 Ralchenko, Y.; Kramida, A. E.; Reader, J.; and NIST ASD Team, NIST Atomic Spectra Database (version 3.1.4) available online at http://physics.nist.gov/asd3

8 Nesbet, R. K. Phys. Rev. A 1864, 135, 460.

9 Nayak, S. K.; Jena, P. Chem. Phys. Lett. 1998, 289, 47.

10 Desmarais, N.; Reuse, F. A.; Khanna, S. N. J. Chem. Phys. 2000, 112, 5576.

11 Barden, C. J.; Rienstra-Kiracofe, J. C.; Shaeffer III, H. F. J. Chem. Phys. 2000, 113, 690.

12 Gutsev, G. L.; Bauschlicher Jr., C. W. J. Phys. Chem. A 2003, 107, 4755.

13 Yanagisawa, S.; Tsuneda, T.; Hirao, K. J. Chem. Phys. 2000, 112, 545.

14 Yamanaka, S.; Ukai, T.; Nakata, K.; Takeda, R.; Shoji, M.; Kawakami, T.; Takada,T.; Yamaguchi, K. Int. J. Quant. Chem. 2007, 107, 3178.

15 Bauschlicher Jr., C. W. Chem. Phys. Lett. 1989, 156, 95.

16 Wang, B.; Chen, Z. Chem. Phys. Lett. 2004, 387, 395.

17 Yamamoto, S.; Tatewaki, H.; Moriyama, H.; Nakano, H. J. Chem. Phys. 2006, 124, 124302.

18 Negodaev I.; de Graaf, C.; Caballol, R. Chem. Phys. Lett. 2008, 459, 73 76

19 Angeli, C.; Cavallini, A.; Cimiraglia, R. J. Chem. Phys. 2008, 128, 244317.

ISBN:978-84-694-2171-0/DL:T. 1032-2011

20 Queralt, N.; Taratiel, D.; de Graaf, C.; Caballol, R.; Cimiraglia, R.; Angeli, C. J. Comp. Chem. 2008, 29, 994.

21 Andersson, K.; Malmqvist, P.-Å.; Roos, B. O.; Sadlej, A. J.; Wolinski, K. J. Phys. Chem. 1990, 94, 5483.

22 Andersson, K.; Malmqvist, P.-Å.; Roos, B. O. J. Chem. Phys. 1992, 96, 1218.

23 Roos,B.; Taylor, P.; Siegbahn, P.Chem. Phys. 1980, 48, 157.

24 Ghigo, G.; Roos, B. O.; Malmqvist, P.-Å. Chem. Phys. Lett. 2004, 396, 142.

25 Miralles, J.; Daudey, J.-P.; Caballol, R. Chem. Phys. Lett. 1992, 198, 555.

26 Miralles, J.; Castell, O.; Caballol, R.; Malrieu, J.-P. Chem. Phys. 1993, 172, 33.

27 García, V.M.; Caballol, R.; Malrieu, J.-P. J. Chem. Phys. 1998, 109, 504.

28 Rodríguez, E.; Reguero, M.; Caballol, R.J. Phys. Chem. A 2000, 104, 6253.

29 van Duijneveldt, F.B.; van Duijneveldt-van de Rijdt, J.G.C.M.; van Lenthe, J.H. Chem. Rev. 1997, 94, 1873.

30 Karlström, G.; Lindh, R.; Malmqvist, P.-Å.; Roos, B.O.; Ryde, U.; Veryazov, V.; Widmark, P.-O.; Cossi, M.; Schimmelpfennig, B.; Neograd y, P.; Seijo, L. Comput. Mater. Sci. 2003, 28, 222.

31 Ben Amor, N.; Maynau, D. Chem. Phys. Lett. 1998, 286, 221.

32 Calzado, C.J.; Cabrero, J.; Malrieu, J.-P.; Caballol, R. J. Chem. Phys. 2002, 116, 2728.

33 Anderson, P.W. In Theory of Magnetic Interaction: Exchange in Insulators and Superconductors, Academic Press (New York, 1963).

34 Langhoff, S. R.; Davidson, E. R. Int. J. Quant. Chem. 1974, 8, 61.

35 Lombardi, J. R.; Davis, B. Chem. Rev. 2002, 102, 2441.

36 Angeli, C.; Cimiraglia, R.; Evangelisti, S.; Leninger, T.; Malrieu, J.-P. J. Chem. Phys. 2001, 114, 10252.

37 Angeli, C.; Cimiraglia, R.; Malrieu, J.-P. J. Chem. Phys. 2002, 117, 9138.

38 Lopez, C.; Costa, R.; Illas, F.; de Graaf, C.; Turnbull, M. M.; Landee, C. P.; Espinosa, E.; Mata, I.; Molins, E. J. Chem. Soc., Dalton Trans. 2005, 2322.

ISBN:978-84-694-2171-0/DL:T. 1032-2011

39 Boxwell, C. J.; Bhalla, R.; Cronin, L.; Turner, S. S.; Walton, P. H. J. Chem. Soc., Dalton Trans. 1998, 2449.

40 Mazurek, W.; Kennedy, B. J.; Murray, K. S.; O'Connor, M. J.; Rodgers, J. R.; Snow, M. R.; Wedd, A. G.; Zwack, P. R. Inorg. Chem. 1985, 24, 3258.

41 Tolman, W. B.; Rardin, R. L.; Lippard, S. J. J. Am. Chem. Soc. 1989, 111, 4532.

42 Kogan, V. A.; Lukov, V. V.; Novotortsev, V. M.; Eremenko, I. L.; Aleksandrov, G. G. Russ. Chem. Bull. 2005, 54, 600.

43 Kogan, V. A.; Lukov, V. V.; Shcherbakov, I. N. Russ. J. Coord. Chem. 2010, 36, 401.

44 Suaud, N.; Gaita-Ariño, A.; Clemente-Juan, J. M.; Sánchez-Marín, J.; Coronado, E. J. Am. Chem. Soc. 2002, 124, 15134.

45 Moreira, I. de P. R.; Suaud, N.; Guihéry, N.; Malrieu, J.-P.; Caballol, R.; Bofill, J. M.; Illas, F. Phys. Rev. B 2002, 66, 134430.

46 Gellé, A.; Munzarová, M.; Lepetit, M. B.; Illas, F. Phys. Rev. B 2003, 68, 125103.

47 Bordas, E.; Caballol, R.; de Graaf, C.; Malrieu, J.-P. Chem. Phys. 2005, 309, 259.

48 Calzado, C. J.; Angeli, C.; Taratiel, D.; Caballol, R.; Malrieu, J.-P. J. Chem. Phys. 2009, 131, 044327.

49 Negodaev, I.; Queralt, N.; Caballol, R.; de Graaf, C. Chem. Phys. 2011, in press.

50 Calzado, C. J.; Angeli, C.; Caballol, R.; Malrieu, J.-P. Theor. Chem. Acc. 2010, 126, 185.

51 Gagliardi, L.; Lindh, R.; Karlström, G. J. Chem. Phys. 2004, 121, 4494 4500.

52 Kahn, O. Molecular Magnetism; VCH Publishers, (New York, 1993).

53 Güdel, H. U.; Stebler, A.; Furer, A. Inorg. Chem. 1979, 18, 1021.

54 Ruiz, E.; Alemany, P.; Alvarez, S.; Cano, J. J. Am. Chem. Soc. 1997, 119, 1297.

55 Ruiz, E.; de Graaf, C.; Alemany, P.; Alvarez, S. J. Phys. Chem. A 2002, 106, 4938.

56 Nishida,Y.; Kida, S. J. Chem. Soc., Dalton Trans. 1986, 2633.

57 McKee, V.; Zvagulis, M.; Reed, C. A. Inorg. Chem. 1985, 24, 2914.

ISBN:978-84-694-2171-0/DL:T. 1032-2011

58 Hay, P. J.; Thibeault, J. C.; Hoffmann, R. J. J. Am. Chem. Soc. 1975, 97, 4884.

59 Ruiz, E.; Alemany, P.; Alvarez, S.; Cano, J. Inorg. Chem. 1997, 36, 3683.

UNIVERSITAT ROVIRA I VIRGILI
THE CALCULATION OF THE THERMAL DEPENDENCY OF THE MAGNETIC SUSCEPTIBILITY
IN EXTENDED SYSTEMS WITH AB INITIO ELECTRONIC STRUCTURE PARAMETERS
Igor Negodaev
ISBN:978-84-694-2171-0/DL:T. 1032-2011

UNIVERSITAT ROVIRA I VIRGILI
THE CALCULATION OF THE THERMAL DEPENDENCY OF THE MAGNETIC SUSCEPTIBILITY
IN EXTENDED SYSTEMS WITH AB INITIO ELECTRONIC STRUCTURE PARAMETERS
Igor Negodaev
ISBN:978-84-694-2171-0/DL:T. 1032-2011

Chapter 4

Magnetic coupling in extended systems

UNIVERSITAT ROVIRA I VIRGILI
THE CALCULATION OF THE THERMAL DEPENDENCY OF THE MAGNETIC SUSCEPTIBILITY
IN EXTENDED SYSTEMS WITH AB INITIO ELECTRONIC STRUCTURE PARAMETERS
Igor Negodaev
ISBN:978-84-694-2171-0/DL:T. 1032-2011

After the discussion of the magnetic coupling in two molecular systems in the previous chapter, we now turn our attention to extended structures. In particular, we will focus on the description of the magnetic interaction in the hexagonal layers found in bifunctional materials. To this purpose, the procedure to obtain $\chi(T)$ will be tested in model systems first and then applied to the more interesting hexagonal layers.

4.1 Low-dimensional materials

The four model systems are all based on the Cu(II) – oxalato – Cu(II) structural motif. The set includes three 1D-chain compounds and one material with discrete (virtually) non-interacting dinuclear complexes. The first oxalato-bridged Cu(II) material studied is $[Cu_2(\mu\text{-}ox)_2(ampy)_3]_n$ (1), with ox = oxalate dianion and ampy = 2-amino-3-methylpyridine (Figure 4.1a). The structure consists of corrugated one-dimensional chains in which two types of Cu(II) centres (five- and six-coordinated) are bridged by bis-bidentate oxalate ligands. Magnetic susceptibility measurements[1] reveal an antiferromagnetic intrachain coupling of -22.9 cm^{-1}. The next compound is $[Cu(\mu\text{-}ox)(pyOH)_2]_n$ (2), with pyOH = 3-hydroxy-pyridine (Figure 4.1b). From the magnetic susceptibility curve in the 2-300 K temperature range, a ferromagnetic coupling was derived[2] with a J = +1.3 cm^{-1}. A moderate antiferromagnetic coupling was observed in $\{[Cu_2(\mu\text{-}ox)_2ampy'3]\cdot ampy'\}_n$ (3) with ampy' = 2-amino-4-methylpyridine (Figure 4.1c).[2] Five- and six-coordinated Cu(II) ions are bridged by two oxalate ligands with slightly different geometry, giving rise to a spin chain with two different J-values: J_1 = -66.6 cm^{-1} and J_2 = -58.6 cm^{-1}. The fourth Cu(II) compound is $[Cu_2(\mu\text{-}ox)(dpa)_2(CH_3CN)_2](ClO_4)_2$ (4) with dpa = di-2-pyridylamine (Figure 4.1d).[3] The crystal contains discrete moieties with two Cu(II) ions showing strong magnetic

coupling (J = -382 cm^{-1}). These units interact through hydrogen bridges, but they are magnetically not coupled and can be considered as isolated molecules.

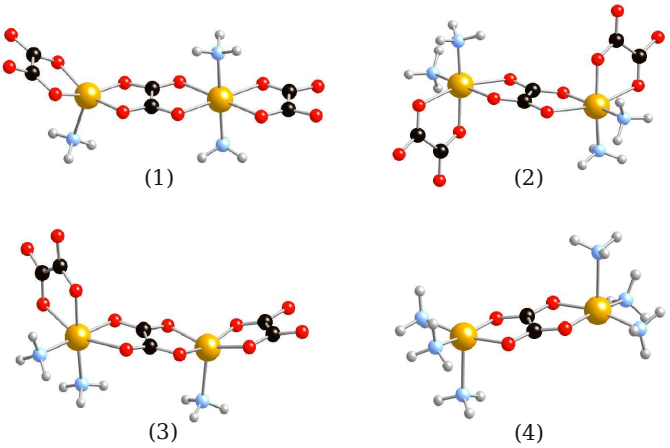

Figure 4.1. Ball and stick representations of the studied structures. Yellow - Cu; Red - O; Blue - N; Black - C; Grey - H.

Although there are two different TMs in the large majority of the hexagonal oxalate lattices, we concentrated here on the description of homometallic oxalato-bridged lattices. The ideal system to start with would be a lattice containing Cu(II) ions. However, we have not found any regular hexagonal lattice in the literature. This is probably due to the Jahn-Teller active nature of the Cu(II) ion, being unstable in the quasi octahedral coordination mode generally found in the regular hexagonal lattices. A recent study of Duan and co-workers[4] reported the structure of $(A)_2[M^{II}_2(C_2O_4)_3]$ lattices with M = Fe and Co, and A = diethylene-triamine derived ammonium salt. We have used this structure to calculate the magnetic coupling in regular hexagonal oxalato-bridged lattices. In addition, we replaced the Co ion with Ni and Cu for testing purposes. These structures will be referred to as TM-oxal in the remainder with TM = Cu, Ni, Co, Fe.

4.1.1 Computational details

ISBN:978-84-694-2171-0/DL:T. 1032-2011

The electronic structure of the dinuclear Cu(II) – oxalato – Cu(II) fragments shown on Figure 4.1 was determined with two quantum chemical methods. In the first place, we used the CASPT2 method[5,6] as implemented in Molcas 7.0 code.[7] As mentioned before, this method provides reasonably accurate estimates of J for moderately to strongly coupled spin moments[8], but should be used with caution for weakly coupled systems.[9] In some cases, we encountered intruder states. The artificial effect of these states on the second-order estimate of the energy has been eliminated by applying a level shift.[10] Dealing with Cu(II)-based systems, the minimal CAS (2, 2) has been used. J is calculated from the energy difference of the singlet in triplet state in all systems.

The second method is based on the difference-dedicated configuration interaction (DDCI)[11,12] implemented in the CASDI program.[13] Because of the low spatial symmetry of the fragments and the elevated spin moment in some of them, the standard DDCI calculation leads to a prohibitively large CI space. Therefore, we follow the extended (CAS_{ext}/DDCI2) method, which has successfully been applied in similar studies.[14,15]

The used ANO basis set is already cited in chapter 3 (Table 3.5). This basis set has been shown to be sufficiently large for the description of magnetic coupling parameters.[16]

ISBN:978-84-694-2171-0/DL:T. 1032-2011

4.1.2 Results and discussion

(1) $[Cu_2(\mu\text{-ox})(dpa)_2(CH_3CN)_2](ClO_4)_2$

Here, ox = oxalate dianion, and dpa = di-2-pyridylamine. The crystal contains discrete moieties with two Cu(II) ions showing strong magnetic coupling (J = -382 cm^{-1}). Although these units interact through hydrogen bridges, they are magnetically not coupled. This Cu(II) dimer is considered here as one of the simplest oxalato-bridged systems to test the procedure to obtain the magnetic susceptibility curve, since it contains only discrete magnetic units of two magnetic centres.

The strength of the coupling of the S=1/2 moments on Cu(II) through the oxalato bridge is largely determined by the relative orientation of the magnetic orbitals as shown in Figure 4.2.[1,17,40] Strong coupling is observed when these orbitals are co-planar, while no coupling or weak ferromagnetic coupling is expected in the case when these orbitals have a parallel orientation with respect to each other. Intermediate coupling can be expected for the combination of one in-plane magnetic orbital with an out-of-plane magnetic orbital. The studied compound belongs clearly to the co-planar class: the CASSCF magnetic orbitals are co-planar (see Figure 4.3). The obtained coupling constant is -244.4 cm^{-1} at CASPT2 and -329.8 cm^{-1} at CAS_{ext}/DDCI2 level. CASPT2 underestimates the coupling by a non-negligible amount. This is not unexpected since the results are obtained with an active space that only contains the magnetic orbitals. For strong magnetic coupling, the active space should be extended with orbitals on the bridge and extra TM-d orbitals to give a more accurate account of the most important non-dynamical electron correlation effects.[8] The CAS_{ext}/DDCI2 result is in good agreement with the experimental estimate.

UNIVERSITAT ROVIRA I VIRGILI
THE CALCULATION OF THE THERMAL DEPENDENCY OF THE MAGNETIC SUSCEPTIBILITY
IN EXTENDED SYSTEMS WITH AB INITIO ELECTRONIC STRUCTURE PARAMETERS
Igor Negodaev
ISBN:978-84-694-2171-0/DL:T. 1032-2011

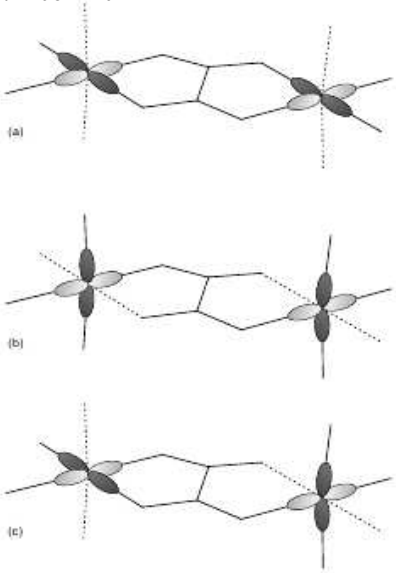

Figure 4.2. Schematic representation of the magnetic orbitals in oxalato-bridged TM complexes. The dashed lines represent the longer TM–ligand distance. (a) co-planar magnetic orbitals; (b) parallel magnetic orbitals; (c) combination of in-plane and out-of-plane magnetic orbitals.

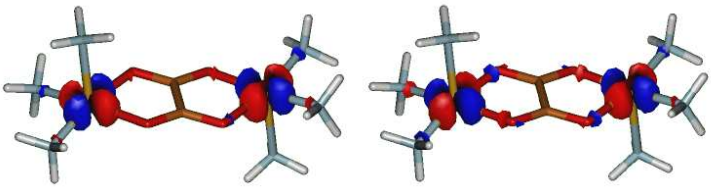

Figure 4.3. CASSCF optimized magnetic orbitals of compound (1).

The thermal dependency of magnetic susceptibility is now analysed. After applying a correction for 0.7% impurities and subtracting the estimate of 1.6×10^{-3} cm^3/mol for the temperature independent paramagnetism given in the experimental paper, we obtain a perfect agreement with the calculated curve using the experimental J value of -382.3 cm^{-1}. The two curves are indistinguishable in Figure 4.4.

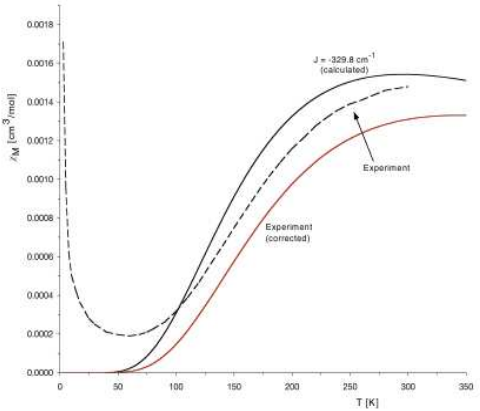

Figure 4.4. Calculated magnetic susceptibility as function of the temperature of compound (1) for different choices of J (full curves). The dashed curve represent the raw experimental data.

Using the CAS_{ext}/DDCI2 estimate for J, we obtain a curve that is in reasonable agreement with the corrected experimental curve. The maximum appears at lower temperature and the magnetic susceptibility is higher in the considered temperature interval due to the smaller J value used in the calculation of $\chi(T)$. The CASPT2 curve is not shown since the J-value is significantly smaller than the experimental estimate.

ISBN:978-84-694-2171-0/DL:T. 1032-2011

(2) $[Cu_2(\mu\text{-}ox)_2(ampy)_3]_n$

Here, ox = oxalate dianion, and ampy = 2-amino-3-methyl-pyridine. The structure consists of corrugated one-dimensional chains in which two types of Cu(II) centres (five- and six-coordinated) are bridged by bis-bidentate oxalate ligands. Magnetic susceptibility measurements reveal an antiferro-magnetic intrachain coupling of -22.9 cm^{-1}.

The overview of magnetic orbitals (Figure 4.5) identifies this compound to class (c) (see Figure 4.2).

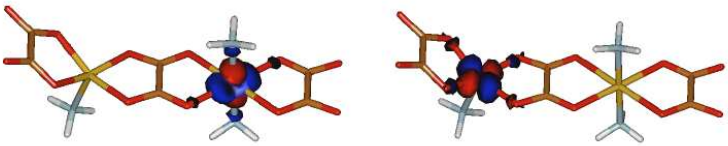

Figure 4.5. CASSCF optimized magnetic orbitals of compound (2).

Here, CASPT2 result is in reasonable agreement with experiment, -9.0 cm^{-1}, and a more quantitative estimate is obtained with CAS_{ext}/DDCI2 (-16.5 cm^{-1}). The precise reproduction of the experimental J is a difficult process, since the molecule is close to the border between type (b) and type (c) behaviour. A small enlargement of the distance between Cu(II) and the axial ligand converts the in-plane magnetic orbital to an out-of-plane magnetic orbital (see Figure 4.5) with a parallel orientation with respect to the magnetic orbital localized on the other Cu(II) ion. This weakens the magnetic coupling significantly. CASSCF seems to overestimate the parallel component in the magnetic orbital (J = -0.75 cm^{-1}), which is only partially repaired by CASPT2 and slightly better with CAS_{ext}/DDCI2.

The system (2) has a one-dimensional magnetic chain

topology with negligible inter-chain interactions. The magnetic susceptibility curve (Figure 4.6) can be accurately fitted with the standard expression for 1D chains.[18] The corrected experimental data nearly coincide with the curve that we obtain by diagonalizing the Heisenberg Hamiltonian of a 14 centre model with the experimental J-value. The source of the discrepancy could be the temperature independent paramagnetism for which no estimate was given in the experimental paper.

The finite size effects were addressed in this system by comparing the results obtained with models of different sizes. In the first place, it was observed that the application of periodic boundary conditions (closing the 1D chain to give a ring) has only a small effect on the calculated curves. Important size effects are observed for systems up to 14 centres, but the 16-centre-curve is identical to the one obtained with the 14 centre model as shown in Figure 4.6. These curves were obtained with the CAS_{ext}/DDCI2 J-value, which is about 25% smaller than the experimental one. This leads again to a maximum in the curve at slightly lower temperature and higher magnetic susceptibilities at low temperatures.

ISBN:978-84-694-2171-0/DL:T. 1032-2011

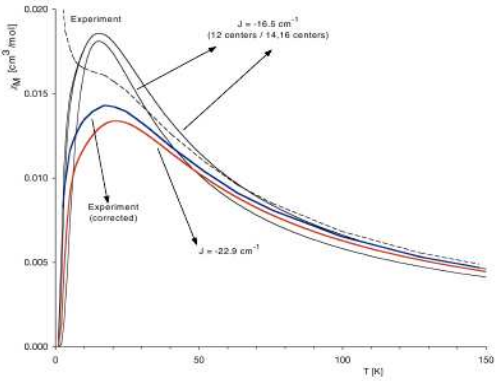

Figure 4.6. Calculated magnetic susceptibility as function of the temperature of compound (2). The CAS_{ext}/DDCI2 and experimental estimates of J are used in the full curves. The dashed curve represent the experimental data.

(3) $[Cu(\mu\text{-}ox)(pyOH)_2]_n$

Here, ox = oxalate dianion, pyOH = 3-hydroxypyridine. From the magnetic susceptibility curve in the 2-300 K temperature range, a ferromagnetic coupling was derived with a coupling constant of +1.3 cm^{-1} .

The behaviour of compound (3) in comparison with previously described structures is completely different. The calculated magnetic orbitals are parallel (see Figure 4.7) and the spin moments are basically uncoupled. This is reflected in both the CASPT2 (-3.5 cm^{-1}) and CAS_{ext}/DDCI2 (0.6 cm^{-1}) results, which indicate a very small antiferromagnetic coupling. In this case, the calculations are not capable to predict the sign of the interaction. Probably more elaborate schemes such as full DDCI or

decontracted NEVPT2[19] can provide a more precise description but this is beyond the scope of the thesis.

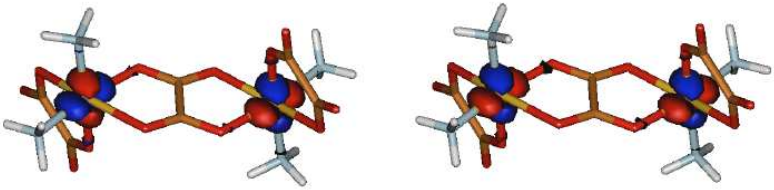

Figure 4.7. CASSCF optimized magnetic orbitals of compound (3).

We did not intend to reproduce the experimental magnetic susceptibility curve for compound (3) due to the fact that the calculated estimates indicate an antiferromagnetic behaviour, while experimentally ferromagnetic coupling is observed. Again, we would like to stress that the coupling is very weak and that one cannot expect a precision of the computational schemes applied that is better than a few wave numbers.

(4) $\{[Cu_2(\mu\text{-}ox)_2ampy'_3]\cdot ampy'\}_n$

Here, ox = oxalate dianion, ampy'=2-amino-4-methyl-pyridine. Five- and six-coordinated Cu(II) ions are bridged by two oxalate ligands with slightly different geometry, giving rise to a spin chain with two different J-values: J_1 =-66.6 cm^{-1} and J_2 = -58.6 cm^{-1} .

This is also an intermediate case of coupling, as found for compound (2) but not so close to type (b) behaviour (see Figure 4.2). Magnetic orbitals are presented in Figure 4.8. J_1 = -23.8 cm^{-1} and J_2 = -27.2 cm^{-1} were found at CASPT2 level, while CAS_{ext}/DDCI2 gives -51.8 cm^{-1} and -63.5 cm^{-1} respectively, with a perfect agreement with experimental values. This system

has a magnetic topology that is not as well established as the previous. The magnetic susceptibility of alternating chain compounds is usually fitted to an expression derived by Hall et al.[20] The correction due to impurities is small and hardly changes the curve of the experimental data. Therefore, it has not been included in Figure 4.9. Before comparing with the experimental curve, we first comment the finite size effects in the theoretical estimates of the magnetic susceptibility curve. As in the uniform 1D chain, we find small differences between the open and closed models. While there are small finite size effects in the open models, the closed systems produce nearly the same curves for the 12-, 14-, and 16-centre models. The Heisenberg Hamiltonian for these models was built using the CAS_{ext}/DDCI2 J-values, which are only slightly smaller than those extracted from experiment. The curve obtained with the experimental estimates is similar to the previous ones, the maximum shifts to higher energy and magnetic susceptibility values are somewhat smaller.

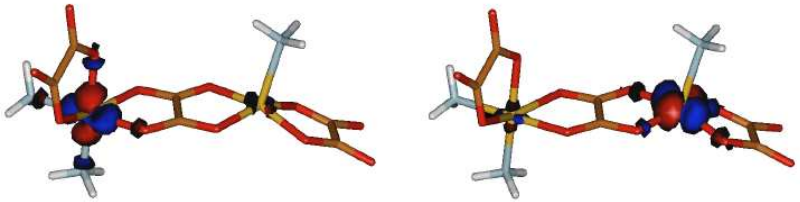

Figure 4.8. CASSCF optimized magnetic orbitals of compound (4).

However, the comparison with the experimental curve is not as satisfactory as in the previous cases. In the high temperature limit agreement is excellent, but at lower temperatures the experimental curve falls off faster than the curve obtained from a 14 centre model with the experimental J-values. This discrepancy cannot be explained by the neglect of the impurities present in the

ISBN:978-84-694-2171-0/DL:T. 1032-2011

sample, since this only causes a decrease of the experimental χ(T) values.

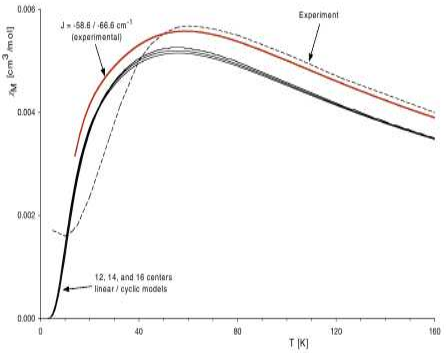

Figure 4.9. Calculated magnetic susceptibility as function of the temperature of compound (4). The CAS_{ext}/DDCI2 estimate of J is used to obtain the full curves. Open and closed models of different size are compared. The dashed curve represent the experimental data.

4.1.3 Conclusion

The CASPT2 and CAS_{ext}/DDCI2 computational schemes applied to a series of compounds containing Cu(II) ions in different topologies give reasonable estimates of J at a limited computational cost, and the diagonalization of the Heisenberg Hamiltonian for larger models gives good estimates of χ(T). In the next section, this method is applied to higher dimensionality oxalato-bridged materials.

ISBN:978-84-694-2171-0/DL:T. 1032-2011

The most interesting classes of magnetic materials are 2D- and 3D-systems both for the experimentalists and theoreticians. A very special group is constituted by the two-dimensional oxalato-bridged networks of TMs. The negative charge of this magnetic layer is compensated by a countercation with additional properties, eventually giving rise to bifunctional materials such as ferromagnetic molecular metals,[21] magnetic multilayers,[22] photochromic magnets,[23] or nonlinear optical active magnets.[24] Among oxalate-based 3D-networks, an interesting family incorporates chiral counteractions, giving rise to chiral magnets[25,26,27] and recently hybrid magnets with coexistence of magnetic ordering and spin crossover.[28]

4.2.1 *Catena*-μ-Tris[oxalato(2-)-O^1,O^2;O^3,O^4]-dicopper

Many 3D-extended systems are also reported. Catena-μ-Tris[oxalato(2-)-O^1,O^2;O^3,O^4]-dicopper complex[29] was the first extended 3D-structure in which the copper ion is surrounded by three coordinated oxalate anions. Although six oxygen atoms of three ligands are bound to a copper ion and each oxalate ion acts as a bridge between two of them, the metal ions are not in a plane but in a real 3-D arrangement and the crystal does not present the honeycomb structure typical for the bifunctional materials. Instead, the structure was described as a network of interlocked helical chains. As shown in Figure 4.10, the central copper ion is coordinated to three oxalate anions in a deformed octahedral environment. This periodic unit shows three different oxalate-bridged binuclear copper units, and therefore three different magnetic coupling interactions. Since the magnetic topology of

ISBN:978-84-694-2171-0/DL:T. 1032-2011

this material cannot be directly determined from the crystalline structure due to its complexity, we decided to undertake the theoretical investigation of the magnetic coupling in this system. To our knowledge, no experimental data have been given until now on the magnetic behaviour of this compound.

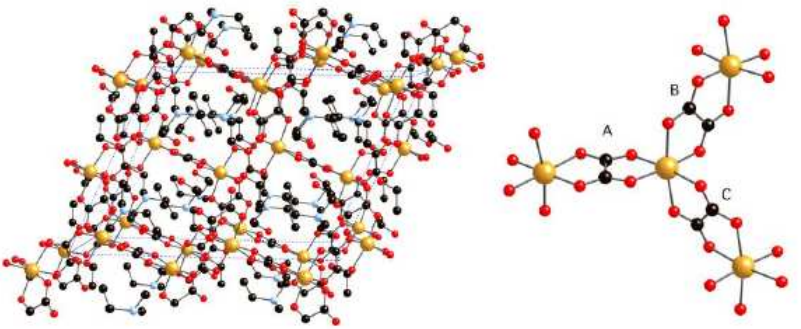

Figure 4.10. Left: Catena-μ-Tris[oxalato(2-)-O^1,O^2;O^3,O^4]-dicopper with diethyl-(2-hydroxyethyl)-ammonium cations located in the channels of the structure. Yellow: Cu; red: oxygen; black: carbon. Right: a repeated structural motif, where A, B and C are different dimers with distinct geometrical parameters.

Computational details

Firstly, the adequate modeling of the material should be designed to calculate the magnetic coupling between the spin moments localized on the Cu(II) ions. In a first step the three binuclear units $Cu(C_2O_4)Cu$ shown in Figure 4.10, A, B, and C, were considered, and the potential cooperative role of a third spin moment was investigated in trimers AB, AC and BC. The coupling parameters were extracted from the phenomenological Heisenberg Hamiltonian spectrum, as described before. To reduce the computational time of the comparison between two- and three-centre clusters, the external oxalato ligands were modelled by

water molecules. It has previously been shown that the exact nature of the coordinating external ligands is in general not decisively relevant for the magnetic coupling as long as the electronegativity of the atoms bonded to the TM is maintained.[33] The geometry of the metal-oxalate units is the experimental one, and the position of the oxygen atoms of the external water molecules is the same as the position of the oxygens in the oxalate ligands in the crystal structure. In a final step, dinuclear units with external oxalate ligands were also considered.

As in section 4.1, CASPT2, DDCI and CAS_{ext}/DDCI2 methods were used to determine the electronic structure of these fragments. The one-electron basis set cited before (Table 3.5) has been shown to be sufficiently large (basis 2) for the description of magnetic coupling parameters and even a reduction to Cu(5s,4p,3d) / C,O(3s,2p) / H(2s) gives reasonable estimates.[16,30] Hence, this smaller basis (basis 1) was applied in the trinuclear clusters to reduce the computational burden of the DDCI calculations in these models.

The procedure of extraction of the coupling parameters for trinuclear systems is less trivial. Than for dinuclear ones. In the trinuclear case the Heisenberg Hamiltonian reads:

$$\hat{H} = -J_{12}\hat{S}_1\hat{S}_2 - J_{23}\hat{S}_2\hat{S}_3 - J_{13}\hat{S}_1\hat{S}_3 \qquad 4.1$$

with three eigenfunctions, one quartet and two doublets. The difficulty of the extraction of the three coupling parameters of expression 4.1 from the energy spectrum associated to these three states obtained from *ab initio* calculations is obvious. The two energy differences are not enough to determine the three magnetic coupling parameters unless symmetry imposes restrictions on the J values, which is not the case in the structure studied here. The extra necessary information is contained in the wave-functions of the spin states. To obtain the coupling parameters from the calculated energies and wave-functions, let

UNIVERSITAT ROVIRA I VIRGILI
THE CALCULATION OF THE THERMAL DEPENDENCY OF THE MAGNETIC SUSCEPTIBILITY
IN EXTENDED SYSTEMS WITH AB INITIO ELECTRONIC STRUCTURE PARAMETERS
Igor Negodaev
ISBN:978-84-694-2171-0/DL:T. 1032-2011

as write the matrix representation of the Heisenberg Hamiltonian in the basis of the M_s = 1/2 determinants, $|\alpha\alpha\beta\rangle$, $|\alpha\beta\alpha\rangle$ and $|\beta\alpha\alpha\rangle$:

	$\alpha\alpha\beta$	$\alpha\beta\alpha$	$\beta\alpha\alpha$
$\alpha\alpha\beta$	$\frac{1}{4}(J_{13}+J_{23}-J_{12})$	$\frac{-J_{23}}{2}$	$\frac{-J_{13}}{2}$
$\alpha\beta\alpha$	$\frac{-J_{23}}{2}$	$\frac{1}{4}(J_{12}+J_{23}-J_{13})$	$\frac{-J_{12}}{2}$
$\beta\alpha\alpha$	$\frac{-J_{13}}{2}$	$\frac{-J_{12}}{2}$	$\frac{1}{4}(J_{12}-J_{23}+J_{13})$

4.2

The relation between the N-electron wave-functions and energies and the matrix elements of expression 4.2, is provided by Bloch's effective Hamiltonian theory.[31] As mentioned before in equation 2.34, the Bloch's formula reads $\hat{H}_{eff}=\sum_k |P\Psi_k\rangle E_k \langle P\Psi_k|$ where $|P\Psi_k\rangle$ are the orthogonalized projections of the *ab initio* wave-functions onto the model space spanned by the M_s = 1/2 determinants, $|P\Psi_Q\rangle$, $|P\Psi_{D_1}\rangle$ and $|P\Psi_{D_2}\rangle$. There are several ways to project the *ab initio* wave-functions onto the model space. Here, we follow the method proposed by des Cloizeaux involving the $S^{-1/2}|P\tilde{\Psi}_k\rangle$ transformation,[32] where S is the overlap matrix of the projected wave-functions $|P\tilde{\Psi}_k\rangle$. The mapping of the $\hat{H}_{eff}$ matrix elements and the matrix elements of the model Hamiltonian shown in equation 4.2 give the *ab initio* values of J_{12}, J_{23} and J_{13}.

Results and discussion

Firstly, the local character of the magnetic coupling is discussed. The smallest subunits that can be used to extract the

nearest neighbour magnetic coupling parameters are the three binuclear systems marked as A, B and C in Figure 4.10. The extension of these units with an extra magnetic centre allows us to answer two questions: (i) Can the next nearest neighbour interaction be neglected in the simulation of the macroscopic magnetic behaviour, and (ii) is a binuclear cluster large enough to accurately determine the nearest neighbour interaction. Figure 4.11 defines the six different interaction parameters that have been studied to describe the magnetic topology of the system. The binuclear clusters A, B, and C contain the interactions J_{12}, J_{13} and J_{14}, respectively. The trinuclear system AB contains the copper atoms 1, 2 and 3, and we calculate J_{12}, J_{13} and J_{23} for this cluster. System AC with copper atoms 1, 2 and 4 allows us to determine J_{12}, J_{14} and J_{24}. Finally, we can extract J_{13}, J_{14} and J_{34} from the three-centre cluster BC involving the copper atoms 1, 3 and 4.

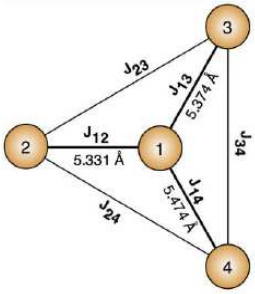

Figure 4.11. Schematic representation of the nearest and next nearest magnetic interactions in a subunit of the catena structure containing three connected copper-copper dimers. Copper-copper distances in the subunits are given in Ångstrom.

Table 4.1 lists the results obtained for the three binuclear clusters using different approximations for the N-electron wave-function and the Table compares the different basis sets and the influence of the modeling of the external ligands. Several conclusions can be drawn for the Table. In the first place, it is

obvious that the quality of the small basis set is good enough for comparing the two- and three-centre clusters. The differences in the calculated J-values with DDCI are due to the f function on Cu that artificially lowers the antiferromagnetic coupling in these systems.[16] Secondly, we observe an unexpected influence of the modeling of the external ligands by H_2O molecules instead of the real oxalato ions. In earlier applications to Ni(II)-based systems, the perfect agreement between H_2O and oxalato external ligands was found.[33] Given this difference between H_2O and oxalato external ligands, it would be preferable to use the oxalato ions as external ligands in the three-centre cluster. Nevertheless, this leads to a computational problem of inaccessible size and we opted to use H_2O ligands for the comparison.

Table 4.1. Magnetic coupling parameters (in cm^{-1}) obtained from binuclear clusters at different approximation to the N-electron wave-function.

Cluster	J	Basis	Ext. Ligand	CASPT2	DDCI	CAS_{ext}/DDCI2
A	J_{12}	1	H_2O	-56.2	-113.4	-138.7
	J_{12}	1	Oxalato	-48.1	-81.1	-103.7
	J_{12}	2	Oxalato	-53.3	-64.8	-118.7
B	J_{13}	1	H_2O	-40.2	-80.5	-106.3
	J_{13}	1	Oxalato	-31.3	-54.7	-79.2
	J_{13}	2	Oxalato	-36.2	-44.4	-91.7
C	J_{14}	1	H_2O	-4.6	-3.7	-3.2
	J_{14}	1	Oxalato	-2.8	-4.4	-3.3
	J_{14}	2	Oxalato	-5.3	-4.0	-4.7

The third conclusion concerns the comparison of the CASPT2 and DDCI results. For clusters A and B, we observe that CASPT2 gives a smaller value for the coupling than the two DDCI variants. This underestimation of CASPT2 finds its origin in the

application of a reference wave-function without ligand-to-metal charge-transfer (LMCT) configurations. The perturbative treatment of the electron correlation is not sufficient to account for these important LMCT configurations, which leads to an underestimation of the coupling.[8] The variational treatment of these configurations by DDCI and CAS_{ext}/DDCI2 gives a more complete description of the LMCT process and produces more accurate estimates of J. The CAS_{ext}/DDCI2 method reasonably reproduces the DDCI values, albeit larger in (almost) all cases. This is the expected behaviour and is well documented in the literature.[15,34] The lack of some specific ferromagnetic contributions to the wave-function in CAS_{ext}/DDCI2 leads in general to a slight overestimation of the J values. Finally, we notice that J_{12} and J_{13} are of the same magnitude, while J_{14} is much smaller. This will be discussed in more detail below.

The results on the trinuclear systems are resumed in Table 4.2. Only DDCI and CASext/DDCI2 results are included since the determination of the J values at the CASPT2 level is not possible. As explained above, the extraction of the J's in the trinuclear clusters requires the information from both the energy and the wave-function. The latter information is not available for CASPT2.

The Table 4.2 clearly shows that the next-nearest neighbour interactions can possibly be neglected, since the absolute value of this interaction is smaller than 5 cm^{-1} in all cases. Furthermore, we observe that the estimates of the coupling between two copper ions extracted from different clusters is rather similar and that the coupling parameters J_{12} and J_{13} are of the same order of magnitude, while J_{14} is much smaller as was already found for the dinuclear complexes. The comparison of the parameters with those obtained in the smaller clusters shows some, at first sight unexpected, differences. For example, the DDCI value of J_{13} is -80.5 cm^{-1} calculated in the dinuclear cluster using H_2O as external ligand. The same interaction extracted from a trinuclear

cluster with H_2O external ligands is -65.2 or -69.7 cm^{-1} for the AB and BC clusters, respectively. This difference between two- and three centre cluster is significantly larger than observed in other studies of the cluster size dependence.[35,36,37,38]

Table 4.2. Nearest neighbour and next nearest neighbour magnetic coupling parameters (in cm^{-1}) calculated from three different trinuclear clusters.

Cluster	J	DDCI	CAS_{ext}/DDCI2
AB	J_{12}	-80.3	-91.8
	J_{13}	-65.2	-83.0
	J_{23}	-3.3	0.6
AC	J_{12}	-77.0	-103.3
	J_{14}	-2.7	-2.3
	J_{24}	0.9	0.7
BC	J_{13}	-69.7	-87.4
	J_{14}	-4.1	-4.1
	J_{34}	0.0	0.0

The explanation lies in the fact that the central Cu(II) ion in the three centre clusters has a different surrounding (two oxalato ligands and one H_2O) than in the two centre clusters (one oxalato and two H_2O). Given the observation that the use of oxalato ligands as external ligands tends to lower the absolute value of J (see Table 4.1), it is not surprising to see a weaker magnetic coupling in the three-centre clusters compared to the two-centre ones with H_2O external ligands and similar or slightly stronger than the two-centre clusters with oxalato external ligands.

In summary, the magnetic coupling parameters extracted from the dinuclear complexes with oxalato external ligands can be considered not to be largely affected by the modeling of the extended material with a cluster model. The cluster size effects

are small when the correct (*i.e.* oxalato) external ligands are used. In the following, we will base our discussion of the magnetic topology of the material on the DDCI values listed in Table 4.1 for the clusters with oxalato external ligands using basis 1. Note that the conclusions will not be altered significantly if we take a set of J values obtained with one of the other methods.

The magnetic topology of compound is the second subject to be discussed. The relative magnitude of the different J-values define the magnetic structure of the crystal. As mentioned in the previous paragraphs, the material has two dominant magnetic interaction of approximately equal strength and one additional weak interaction. The key to the explanation of this observation lie in the magnetic orbitals and and the relative orientation of these along the magnetic interaction paths,[1,2,39,40] as mentioned in section 4.1.2. Figure 4.12 presents the magnetic orbitals for the dinuclear clusters. In cluster A, from which J_{12} is extracted, both magnetic orbitals lie in the plane of the bridging oxalato ligand. Following the reasoning of the Kahn-Briat model,[41] this orientation leads to an optimal overlap of the non-orthogonal localized magnetic orbitals, maximizing the magnetic coupling. The Hay-Thibeault-Hoffmann model[42] relates J with the difference in orbital energy of the magnetic orbitals. The in-plane orientation leads to maximum interaction of the magnetic orbitals with the orbitals on the bridge, and hence, a large difference in the orbital energy. The same reasoning holds for cluster B. The orientation of the magnetic orbitals is similar as in cluster A and therefore the interaction J_{13} is of similar magnitude as J_{12}. The small differences may be explained by the slightly larger distance between the magnetic centres in cluster B and the less planar oxalato-bridge.

UNIVERSITAT ROVIRA I VIRGILI
THE CALCULATION OF THE THERMAL DEPENDENCY OF THE MAGNETIC SUSCEPTIBILITY
IN EXTENDED SYSTEMS WITH AB INITIO ELECTRONIC STRUCTURE PARAMETERS
Igor Negodaev
ISBN:978-84-694-2171-0/DL:T. 1032-2011

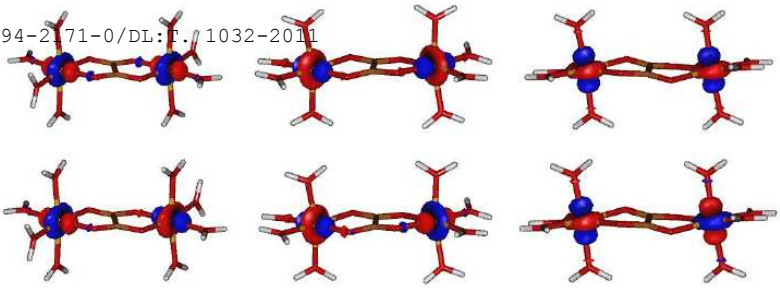

Figure 4.12. CASSCF optimized magnetic orbitals for the dinuclear cluster A (left), B (middle) and C (right) with H_2O external ligands. Similar orbitals were obtained for the clusters with oxalato external ligands.

The situation is entirely different in cluster C used to calculate J_{14}. The shortest Cu-O distances are found perpendicular to the oxalato plane. This leads to a parallel orientation of the magnetic orbitals with almost no overlap and weak metal-bridge interaction, explaining the small J value obtained for cluster C.

With the calculated J-values at hand, we can determine the magnetic structure of the compound. Figure 4.13 plots the magnetic topology by connecting the Cu(II) ions with the corresponding J_{12}, J_{13} and J_{14}. Except for one Cu(II) ion, the oxalato ligands are removed for clarity. The stronger interactions J_{12} and J_{13} are represented by solid lines while the weak J_{14} is drawn as a dashed line. From this drawing, it is clear that the magnetic topology is best characterized as an alternating 1D chain compound with weak interchain interactions. The magnetic chains are located in the xz-plane of the crystal.

The next step in the procedure is the calculation of the temperature dependence of the magnetic susceptibility with a strategy outlined before. Two magnetic models were compared. The first one is a one-dimensional model that only considers J_{12} and J_{13}, *i.e.* an alternating chain model. The second one (drawn in

Figure 4.14) reproduces the 3D magnetic structure containing alternating chains connected through J_{14}. We apply periodic boundary conditions in both models to minimize the finite size effects on the magnetic susceptibility. The complete diagonalization of the Heisenberg Hamiltonian is still affordable for magnetic clusters with 16 S=1/2 centres, larger clusters lead to matrix dimensions that make the diagonalization procedure extremely CPU-time consuming.

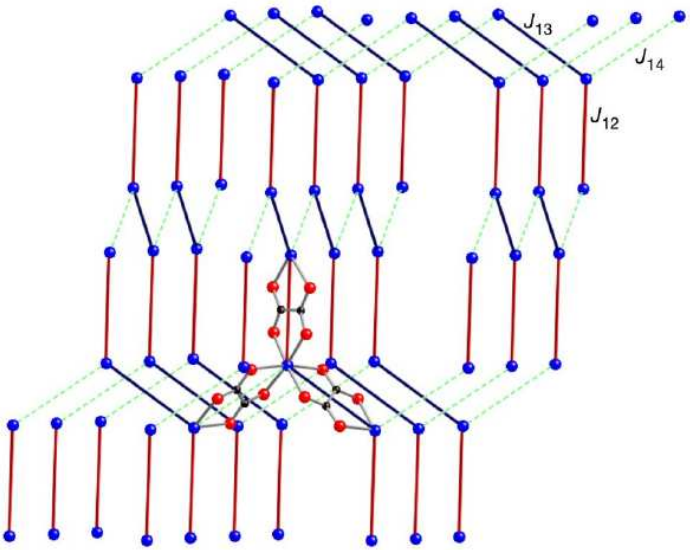

Figure 4.13. Magnetic topology of Catena-μ-Tris[oxalato(2-)-O^1,O^2;O^3,O^4]-dicopper. Blue spheres represent Cu, while all oxalato ligands are omitted, except for one Cu ion. Solid lines represent the strong magnetic couplings (Red = J_{12} ; Dark Blue = J_{13}), the dashed green line is the weak interaction J_{14}.

For systems with elevated magnetic moments the number of centres that can be considered is smaller. We have checked the stability of the results obtained with the one-dimensional model by

reducing the number of centres. We observed extremely small differences for these smaller models. For shorter chains, the maximum in the magnetic susceptibility shifts to higher temperatures by less than 1 K, which is irrelevant given the uncertainty in the calculated magnetic coupling constants.

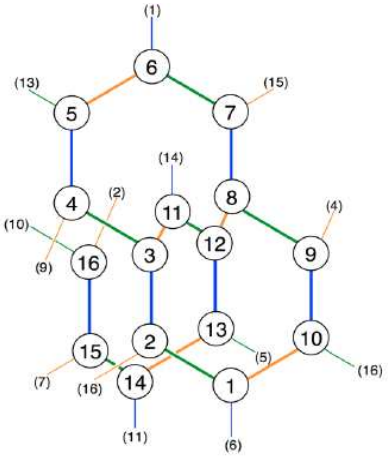

Figure 4.14. Three-dimensional magnetic 16-centre model. The numbers in parentheses indicate how the periodic boundary conditions are applied. Blue lines represent J_{12} =-81.1 cm^{-1}; Green lines represent J_{13} = -54.7 cm^{-1}; Orange lines represent J_{14} = -4.4 cm^{-1}.

Figure 4.15 presents the theoretical estimate of the magnetic susceptibility of the studied structure. No experimental data have been published so far, hence we cannot make a direct comparison. The smallness of J_{14} makes that the estimates of $\chi(T)$ in both magnetic models is rather similar. Both the maximum in the susceptibility and the overall shape of the curve are not affected by the interchain interaction. Note, however, that the existence of J_{14} is essential for the presence at low temperatures, since a true 1D magnetic system cannot have long range magnetic order at any finite temperature.[43]

UNIVERSITAT ROVIRA I VIRGILI
THE CALCULATION OF THE THERMAL DEPENDENCY OF THE MAGNETIC SUSCEPTIBILITY
IN EXTENDED SYSTEMS WITH AB INITIO ELECTRONIC STRUCTURE PARAMETERS
Igor Negodaev
ISBN:978-84-694-2171-0/DL:T. 1032-2011

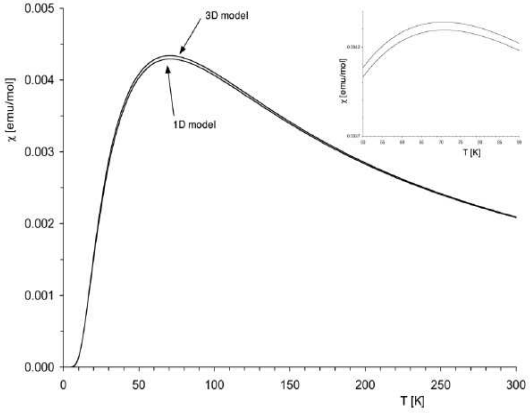

Figure 4.15. Thermal dependency of the magnetic susceptibility calculated with 1D and 3D magnetic models. The inset zooms in on the region around the maximum.

Conclusion

A strategy has been described for the determination of the temperature dependence of the magnetic susceptibility starting from the calculation of the magnetic coupling strength in oxalato-bridged structures with transition metal atoms as magnetic centres. In this work, we apply this strategy to the first synthesized compound of this kind, but can also be applied to the magnetic layers in bifunctional materials which are similar to the structure investigated here. In the first place, we have established that the interactions between next nearest neighbours can be neglected and that the minimal magnetic unit to obtain reliable estimates of J is a binuclear cluster with preferable oxalato ligands as external ligands. The magnetic topology of the structure has been explored and found to best fit the alternating chain description augmented with weak interchain interactions.

ISBN:978-84-694-2171-0/DL:T. 1032-2011

The comparison of the different computational schemes to estimate J shows that CASPT2 based on a minimal active space underestimates the coupling. The results obtained with CAS_{ext}/DDCI2 slightly overestimates the coupling in comparison to those at the full DDCI level, the latter being well established as an accurate, but expensive computational method for calculating energy differences between electronic states involved in the magnetic coupling process. Therefore, the CAS_{ext}/DDCI2 methodology can be applied to other 3D extended structures for magnetic coupling constant calculations, especially interesting when the number of unpaired electrons per magnetic sites increases and DDCI becomes infeasible.

The results of the extraction of χ(T) may serve as a guideline for the interpretation of a experimental determination of the magnetic susceptibility in the compound studied and the strategy can also be applied to clarify the magnetic behaviour in other, related materials.

4.2.2 Hexagonal lattices

As mentioned before, a special group is constituted by the two-dimensional oxalato-bridged networks of TMs. The magnetic centres form a hexagonal lattice as shown in Figure 4.16 with (anti-)ferromagnetic inter-site coupling. The calculation of the magnetic coupling strength between the TM ions in the hexagonal oxalato-bridged lattices follows to a large extent the same procedure as for the molecular complexes. We study three different clusters cut from the lattice (see Figure 4.16), since there are three slightly different magnetic pathways in the compounds reported by Duan et al.[4] These clusters contain the two TM ions, the oxalato bridge and the four external oxalato ligands that take the role of external ligand. We have tested this

representation against a model in which the cluster is embedded in a set of point charges and pseudopotentials for the nearby TM ions. In line with previous findings, the latter representation gives virtually the same results as the isolated fragments. The J for the systems with two Cu(II) ions is obtained as outlined before. In the hexagonal lattices with Ni, Co and Fe, the Heisenberg spectrum contains more states. Following the conclusions of Queralt *et al.*[9] we used the lowest two states of the Heisenberg spectrum to calculate J.

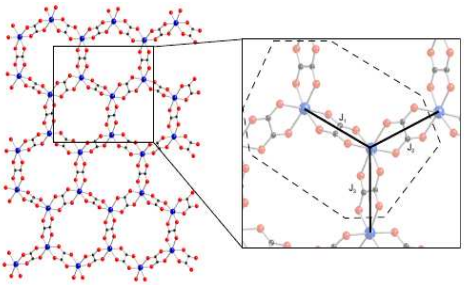

Figure 4.16. Left: Hexagonal, oxalato-bridged transition metal lattice. Larger Blue spheres are the TM ions, Red is oxygen and Black is carbon. Right: Zoom on the hexagonal lattice showing the three interaction paths (thick lines) and the cluster used to calculate one of the coupling parameters (enclosed by the dashed line).

The orientation of the magnetic orbital in the Cu-oxal lattice only leads to a certain overlap of the magnetic orbitals on neighbouring centres along the J_2 pathway (see Figure 4.17 a). For the other two magnetic pathways the relative orientation of the orbitals is a combination of in-plane and out-of-plane orientations as shown in Figure 4.2 b. This is reflected in the three different J-values that we obtain for this hypothetical lattice: $J_2 > J_1 \approx J_3$. Since there are two, mutually orthogonal, open-shell orbitals per

magnetic centre in the Ni-oxal lattice, the overlap of magnetic orbitals in all three directions is similar (see Figure 4.17 b) and leads to three nearly identical J values, see Table 4.3. Magnetic coupling strengths are similar in the Co(II) lattice and significantly smaller in the lattice with Fe ions. Magnetic orbitals are plotted in Figure 4.17 c, d. This gradual decrease of J with decreasing atomic number is not unexpected and can be explained by the decreasing electron affinity going to the left in the first-row of TM ions in the periodic table. These values are obtained with CASPT2 based on a minimal active space. Therefore, the values are subject to a (small) underestimation, which is more important for the Cu-based material than for Fe-oxal as ligand-to-metal charge transfer effects have larger effects on the coupling between Cu(II) ions than the less electronegative Fe(II) ions.[21]

Table 4.3. CASPT2 magnetic coupling parameters (in cm^{-1}) in TM-oxal lattices.

	Fe	Co	Ni	Cu
Unit 1	-3.8	-11.6	-10.7	-6.8
Unit 2	-5.5	-19.1	-10.5	-23.4
Unit 3	-3.8	-11.5	-10.3	-5.0

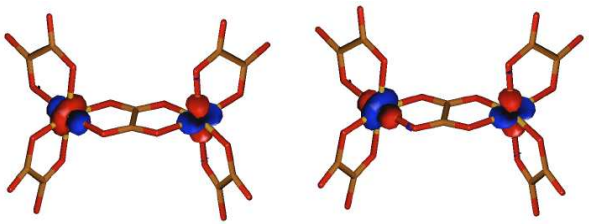

a

Figure 4.17. CASSCF optimized magnetic orbitals of TM-oxal systems. a) TM = Cu; b) TM = Ni; c) TM = Co; d) TM = Fe.

UNIVERSITAT ROVIRA I VIRGILI
THE CALCULATION OF THE THERMAL DEPENDENCY OF THE MAGNETIC SUSCEPTIBILITY
IN EXTENDED SYSTEMS WITH AB INITIO ELECTRONIC STRUCTURE PARAMETERS
Igor Negodaev
ISBN:978-84-694-2171-0/DL:T. 1032-2011

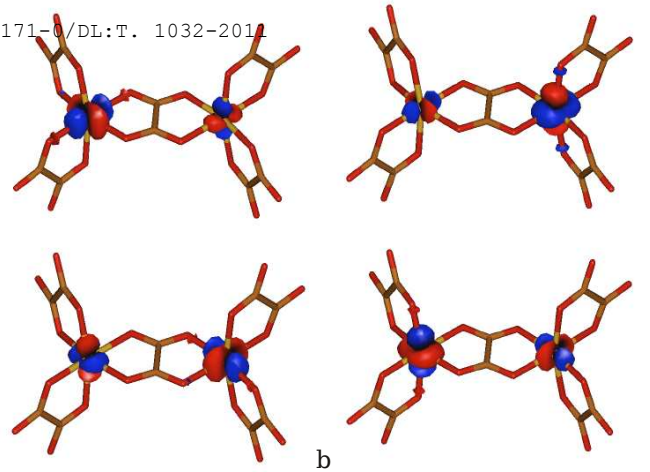

b

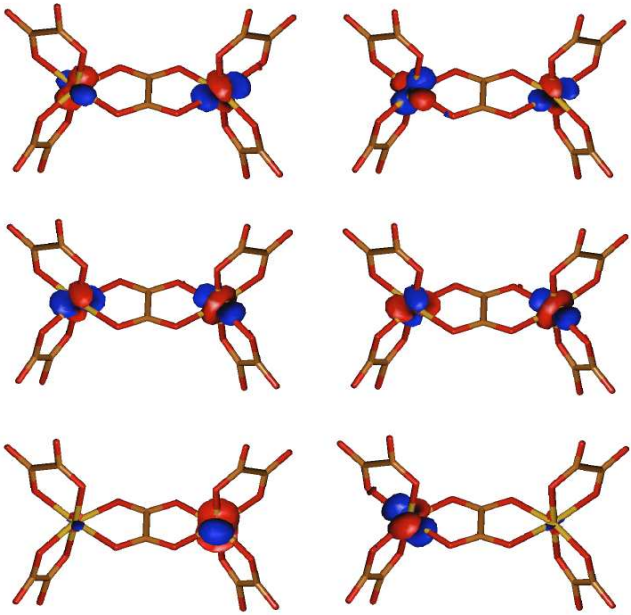

c

Figure 4.17. Continuation.

UNIVERSITAT ROVIRA I VIRGILI
THE CALCULATION OF THE THERMAL DEPENDENCY OF THE MAGNETIC SUSCEPTIBILITY
IN EXTENDED SYSTEMS WITH AB INITIO ELECTRONIC STRUCTURE PARAMETERS
Igor Negodaev
ISBN:978-84-694-2171-0/DL:T. 1032-2011

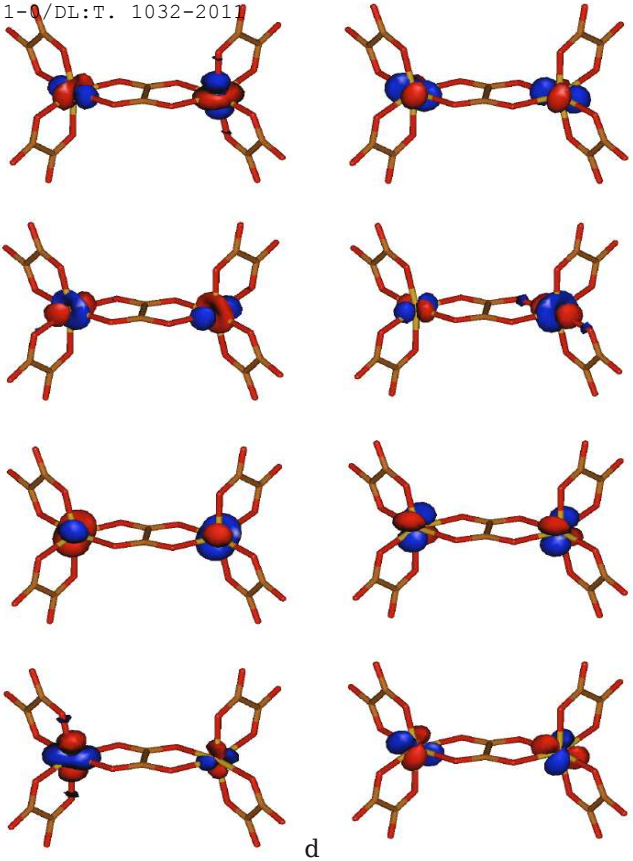

Figure 4.17. Final.

The magnetic topology of the hexagonal lattices needs an additional testing for finite size effects. Cu-oxal is an excellent candidate for this purpose given that models can be built with 16 magnetic centres. The elevated spin moment for the other TM-oxal lattices makes that the dimension of the Heisenberg Hamiltonian increases very fast with increasing model size and even for Ni-oxal it is not possible to diagonalize the Hamiltonian of the 16-centre model. Figure 4.18 shows the three models that we

have considered to study the finite size effects. The encircled numbers represent centres of the models, while the numbers in parenthesis indicate how the periodic boundary conditions are fulfilled.

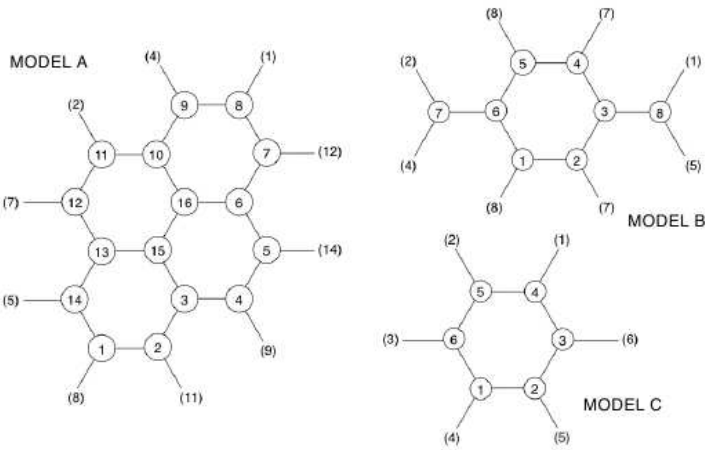

Figure 4.18. Three models used to calculate the magnetic susceptibility in the hexagonal oxalato-bridged TM lattices. Numbers in parenthesis show how the periodic boundary conditions are introduced in the model.

The χ(T) curves obtained with the three models are nearly identical (see Figure 4.19). For higher temperatures the three curves are indistinguishable and only near the maximum in the curve found around 22 K, there are small differences between the largest (A) and the smallest (C) model. The maximum deviation between Model A and Model C is $0.7 \cdot 10^{-3}$ cm^3/mol, which can be considered to be negligible, considering the precision in the calculated J's. Note, however, that we cannot exclude the possibility that finite size effects are more significant for the hexagonal lattices with larger spin moments.

UNIVERSITAT ROVIRA I VIRGILI
THE CALCULATION OF THE THERMAL DEPENDENCY OF THE MAGNETIC SUSCEPTIBILITY
IN EXTENDED SYSTEMS WITH AB INITIO ELECTRONIC STRUCTURE PARAMETERS
Igor Negodaev
ISBN:978-84-694-2171-0/DL:T. 1032-2011

The calculation of the dependence of the magnetic susceptibility on the temperature has been performed with model B for the hexagonal lattices with TM=Cu, Ni, Co, and Fe. The results are presented in Figure 4.19 and compared to the experimental curves of Duan and co-workers[4] for Fe-oxal and Co-oxal. The Ni and Cu based lattices are hypothetical model systems and have been added for comparison.

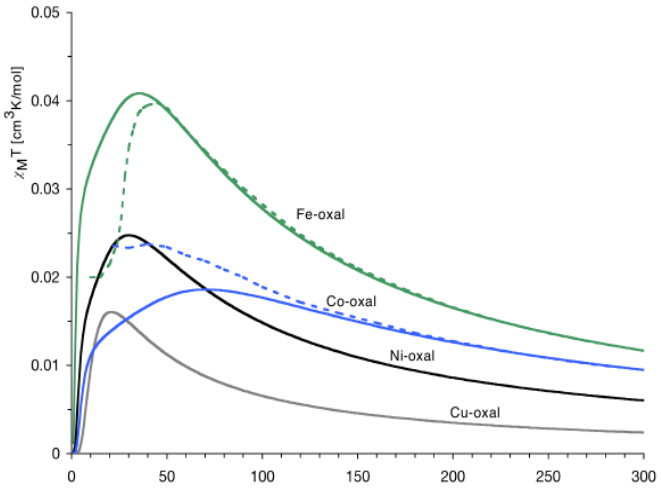

Figure 4.19. Magnetic susceptibility curves for four different hexagonal, oxalato-bridged TM layers. Full lines represent the calculated curves, dotted lines are the experimental curves.[4]

The first observation is that the magnetic susceptibility at higher temperatures gradually increases with the spin moment localized on the TM ions as expected and the accompanying decrease in the coupling between these moments from Cu to Ni/Co to Fe. In the second place, we observe a rather good agreement between the calculated curve for Fe-oxal using the CASPT2 J values and the experimental magnetic susceptibility. The maximum in the curve obtained by diagonalizing the Heisenberg Hamiltonian with the calculated J lies at 35 K, while

the maximum in the experimental curve is found around 44 K. This discrepancy can be attributed to the small underestimation of the coupling obtained with CASPT2 based on a minimal active space, some corrections that should be applied to the experimental curve (impurities and TIP), and probably finite size effects in the model used for the diagonalization.

This establishes the magnetic coupling strength between the Fe(II) ions in the hexagonal oxalato-bridged lattices to be of the order of -5 cm^{-1} to -10 cm^{-1}, see Table 4.3. On the other hand the comparison between the experimental and calculated χ curve for Co-oxal is less favourable. The maximum in the theoretical curve (71 K) deviates significantly from the maximum in the experimental magnetic susceptibility (~30 K). The main reason for this difference is the neglect of the spin-orbit coupling in the theoretical determination of χ. The nearly octahedral environment of the Co(II)-$3d^7$ ions in the hexagonal lattices lead to strong magnetic anisotropy and spin-orbit coupling should be taken into account.

Finally, we compare our theoretical estimates to those obtained from the expression to relate $\chi(T)$ to $J_1 > J_2 = J_3$ in a hexagonal lattice proposed by Curély and co-workers:[44]

$$\chi = \frac{g^2}{3kT}\frac{(1+u_1u_2)^2(1+u_2^2)+2u_2(1+u_1u_2)^2+u_1(1-u_2^2)^2}{(1-u_1^2u_2^2)(1-u_2^2)} \qquad 4.3$$

with

$$u_i = \coth\left(\frac{S(S+1)J_i}{kT}\right) - \frac{kT}{S(S+1)J_i} \qquad 4.4$$

Here, g is the Landé factor and k the Boltzmann constant. In the original publication, the authors indicate that J_i should be multiplied by a normalization factor S(S+1) to take into account that the spins are treated in a classical way in the derivation of equation 4.3.[45,46,47] However, it appears from the literature that

this criterion is not universally followed in the fitting procedures. Apparently no scaling factor was used in the fitting of the magnetic susceptibility by Wang and co-workers[48]. The comparison of the two strategies is made in Table 4.4, where we list the temperature for which χ reaches a maximum (T_{max}) for the four hexagonal lattices considered.

Table 4.4. Temperature (in K) for which the magnetic susceptibility reaches a maximum in hexagonal lattices obtained from diagonalization of the Heisenberg Hamiltonian or through the theoretical expression proposed by Curély and co-workers.

Lattice	Spin	Heisenberg	Curély et al.[44]
Fe-oxal	2	35	41
Co-oxal	3/2	74	84
Ni-oxal	1	29	32
Cu-oxal	1/2	20	14
Cu-oxal	1/2		19[a)]

a) Calculated without the S(S+1) scaling factor in front of J in equation 4.3.

The estimates of T_{max} are in general reasonably similar in the two approaches. The lattice with S = 2 spins (Fe-oxal) is the best approximation to the classical spin limit for which the Curély expression was derived. The slightly lower value of T_{max} obtained by diagonalization of the Heisenberg Hamiltonian in this lattice may partially be due to the fact that one can only use the relatively small model B in the diagonalization procedure. On the other hand, for the S = 1/2 lattice (Cu-oxal), the approximation of classical spins is less valid, making the application of the Curély expression problematic. In fact, we obtain very good agreement

ISBN:978-84-694-2171-0/DL:T. 1032-2011

with the diagonalization method by removing the S(S+1) factor from the expression. Not only T_{max} is the same in both approaches, but also the overall shape of the $\chi(T)$ curve is similar in both methods. The curves of thermal dependency of the magnetic susceptibility for TM-oxal systems obtained by diagonalization of Heisenberg Hamiltonian and applying Curély expression are presented on Figures 4.20 – 4.23.

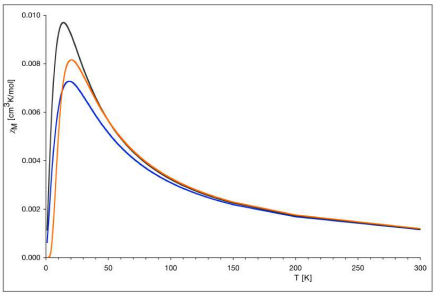

Figure 4.20. χ(T) curve for Cu-oxal obtained by diagonalization of the Heisenberg Hamiltonian (Orange) and the Curély expression with k·J = S(S+1)J = 3/4 J (Dark Grey); k·J = 1·J (Blue). Model A was used in the diagonalization procedure. J_1=-23, J_2=J_3=-5 cm^{-1}.

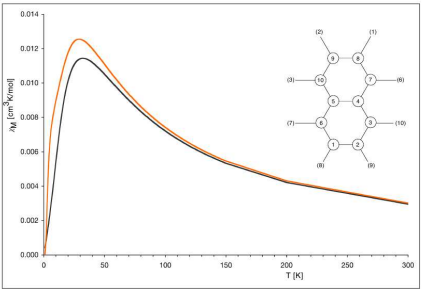

Figure 4.21. χ(T) curve for Ni-oxal obtained by diagonalization of the Heisenberg Hamiltonian (Orange) and the Curély expression with k·J = S(S+1)J = 2 J (Dark Grey). A 10-centre (see inset) was used in the diagonalization procedure. J_1=J_2=J_3=-10.5 cm^{-1}. No significant cluster size effects were found comparing the diagonalization of the 10-centre and 8-centre (model B) cluster. T_{max} differs by 1 K for both clusters.

UNIVERSITAT ROVIRA I VIRGILI
THE CALCULATION OF THE THERMAL DEPENDENCY OF THE MAGNETIC SUSCEPTIBILITY
IN EXTENDED SYSTEMS WITH AB INITIO ELECTRONIC STRUCTURE PARAMETERS
Igor Negodaev
ISBN:978-84-694-2171-0/DL:T. 1032-2011

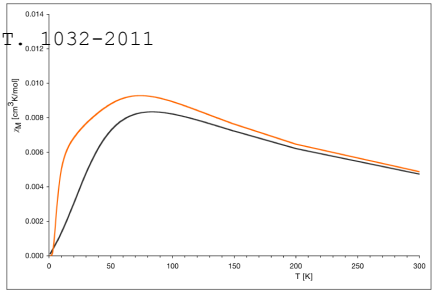

Figure 4.22. χ(T) curve for Co-oxal obtained by diagonalization of the Heisenberg Hamiltonian (Orange) and the Curély expression with k·J = S(S+1)J = 15/4 J (Dark Grey). Model B was used in the diagonalization procedure. J_1=-19.1 and J_2=J_3=-11.5 cm^{-1}.

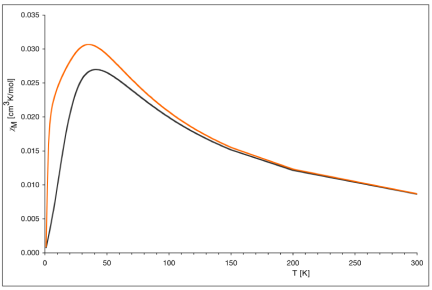

Figure 4.23. χ(T) curve for Fe-oxal obtained by diagonalization of the Heisenberg Hamiltonian (Orange) and the Curély expression with k·J = S(S+1)J = 6J (Dark Grey). Model B was used in the diagonalization procedure. J_1=-5.5 and J_2=J_3=-3.8 cm^{-1}.

In summary, we conclude that the diagonalization method and the Curély expression predict the same behaviour of the magnetic susceptibility in hexagonal lattices. The latter is probably preferable for lattices with high spin moments since finite size effects do not play a role in this method, while the diagonalization of the Heisenberg Hamiltonian is the best choice for lattice with smaller spin moments.

ISBN:978-84-694-2171-0/DL:T. 1032-2011

The magnetic coupling strength of the spin moments localized on the TM centres in hexagonal lattices is addressed by *ab initio* calculations of relevant fragments containing two TM ions and the ligands coordinating them. The calculated J values were used to construct a Heisenberg Hamiltonian of a larger model with either 6, 8 or 16 centres with periodic boundary conditions. By diagonalizing the Heisenberg Hamiltonian of this larger model, we obtain an energy spectrum from which the magnetic susceptibility can be calculated through standard statistical mechanics. The temperature dependence of the magnetic susceptibility is compared to experimental measurements of this quantity. Before applying the method to the hexagonal lattices, we first applied it to a series of compound containing Cu(II) ions (section 4.1) in different topologies.

In the case of the hexagonal lattice with Fe(II) ions the comparison between experiment and theory is good, validating the calculated J values of approximately -5 to -10 cm^{-1} . For the compound with Co(II) ions the calculated $\chi(T)$ curve agrees to a lesser extent with the experimental one due to the important magnetic anisotropy effects. The method can now be applied to the hexagonal lattices that form part of the bifunctional materials and can be considered to be an interesting alternative to calculate J-values instead of the use of the analytical expression of Curély and co-workers.

ISBN:978-84-694-2171-0/DL:T. 1032-2011

4.3 References

1 Castillo, O.; Luque, A.; Lloret, F.; Román, P. Inorg. Chem. Commun. 2001, 4, 350.

2 Castillo, O.; Luque, A.; Julve, M.; Lloret, F.; Román, P. Inorg. Chim. Acta 2001, 315, 9.

3 Du, M.; Guo, Y.-M.; Chen, S.-T.; Bu, X.-H.; Ribas, J. Inorg. Chim. Acta 2003, 346, 207.

4 Duan, Z.; Zhang, Y.; Zhang, B.; Pratt, F. L. Inorg. Chem. 2009, 48, 2140.

5 Andersson, K.; Malmqvist, P.-Å.; Roos, B. O.; Sadlej, A. J.; Wolinski, K. J. Phys. Chem. 1990, 94, 5483.

6 Andersson, K.; Malmqvist, P.-Å.; Roos, B. O. J. Chem. Phys. 1992, 96, 1218.

7 Karlström, G.; Lindh, R.; Malmqvist, P.-Å.; Roos, B.O.; Ryde, U.; Veryazov, V.; Widmark, P.-O.; Cossi, M.; Schimmelpfennig, B.; Neogrady, P.; Seijo, L. Comput. Mater. Sci. 2003, 28, 222.

8 de Graaf, C.; Sousa, C.; de P. R. Moreira, I.; Illas, F. J. Phys. Chem. A 2001, 105, 11371.

9 Queralt, N.; Taratiel, D.; de Graaf, C.; Caballol, R.; Cimiraglia, R.; Angeli, C. J. Comp. Chem. 2008, 29, 994.

10 Forsberg, N.; Malmqvist, P.-Å. Chem. Phys. Lett. 1997, 274, 196204.

11 Miralles, J.; Daudey, J.-P.; Caballol, R. Chem. Phys. Lett. 1992, 198, 555.

12 Miralles, J.; Castell, O.; Caballol, R.; Malrieu, J.-P. Chem. Phys. 1993, 172, 33.

13 Ben Amor, N.; Maynau, D. Chem. Phys. Lett. 1998, 286, 221.

14 Gellé, A.; Munzarová, M.; Lepetit, M. B.; Illas, F. Phys. Rev. B 2003, 68, 125103.

15 Bordas, E.; Caballol, R.; de Graaf, C.; Malrieu, J.-P. Chem. Phys. 2005, 309, 259.

16 Muñoz, D.; de Graaf, C.; Illas, F. J. Comp. Chem. 2004, 25, 1234.

17 Ruiz, E.; Alvarez, S.; Rodríguez-Fortea, A.; Alemany, P.; Pouillon, Y.; Massobrio, C. Electronic structure and magnetic behaviour in polynuclear transition-metal complexes. In Magnetism: Molecules to Materials II; Miller, J. S., Drillon, M., Eds.; Wiley-VCH, 2001; Chapter 7, 227.

18 Bonner, J. C.; Fisher, M. E. Phys. Rev. 1964, 135, A640.

19 Angeli, C.; Calzado, C. J.; Cimiraglia, R.; Malrieu, J.-P. J. Chem. Phys. 2006, 124, 234109.

20 Hall, J. W.; Marsh, W. E.; Weller, R. R.; Hatfield, W. E. Inorg. Chem. 1981, 20, 1033.

21 Coronado, E.; Galán-Mascarós, J. R.; Gómez-Garcia, C. J.; Laukhin, V. Nature 2000, 408, 447.

22 Coronado, E.; Galán-Mascarós, J. R.; Gómez-Garcia, C. J.; Ensling, J.; Gütlich, P. Chem. Eur. J. 2000, 6, 552.

23 Bénard, S.; Yu, P.; Audière, J. P.; Rivière, E.; Clément, R.; Guilhem, J.; Tchertanov, L.; Nakatami, K. J. Am. Chem. Soc. 2000, 122, 9444.

24 Bénard, S.; Rivière, E.; Yu, P.; Nakatami, K.; Delouis, J. F. Chem. Mater 2001, 13, 159.

25 Hernández-Molina, M.; Lloret, F.; Ruiz-Pérez, C.; Julve, M. Inorg. Chem. 1998, 37, 4131.

26 Andrés, R.; Gruselle, M.; Malézieux, B.; Verdaguer, M.; Vaissermann, J. Inorg. Chem. 1999, 38, 4637.

27 Pointillart, F.; Train, C.; Gruselle, M.; Villain, F.; Schmalle, H. W.; Talbot, D.; Gredin, P.; Decurtins, S.; Verdaguer, M. Chem. Mater. 2004, 16, 832.

28 Clemente-León, M.; Coronado, E.; López-Jordà, M.; Minués-Espallargas, G.; Soriano-Portillo, A.; Waerenborgh, J. C. Chem. Eur. J. 2010, 16, 2207.

29 Sundberg, M. R.; Kivekäs, R.; Koskimies, J. K. J. Chem. Soc., Chem. Commun. 1991, 526.

30 Queralt, N.; de Graaf, C.; Cabrero, J.; Caballol, R. Mol. Phys. 2003, 101, 2095.

31 Bloch, C. Nucl. Phys. 1958, 6, 329.

32 des Cloizeaux, J. Nucl. Phys. 1960, 20, 321.

33 Bordas, E.; Caballol, R.; de Graaf, C.; J. Mol. Struct. THEOCHEM, 2005, 727, 173.

34 Calzado, C. J.; Angeli, C.; Caballol, R.; Malrieu, J.-P. Theor. Chem. Acc. 2010, 126, 185.

35 Illas, F.; Moreira, I. de P. R.; de Graaf, C.; Castell, O.; Casanovas, J. J. Phys. Rev. B 1997, 56, 5069.

36 Calzado, C. J.; Malrieu, J.-P.; Phys. Rev. B 2001, 63, 214520.

37 de Graaf, C.; Illas, F.; Phys. Rev. B 2001, 63, 014404.

38 de Graaf, C.; Moreira, I. de P. R.; Illas, F.; Iglesias, Ò.; Labarta, A. Phys. Rev. B 2002, 66, 014448.

39 Cano, J.; Alemany, P.; Alvarez, S.; Verdaguer, M.; Ruiz, E. Chem. Eur. J. 1998, 4, 476.

40 Cabrero, J.; Ben Amor, N.; de Graaf, C.; Illas, F.; Caballol, R. J. Phys. Chem. A 2000, 104, 9983.

41 Kahn, O.; Briat, B. J. Chem. Soc. Faraday Trans. 1976, 72, 268.

42 Hay, P. J.; Thibeault, J. C.; Hoffmann, R. J. Am. Chem. Soc. 1975, 97, 4884.

43 Mermin, N. D.; Wagner, H. Phys. Rev. Lett. 1966, 17, 1133.

44 Curély, J.; Lloret, F.; Julve, M. Phys. Rev. B 1998, 58, 11465.

45 Georges, R.; Borrás-Almenar, J. J.; Coronado, E.; Curély, J.; Drillon, M. One-dimensional magnetism: An overview of the models. In Magnetism: Molecules to Materials; Miller, J. S., Drillon, M., Eds.; Wiley-VCH: Weinheim, 2001; Chapter 1, 1.

46 Armentano, D.; De Munno, G.; Lloret, F.; Julve, M.; Curély, J.; Babb, A. M.; Lu, J. Y. NewJ. Chem. 2003, 27, 161.

47 Armentano, D.; De Munno, G.; Guerra, F.; Julve, M.; Lloret, F. Inorg. Chem. 2006, 45, 4626.

48 Wang, X. T.; Wang, Z. M.; Gao, S. Inorg. Chem. 2007, 46, 10452.

UNIVERSITAT ROVIRA I VIRGILI
THE CALCULATION OF THE THERMAL DEPENDENCY OF THE MAGNETIC SUSCEPTIBILITY
IN EXTENDED SYSTEMS WITH AB INITIO ELECTRONIC STRUCTURE PARAMETERS
Igor Negodaev
ISBN:978-84-694-2171-0/DL:T. 1032-2011

Chapter 5

Magnetic coupling and anisotropy

UNIVERSITAT ROVIRA I VIRGILI
THE CALCULATION OF THE THERMAL DEPENDENCY OF THE MAGNETIC SUSCEPTIBILITY
IN EXTENDED SYSTEMS WITH AB INITIO ELECTRONIC STRUCTURE PARAMETERS
Igor Negodaev
ISBN:978-84-694-2171-0/DL:T. 1032-2011

ISBN:978-84-694-2171-0/DL:T. 1032-2011

The recent interest for systems with magnetic anisotropy is easily explained by the discovery of so-called single molecule magnets (SMMs).[1,2,3] Their ability to present two high spin states of different magnetization separated by an energy barrier provides new challenges in the study of quantum mechanics effects. In the first place, the bistability of the two high spin states with opposite M_s values makes these molecules suitable candidates for materials with all kind of interesting applications, in principle. Moreover, the in-plane anisotropy discovered in such systems leads to quantum tunnelling, which in its turn gives a possibility to study coherence and interference effects. Since the magnetic anisotropy plays a key role in the magnetic behaviour of a compound, the control over anisotropy parameters is really important to design materials with higher critical temperatures. Theory provides important relations with experiment by the interpretation of the experimental data using model Hamiltonians[4,5] and gives the possibility to derive magnetostructural correlations.[6,7] Therefore, this final chapter is devoted to the extension of the obtained experience on systems with magnetic anisotropy. We combine the calculation of J on a honeycomb layer in a mixed-valence vanadium-based system with the calculation of the anisotropy parameters of the V(III) centres. A simple estimate is given of the anisotropy on $\chi(T)$.

5.1 Calculations of the anisotropy parameters

The basic requirements for systems to act as SMM are a high spin ground state of spin moment S and a sizeable axial anisotropy characterized by an easy axis of magnetization and a negative axial zero-field splitting (ZFS) parameter D. In fact, these two factors lead to an energy barrier of $|D|\cdot S^2$ between the two

ISBN:978-84-694-2171-0/DL:T. 1032-2011

states of opposite magnetization. A positive D, gives rise to the rather uninteresting case of a singly degenerate M_s = 0 ground state. Moreover, it is important that the complex has a small rhombic anisotropy (characterized by the parameter E) to avoid excessive tunnelling effects through the barrier. Information about the ZFS parameters D and E can be traditionally obtained from different experimental techniques, where electron paramagnetic resonance (EPR) is one of the most relevant methods.[8,9] Theoretical attempts to calculate anisotropy parameters have been started in the last decade. Due to the large number of centres, most of the studies on SMMs use one- or two-component DFT based calculations.[10,11] The interpretation of the results is usually done within the framework of the giant spin Hamiltonian,[8] where only the global ZFS parameters of the whole system in its ground state are accessible, and all information about the coupling between the different magnetic centres is effectively treated. However, one can also approach the ZFS problem from the coupled-spin Hamiltonian.[12] Here, all local information is retained and both the magnetic coupling as the local anisotropy can be studied. Usually a N-electron wave-function approach is used, where the anisotropy can be addressed by perturbation theory[13] or variationally.[14,15] The method proposed by Maurice and co-workers[16] is based on the effective Hamiltonian theory. The procedure provides estimates of the ZFS parameters and determines the magnetic axes frame. In a first step, spin-orbit restricted active space state interaction (SO-RASSI) calculations are performed to determine the energies and wave-functions of the lowest electronic spin-orbit states. These solutions are then used to calculate the matrix elements of the effective Hamiltonian that exactly reproduces the *ab initio* results in a much smaller model space. More details and a validation of the method is given

ISBN:978-84-694-2171-0/DL:T. 1032-2011

in Ref. [16]. The comparison of this effective Hamiltonian and the commonly used spin-only model Hamiltonian directly leads to the determination of the ZFS parameters.

5.2 Computational information

5.2.1 Description of the material

The 2-D layered $\{[N(n\text{-}Bu)_4][V(II)V(III)(ox)_3]\}_n$ system (here $N(n\text{-}Bu)_4$ is tetra-n-butylammonium and ox is oxalate) synthesized by Min and co-workers[17] has been chosen as research object because the honeycomb structure of the vanadium-oxalate layers strongly resemble that of the bifunctional materials. The compound shows ferrimagnetic behaviour with relatively strong antiferromagnetic interactions in the 20-300K range. The magnetic susceptibility in this temperature range can be fitted with the expression of the Curie-Weiss law

$$\chi = C/(T-\Theta) \qquad 5.1$$

where C is the Curie constant and Θ is the Weiss temperature (or the Weiss constant) defined as

$$\Theta = \frac{zJS(S+1)}{3k} \qquad 5.2$$

where z is the number of magnetic neighbours. Here, Θ = -45 K and in principle a rough mean-field estimate of J can be derived from the Curie-Weiss law. Since the spin angular momentum on the two V centres is different, we calculated J for both extremes using S=3/2 and S=1. This leads to -12 K < J < -22.5 K. At lower temperatures, a spin glass behaviour is observed characterized by disordered spins in a frozen configuration. The V(III)-$3d^2$ electronic configuration is expected to give rise to sizeable magnetic anisotropy effects but no

experimental estimate has been published so far. Nevertheless, a precursor of the V(II)V(III) honeycomb structure was characterized in more detail in the article of Min *et al.*[17] This material, $K_3[V(III)(ox)_3]\cdot 3H_2O$, consists of $V(III)(ox)_3$ complexes, which are magnetically isolated from the other anions. The rather large D value of 5.53 K was explained by the nearly octahedral coordination sphere of the V ion. Hence, it can be expected that a similar anisotropy exists in the presently studied material that contains V(III) centres with a comparable coordination sphere.

As has been done for the extended structures described in the previous chapter, an adequate model should be defined to deal with the present 2D V(II)-V(III) layers. For the calculation of the magnetic coupling parameter, we define a V(II)-ox-V(III) fragment with oxalato anions as external ligands. Following the conclusions of the previous chapters, this representation is precise enough to give a reasonable estimate of J. There is only one unique V(II)-ox-V(III) magnetic path, the other two directions are identical due to the symmetry of the crystal structure, unlike the honeycomb structures discussed before. On the other hand, the anisotropy has been approached from a single-ion point of view and a fragment of one V(III) ion with three surrounding oxalate ligands has been used for calculating D and E.

The space group and cell parameters of $\{[N(n\text{-}Bu)_4][V(II)V(III)(ox)_3]\}_n$ were determined from X-ray diffraction[17] but to the best of our knowledge no experimental data has been published on the atomic positions in the unit cell. The structural analysis made by Min *et al.*[17] was based on IR frequency of the C-O stretch vibration of the oxalate ligands. However, the compound is isomorphous to $\{[N(n\text{-}Bu)_4][Mn(II)Fe(III)(ox)_3]\}_n$,[18] and we applied the missing structural data of the latter compound to construct the two centre fragments used for the calculation of J (see Figure 5.1). This strategy may look rather crude at first sight, but it should be

noticed that the ionic radius of six coordinated V(II) is close to that of Mn(II) (93 and 97 pm, respectively) and the ionic radius of V(III) is practically identical to Fe(III) (78.0 and 78.5 pm, respectively). Moreover, the unit cell parameters are rather similar in both compounds as shown in Table 5.1.

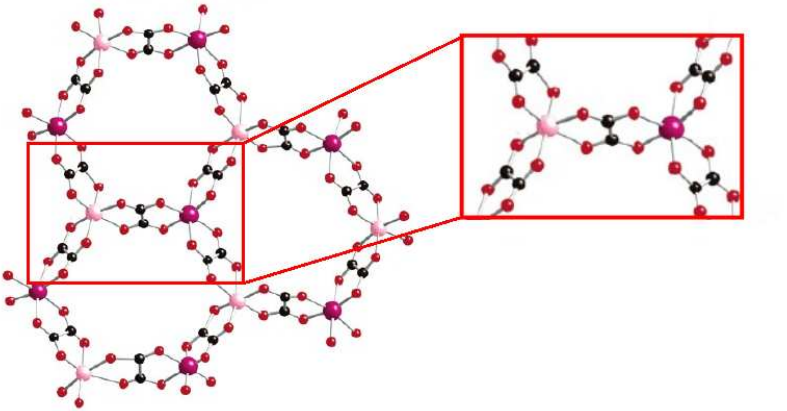

*Figure 5.1. {[N(n-Bu)4][V(II)V(III)(ox)3]}*n *system with a repeated structural motif. Pink: V(III); Violet: V(II); Red: oxygen; Black: carbon.*

Table 5.1. Comparison of crystallographic parameters for {[N(n-Bu)$_4$][V(II)V(III)(ox)$_3$]}$_n$ and {[N(n-Bu)$_4$][Mn(II)Fe(III)(ox)$_3$]}$_n$

	{[N(n-Bu)$_4$][V(II)V(III)(ox)$_3$]}$_n$[17]	{[N(n-Bu)$_4$][Mn(II)Fe(III)(ox)$_3$]}$_n$[18]
a, Å	9.394	9.428
b, Å	9.394	9.428
c, Å	17.710	17.827
α, °	90	90
β, °	90	90
γ, °	120	120

5.2.2 Computational details

ISBN:978-84-694-2171-0/DL:T. 1032-2011

In principle, one could apply the CAS_{ext}/DDCI2 approach to calculate the magnetic coupling of the two V ions. The reference wave-function is a CAS (5, 5) as in the Ni-ox-Cr complex studied previously.[19] However, the lower symmetry and the more bulky external ligand make these calculations computationally rather demanding. Moreover, CASPT2 based on a minimal active space is expected to reproduce the coupling with rather good accuracy. This is based on the fact that the LMCT configurations only get important for the late TM ions in the first row. For Ni and especially in the case of Cu, it is indispensable to give an accurate account of these LMCT configurations, while for Mn a minimal active space gives good results as for the Fe-ox-Fe fragment discussed in the previous chapter. Therefore, we opt for CASPT2 calculations only.

The one-electron basis set used before (Table 3.5) has been reduced to V(5s,4p,3d) / C,O(3s,2p,1d). Since there are two centres with $S_1 = 1$ and $S_2 = 3/2$, three total spin states are possible (S = 1/2, S = 3/2 and S = 5/2). J is estimated from the energy difference of the lowest two states in the spectrum as E(S=1/2)-E(S=3/2)=3/2 J. As shown in the Mn_2 study of chapter 3 and in Ref. [20], this gives the most reliable estimate, since the stabilization of the higher lying state is usually overestimated by CASPT2 resulting in a smaller |J| and strong deviations to the Landé spacing.[20]

The existence of anisotropy due to the V(III) ion adds a couple of terms to the model Hamiltonian that is supposed to describe the local interactions in the extended structure:

$$\hat{H} = -J\hat{S}_1\hat{S}_2 + \hat{S}_1 D_1 \hat{S}_1 + \hat{S}_2 D_2 \hat{S}_2 + \hat{S}_1 D_{12} \hat{S}_2 \qquad 5.3$$

where the first term describes the isotropic Heisenberg magnetic coupling of the local spin moments, used before (chapters 3 - 4).

The second and third terms account for the local single-ions anisotropies. The $3d^3$ electronic configuration of the nearly octahedrally coordinated V(II) ion give rises to very small local anisotropy and we have neglected this effect. The last term in the model Hamiltonian describes the anisotropic exchange interaction between the two ions. The rigorous treatment of this interaction involves a lengthy analysis of the matrix elements of the model Hamiltonian in the (uncoupled) basis set of the M_s components of the spin states.[21] This matrix representation of the model Hamiltonian has a dimension of 12x12 (S=5/2, M_s=5/2, ..., -5/2; S=3/2, M_s=3/2, ..., -3/2; S=1/2, M_s=1/2, -1/2). In a first (probably too simplistic) approach, we neglect the anisotropic interaction based on the assumption that the nearly zero local anisotropy on V(II) also makes the anisotropic exchange small. Then, dealing with local anisotropy only, we calculate the local ZFS parameters D and E following the approach introduced by Maurice *et al.*[16] outlined in section 5.1.

5.3 Results and discussion

The CASPT2 calculations on the dinuclear fragment give J= -13.1 cm^{-1} (-19 K), which is of the same order of magnitude as the estimate derived from the Weiss constant. The CASPT2 may be somewhat underestimated due to the minimal CAS reference wave-function, but this should not be as important as for the interaction between Cu(II) ions as exposed above. The magnetic orbitals are depicted in Figure 5.2. For the V(II) on the left, the three t_{2g}-like orbitals can be recognized, while the two magnetic orbitals associated to the V(III) centre can be classified as V-$3d_{xz}$ and a linear combination of V-$3d_{xy}$ and V-$3d_{yz}$. In this way the interaction between the two centres is maximized and a sizeable

ISBN:978-84-694-2171-0/DL:T. 1032-2011

antiferromagnetic exchange shows up.

The second ingredient for a simulation of the magnetic susceptibility involves the local anisotropy parameters of the V(III) centre. The use of the structural data of the [FeMn(ox)$_3$] used for the calculation of J leads to an unphysically large axial anisotropy of -90 cm^{-1} due to the existence of a nearly degenerate ground state. The three components arising from the $^3T_{1g}$ state are only weakly split by the small deviation from a real octahedral symmetry in the coordination sphere of the V(III) ion. Table 5.2 lists the V—O distances based on the structural data of [FeMn(ox)$_3$].

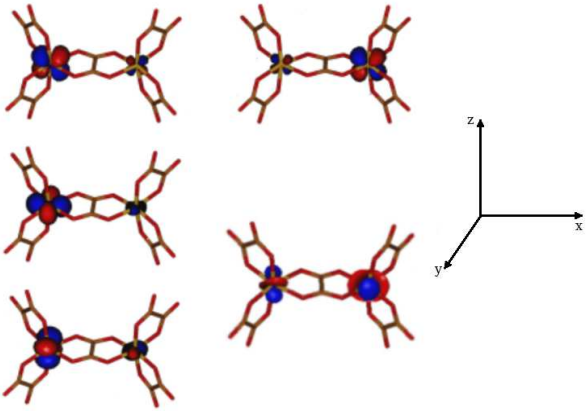

Figure 5.2. CASSCF optimized magnetic orbitals of the studied dimer.

The coordination sphere of the V(III) ion is expected to be at least slightly distorted by the Jahn-Teller effect, and the rather symmetric environment derived from the FeMn compound is probably not the most adequate to estimate the anisotropy parameters. Therefore, we decided to take the structural data of the K$_3$[V(III)(ox)$_3$]·3H$_2$O. In this case the geometrical distortion around the V(III) ion is more significant and the near degeneracy in the ground state disappears. The determination of the ZFS

parameters requires the calculation of the complete S=1 manifold of the V(III) ion, *i.e.* 10 triplets and 15 singlets. This is done in a state average optimization of the orbitals leading to the five V-3d orbitals shown in Figure 5.3.

Table 5.2. V(III)—O distances (in Å) in the studied systems.

	Model based on $\{[N(n\text{-}Bu)_4][Mn(II)Fe(III)(ox)_3]\}_n$[18]	$K_3[V(III)(ox)_3]\cdot 3H_2O$[17]
V-O1	2.075	1.969
V-O2	2.048	1.973
V-O3	2.075	1.995
V-O4	2.048	2.006
V-O5	2.075	2.049
V-O6	2.048	2.051
Average	2.061	2.007

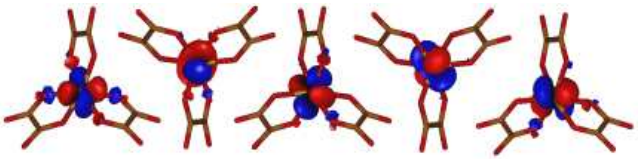

Figure 5.3. CASSCF optimized 3d orbitals of the V(III)(ox)$_3$ monomer.

The obtained axial ZFS parameter D is 9.01 cm^{-1} and in addition we also obtain a sizeable rhombic anisotropy characterized by E = 2.76 cm^{-1}. The ratio E/|D| of 0.30 is close to the limiting value of 1/3 for which the distinction between axial and rhombic anisotropy loose its meaning. The calculated axial anisotropy is at least twice as large as the one reported experimentally, but it should be noted that in the experimental derivation no account is given of the rhombic anisotropy parameter. This could very well

ISBN:978-84-694-2171-0/DL:T. 1032-2011

be the origin of the discrepancy, although computational factors such as the minimal CAS and the limited basis set size cannot be excluded.

Finally, we intend to reproduce the measured magnetic susceptibility of Ref. [17] based on the calculated electronic structure parameters. As far as the isotropic interactions are concerned, the strategy has been established in the previous chapters, but additional modeling is required to account for the anisotropy. For this purpose, we apply the following formulas[22] for the parallel and perpendicular components of χ under the influence of axial anisotropy:

$$\chi_{\parallel}=(C_0 g_{\parallel}^2/T)[2\exp(-x)]/[1+2\exp(-x)] \qquad 5.4$$

$$\chi_{\perp}=(C_0 g_{\perp}^2/T)(2/x)[1-\exp(-x)]/[1+2\exp(-x)] \qquad 5.5$$

with $C_0=\frac{N_A \mu_0 \mu_B^2}{k}$ and $x=\frac{D}{kT}$. Unfortunately, no expressions have been published so far to estimate the effect on χ(T) when both axial and rhombic anisotropy are important. The 6-centre model (see Figure 4.17) has been used to extract χ(T) and Figure 5.4 compares the calculated thermal dependency of the χT product with the experimental one. The red curve is the experimental one, where one should only focus on the regime above approximately 20 K since the material shows spin glass behaviour at lower temperatures. The yellow curve is the calculated susceptibility with isotropic interaction only and the blue one adds the anisotropic correction calculated through equations 5.4 and 5.5 under the complete neglect of the rhombic anisotropy. The agreement with experiment is reasonable. The anisotropic correction improves the comparison with experiment at intermediate temperatures but overshoots at higher temperatures. This is probably due to the fact that (i) we have neglected the rhombic anisotropy, (ii) we have neglected the anisotropic exchange and (iii) we may have overestimated the

axial anisotropy. A complete, detailed account of these three effects is a highly interesting topic for future studies as it may also be applied to improve the agreement between theory and experiment for the hexagonal Co(II)-based layers studied in the previous chapter.

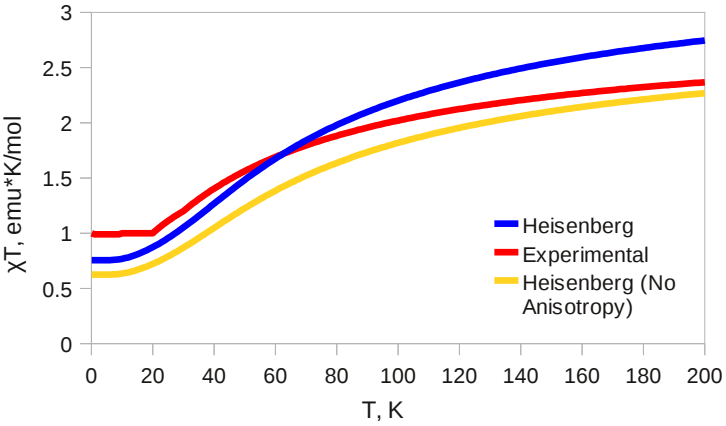

Figure 5.4. Thermal dependency of the magnetic susceptibility of the V(II)-ox-V(III) hexagonal layer. Blue curve: Heisenberg model with anisotropy accounted. Red curve: experimental. Yellow curve: Heisenberg model without anisotropy. J = -13.1 cm^{-1}, D = 9.01 cm^{-1}.

5.4 Conclusion

The magnetic coupling constant and ZFS parameters of the mixed-valence $\{[N(n\text{-}Bu)_4][V(II)V(III)(ox)_3]\}_n$ system with magnetic anisotropy have been found by *ab initio* calculations. The calculated values were used to construct a Heisenberg Hamiltonian of the 6-centre model with periodic boundary

conditions. By diagonalizing the Heisenberg Hamiltonian of this model, we obtain an energy spectrum. This spectrum has been used to calculate the magnetic susceptibility through standard statistical mechanics. The obtained temperature dependence of the magnetic susceptibility is compared to experimental data with a reasonable match due to the simplifications in the treatment of the anisotropy.

The method can probably be applied in the future to the magnetic systems with magnetic anisotropy, which are used, particularly, in field of single molecule magnets, to calculate the thermal dependency of χ. However, a more rigorous treatment seems mandatory.

5.5 References
ISBN:978-84-694-2171-0/DL:T. 1032-2011

1 Caneschi, A.; Gatteschi, D.; Sessoli, R.; Barra, A. L.; Brunel,L. C.; Guillot, M. J. Am. Chem. Soc. 1991, 113, 5873.

2 Friedman, J. R.; Sarachik, M. P.; Tejada, J.; Ziolo, R. Phys. ReV. Lett. 1996, 76, 3830.

3 Thomas, C.; Lionti, F.; Ballou, R.; Gatteschi, D.; Sessoli, R.; Barbara, B. Nature 1996, 383, 145.

4 Duboc, C.; Phoeung, T.; Zein, S.; Pecaut, J.; Collomb, M.-N.; Neese, F. Inorg. Chem. 2007, 46, 4905.

5 Chibotaru, L.; Ungur, L.; Aronica, C.; Elmoll, H.; Pilet, G.; Luneau, D. J. Am. Chem. Soc. 2008, 130, 12445.

6 Ruiz, E.; Cirera, J.; Cano, J.; Alvarez, S.; Loose, C.; Kortus, J. Chem. Commun. 2008, 52.

7 Cirera, J.; Ruiz, E.; Alvarez, S.; Neese, F.; Kortus, J. Chem. Eur. J. 2009, 15, 4078.

8 Abragam, A.; Bleany, B. Electron Paramagnetic Resonance of Transition Ions; Dover Publications: Dover, NY, 1986.

9 Bencini, A.; Gatteschi, D. EPR of Exchange Coupled Systems; Springer-Verlag: Berlin, 1990.

10 Kortus, J.; Hellberg, C. S.; Pederson, M. R. Phys. Rev. Lett. 2001, 86, 3400.

11 Neese, F. J. Chem. Phys. 2007, 127, 164112.

12 Borras-Almenar, J. J.; Clemente-Juan, J. M.; Coronado, E.; Tsukerblatt, B. S. Inorg. Chem. 1999, 38, 6081.

13 Neese, F. J. Am. Chem. Soc. 2006, 128, 10213.

14 de Graaf, C.; Sousa, C. Int. J. Quantum Chem. 2006, 106, 2470.

15 Chibotaru, L.; Ungur, L.; Soncini, A. Angew. Chem., Int. Ed. 2008, 47, 4126.

16 Maurice, R.; Bastardis, R.; de Graaf, C.; Suaud, N.; Mallah.; T.; Guihéry N. J. Chem. Theory Comput. 2009, 5, 2977.

17 Min, K. S.; Rhinegold, A. L.; Miller, J. S. Inorg. Chem. 2005, 44, 8433.

18 Pellaux, R.; Schmalle, H. W.; Huber, R.; Fischer, P.; Hauss, T.; Ouladdiaf, B.; Decurtins, S. Inorg. Chem. 1997, 36, 2301.

19 Queralt, N.; Taratiel, D.; de Graaf, C.; Caballol, R.; Cimiraglia, R.; Angeli, C. J. Comp. Chem. 2008, 29, 994.

ISBN:978-84-694-2171-0/DL:T. 1032-2011

20 Negodaev I.; de Graaf, C.; Caballol, R. Chem. Phys. Lett. 2008, 459, 73.

21 Maurice, R.; Guihéry N.; Bastardis, R.; de Graaf, C. J. Chem. Theory Comput. 2010, 6, 55.

22 Boča, R. In Theoretical Foundations of Molecular Magnetism, Elsevier 1999.

UNIVERSITAT ROVIRA I VIRGILI
THE CALCULATION OF THE THERMAL DEPENDENCY OF THE MAGNETIC SUSCEPTIBILITY
IN EXTENDED SYSTEMS WITH AB INITIO ELECTRONIC STRUCTURE PARAMETERS
Igor Negodaev
ISBN:978-84-694-2171-0/DL:T. 1032-2011

Conclusions

UNIVERSITAT ROVIRA I VIRGILI
THE CALCULATION OF THE THERMAL DEPENDENCY OF THE MAGNETIC SUSCEPTIBILITY
IN EXTENDED SYSTEMS WITH AB INITIO ELECTRONIC STRUCTURE PARAMETERS
Igor Negodaev
ISBN:978-84-694-2171-0/DL:T. 1032-2011

ISBN:978-84-694-2171-0/DL:T. 1032-2011

The research described in this thesis has led to the following main conclusions.

1. CASPT2 is shown to be reasonably good to study oxalato-based materials as well as asymmetric bridged complexes. The systematic underestimation of the magnetic coupling at this level is compensated by the relatively low computational cost.

2. A good agreement of equilibrium distance, dissociation energy and magnetic coupling constant has been achieved with experimental data for the Mn_2 system when using the combined CCSD(T) + DDCI2 approach.

3. In the Mn_2 dimer, CASPT2 leads to large artificial deviations in the values of coupling parameter J depending on the states used in its calculation due to numerical noise that overstabilizes the higher states in the Heisenberg spectrum.

4. DDCI gives accurate estimations of the magnetic coupling parameter, but its application to extended systems is limited to a small number of electrons per magnetic site.

5. The CAS_{ext}/DDCI2 methodology can be considered in general as a good alternative to evaluate J. The precision of this technique is combined with a reasonable computational cost.

6. The Ising model does not reproduce satisfactorily the dependence of the magnetic susceptibility on the temperature, when compared to the Heisenberg model. The best behaviour corresponds to intermediate spin systems, as Ni(II) and Co(II).

7. The exact diagonalization of the Heisenberg Hamiltonian is the best choice to obtain the thermal dependency of the magnetic

ISBN:978-84-694-2171-0/DL:T. 1032-2011

susceptibility, as demonstrated in dinuclear systems.

8. In the asymmetrically bridged Cu(II) dinuclear complexes with carboxylato- and alkoxo-bridges, the magnetic coupling appears strongly dominated by the alkoxo-bridge. The carboxylato bridge plays a secondary role, that can be explained with simple qualitative models. The influence of substituents with different electronegativity on the carboxylato-bridge is negligible.

9. The crystalline geometry is found to be responsible for the difference of J experimentally observed for asymmetrically bridged Cu(II) dinuclear complexes with different substituents on the carboxilato fragment.

10. The modeling of the Catena-μ-Tris[oxalato(2-)-O^1,O^2;O^3,O^4]-dicopper compound shows that next-nearest interactions of magnetic sites can be neglected, and that dinuclear models are sufficient to describe the coupling.

11. The magnetic topology of this structure is found to best fit the alternating chain description with weak interchain interactions.

12. The determination of thermal dependency of the magnetic susceptibility for Cu(II)-, Ni(II)-, Co(II)- and Fe(II)-based 2D hexagonal lattices presented in this thesis is interesting as an alternative for the use of the analytical expression of Curély and co-workers.

13. As shown previously by Novoa and collaborators in extended systems where the extraction of the coupling parameter J from the experimental $\chi(T)$ is not possible, the calculation of J by accurate quantum chemistry methods and the theoretical evaluation of $\chi(T)$ provides an alternative way of estimating J.

14. The susceptibility curve of the V(II)-ox-V(III) system has been determined using the calculated isotropic magnetic coupling constant and the axial anisotropy parameter for V(III). The comparison with experiment is reasonably good. The method can probably be applied in the future to the systems with magnetic anisotropy.

UNIVERSITAT ROVIRA I VIRGILI
THE CALCULATION OF THE THERMAL DEPENDENCY OF THE MAGNETIC SUSCEPTIBILITY
IN EXTENDED SYSTEMS WITH AB INITIO ELECTRONIC STRUCTURE PARAMETERS
Igor Negodaev
ISBN:978-84-694-2171-0/DL:T. 1032-2011

UNIVERSITAT ROVIRA I VIRGILI
THE CALCULATION OF THE THERMAL DEPENDENCY OF THE MAGNETIC SUSCEPTIBILITY
IN EXTENDED SYSTEMS WITH AB INITIO ELECTRONIC STRUCTURE PARAMETERS
Igor Negodaev
ISBN:978-84-694-2171-0/DL:T. 1032-2011

Annexes

UNIVERSITAT ROVIRA I VIRGILI
THE CALCULATION OF THE THERMAL DEPENDENCY OF THE MAGNETIC SUSCEPTIBILITY
IN EXTENDED SYSTEMS WITH AB INITIO ELECTRONIC STRUCTURE PARAMETERS
Igor Negodaev
ISBN:978-84-694-2171-0/DL:T. 1032-2011

ISBN:978-84-694-2171-0/DL:T. 1032-2011

Annex 1. Exact energies of Heisenberg homogeneous linear systems, with J = -1 K, referred to singlet state.

4-sites linear model:

Energy (K)	2S + 1		
	1	3	5
1	0.000	0.659	2.366
2	1.732	1.366	
3		2.073	

ISBN:978-84-694-2171-0/DL:T. 1032-2011

8-sites linear model:

Energy (K)	2S + 1				
	1	3	5	7	9
1	0.000	0.393	1.543	3.201	5.125
2	1.041	0.871	1.909	3.418	
3	1.458	1.267	2.149	3.742	
4	1.730	1.318	2.337	4.125	
5	1.980	1.526	2.573	4.508	
6	2.254	1.700	2.753	4.832	
7	2.677	1.951	2.924	5.049	
8	2.754	2.147	3.074		
9	2.996	2.378	3.296		
10	3.359	2.392	3.327		
11	3.723	2.646	3.629		
12	3.792	2.647	3.730		
13	4.229	2.758	4.022		
14	4.757	2.889	4.189		
15		2.928	4.351		
16		3.058	4.414		
17		3.158	4.561		
18		3.255	4.768		
19		3.503	4.964		
20		3.543			
21		3.696			
22		3.910			
23		3.974			
24		4.152			
25		4.326			
26		4.545			
27		4.698			
28		4.869			

ISBN:978-84-693-2176-0/D.L.:T. 1032-2011

1-2-sites linear model (only low states are reported for low multiplicities).

Energy (K)	2S + 1						
	1	3	5	7	9	11	13
1	0.000	0.281	1.132	2.438	4.075	5.926	7.892
2	0.734	0.629	1.438	2.682	4.248	6.026	
3	1.068	0.950	1.699	2.868	4.355	6.185	
4	1.350	0.954	1.762	2.965	4.472	6.392	
5	1.441	1.224	1.897	2.984	4.579	6.633	
6	1.565	1.269	2.019	3.149	4.733	6.892	
7	1.698	1.431	2.021	3.264	4.750	7.151	
8	1.725	1.537	2.073	3.265	4.839	7.392	
9	1.940	1.561	2.215	3.388	5.009	7.599	
10	2.043	1.602	2.317	3.447	5.011	7.758	
11	2.063	1.731	2.326	3.503	5.117	7.858	
12	2.075	1.740	2.327	3.558	5.229		
13	2.279	1.867	2.337	3.561	5.285		
14	2.307	1.867	2.511	3.684	5.286		
15	2.413	1.964	2.519	3.685	5.391		
16	2.507	2.013	2.575	3.738	5.504		
17	2.564	2.068	2.620	3.798	5.537		
18	2.613	2.173	2.632	3.816	5.558		
19	2.632	2.194	2.640	3.851	5.641		
20	2.699	2.198	2.763	3.959	5.742		

UNIVERSITAT ROVIRA I VIRGILI
THE CALCULATION OF THE THERMAL DEPENDENCY OF THE MAGNETIC SUSCEPTIBILITY
IN EXTENDED SYSTEMS WITH AB INITIO ELECTRONIC STRUCTURE PARAMETERS
Igor Negodaev
ISBN:978-84-694-2171-0/DL:T. 1032-2011

UNIVERSITAT ROVIRA I VIRGILI
THE CALCULATION OF THE THERMAL DEPENDENCY OF THE MAGNETIC SUSCEPTIBILITY
IN EXTENDED SYSTEMS WITH AB INITIO ELECTRONIC STRUCTURE PARAMETERS
Igor Negodaev
ISBN:978-84-694-2171-0/DL:T. 1032-2011

Resumen

UNIVERSITAT ROVIRA I VIRGILI
THE CALCULATION OF THE THERMAL DEPENDENCY OF THE MAGNETIC SUSCEPTIBILITY
IN EXTENDED SYSTEMS WITH AB INITIO ELECTRONIC STRUCTURE PARAMETERS
Igor Negodaev
ISBN:978-84-694-2171-0/DL:T. 1032-2011

ISBN:978-84-694-2171-0/DL:T. 1032-2011

El estudio del magnetismo es uno de los campos importantes de la ciencia moderna. Los logros de la investigación en este campo se aplican con éxito en muchas áreas de la actividad humana, y los materiales con diferentes propiedades magnéticas son ampliamente utilizados en la ciencia y la industria. Los materiales magnéticos de tipo molecular se basan en complejos moleculares o estructuras mayor dimensionalidad usualmente con metales de transición (TM) en los centros magnéticos. Uno de los factores clave para comprender las propiedades magnéticas es la interacción de intercambio entre iones paramagnéticos por medio de ligandos puente de naturaleza diamagnética. Entre los distintos ligando multidentados, el oxalato (ox) es de uso frecuente como puente por su versatilidad. Un subgrupo especial de estos materiales está constituido por redes bidimensionales, donde los centros magnéticos forman una red hexagonal. Estas estructuras se pueden encontrar en algunos materiales bifuncionales.

El presente trabajo está dedicado al estudio teórico de las interacciones de intercambio magnético en dichos sistemas. En los sistemas de alta dimensionalidad, no puede extraerse el parámetro microscópico de acoplamiento a partir de la dependencia de la susceptibilidad magnética con la temperatura por lo que un objetivo de este trabajo consiste en calcular este propiedad a partir de los parámetros calculados y establecer así la comparación con la experiencia.

La tesis comienza con la descripción de los métodos computacionales utilizados, basados en la función de onda, de carácter multireferencial. Los métodos utilizados en este trabajo son el *Complete Active Space Self-Consistent Field* (CASSCF), con inclusión de correlación dinámica mediante Teoría de Perturbaciones, hasta segundo orden (CASPT2) e Interacción de Configuraciones, mediante distintos variantes, del método *Difference-Dedicated Configuration Interaction* (DDCI) y CAS

ISBN:978-84-694-2171-0/DL:T. 1032-2011

extendido y DDCI2 (CAS_{ext}/DDCI2).

Este capítulo describe también la obtención de una propiedad macroscópica como la susceptibilidad magnética en función de la temperatura, a partir del parámetro microscópico de acoplamiento, J. Los diferentes modelos de Hamiltoniano (Ising y Heisenberg) se examinan en detalle, comparando la susceptibilidad magnética obtenida con estos modelos. Hemos utilizado la diagonalización exacta del Hamiltoniano de Heisenberg para lograr este objetivo, y se ha también explorado un enfoque alternativo como el Renormalization Excitonic Method (REM). Se observó que el modelo de Ising no es totalmente compatible con nuestros objetivos. El método de renormalización tampoco se mostró adaptado a este tipo de estudio. En aplicaciones posteriores se optó pues por la diagonalización del modelo de Heisenberg para obtener las curvas de susceptibilidad magnética frente a la temperatura.

Los resultados están organizados en tres capitules. El primero, trata sistemas dinucleares aunque de estudio completo. Comenzado con el sistema más pequeño Mn_2, hemos comprobado el adecuación del modelo de Heisenberg. Hemos logrado distancia de equilibrio, energía de disociación y débil acoplamiento antiferromagnético de acuerdo con los datos experimentales. Se ha corroborado en este caso que las desviaciones del modelo de Heisenberg descritos por otros autores se deben a imprecisiones numéricas. Después se ha analizado un sistema dinuclear de Cu(II) con doble puente asimétrico en un complejo en el que combinan un puente carboxilato y un puente alcóxido en Cu(II). En estos sistemas se ha estudiado la influencia de los sustituyentes electronegativos con la conclusión de que su efecto no es relevante. Se ha discutido además, la importancia relativa de dos puentes en la mediación de la interacción magnética se ha discutido con la conclusión de que el acoplamiento magnético en los sistemas estudiados se debe casi exclusivamente al puente

alcóxido y que el puente carboxilato juega un papel menos importante.

Después la mayor parte de la tesis se dedica a los sistemas con puente oxalato. Se han estudiado materiales con baja dimensionalidad, como cadenas lineales y alternados con iones Cu(II) como centros magnéticos. Los métodos de cálculo CASPT2 y CAS_{ext}/DDCI2 han dado en general estimaciones razonables de J a un costo computacional limitado. La diagonalización del Hamiltoniano de Heisenberg para los modelos más grandes da buenas estimaciones de la dependencia térmica de la susceptibilidad magnética.

Se ha estudiado después el primer sistema sintetizado descrito como 3D constituido por Cu(II) y puentes oxalato. La estrategia se ha basado en cálculos de la constante de acoplamiento en fragmentos de dos y de tres centros magnéticos, comprobando que el modelo bicéntrico es suficiente, siendo despreciable la interacción entre centros no vecinos. La topología magnética de la estructura, que no se desprende de la información experimental de la estructura del cristal, se adapta mejor a una descripción de cadena magnética alternada con interacciones débiles entre cadenas que a un material 3D. Se ha obtenido la dependencia de la susceptibilidad magnética con le temperatura de la que no consta información experimental.

La experiencia obtenida se aplicó a redes hexagonales. Se ha calculado la dependencia térmica de la susceptibilidad magnética para redes 2D con puente oxalato con centros de Cu(II), Ni(II), Co(II) y Fe(II). El método puede aplicarse ahora a las redes hexagonales que forman parte de los materiales bifuncionales descritas en la literatura y comparar curvas de dependencia de la susceptibilidad magnética con la temperatura calculadas y experimentales. En el caso de la red hexagonal de Fe(II) la comparación entre la experiencia y la teoría es buena, mientras que para el compuesto de Co(II), la curva calculada está

de acuerdo en menor medida con la experimental, debido a los importantes efectos de anisotropía.

El paso final fue para tratar el sistema con propiedades adicionales de la anisotropía magnética. Puesto que hemos elegido el dímero V(II)V(III), basado en los cálculos CAS_{ext}/DDCI2 aplicado con éxito antes, sería muy grande. Por lo tanto CASPT2 método se ha utilizado para el cálculo de la constante de acoplamiento magnético. Su uso, la dependencia de la temperatura obtenidos de la susceptibilidad magnética se compara con los datos experimentales con un buen partido. Esto puede permitir a aplicar la metodología de los sistemas magnéticos con anisotropía, que se utilizan, en particular, en el campo de los imanes sola molécula.

Cada capítulo de esta tesis se finaliza con la conclusión y la lista de referencia. Además, unas conclusiones generales de la tesis se resumen en la final del texto.

UNIVERSITAT ROVIRA I VIRGILI
THE CALCULATION OF THE THERMAL DEPENDENCY OF THE MAGNETIC SUSCEPTIBILITY
IN EXTENDED SYSTEMS WITH AB INITIO ELECTRONIC STRUCTURE PARAMETERS
Igor Negodaev
ISBN:978-84-694-2171-0/DL:T. 1032-2011

Publications

UNIVERSITAT ROVIRA I VIRGILI
THE CALCULATION OF THE THERMAL DEPENDENCY OF THE MAGNETIC SUSCEPTIBILITY
IN EXTENDED SYSTEMS WITH AB INITIO ELECTRONIC STRUCTURE PARAMETERS
Igor Negodaev
ISBN:978-84-694-2171-0/DL:T. 1032-2011

Negodaev, I.; de Graaf, C.; Caballol, R.
“On the Heisenberg behaviour of magnetic coupling in the manganese dimer”.
Cnemical Physics Letters, Volume 458, Issues 4-6, 2008, Pages 290-294.

2. Negodaev, I.; de Graaf, C.; Caballol, R.
“Extraction of Magnetic Coupling Parameters in 2-Dimensional Magnetic Honeycomb Layers”.
Journal of Physical Chemistry A, Volume 114, Issue 28, 2010, Pages 7553–7560.

3. Negodaev, I.; Queralt, N.; de Graaf, C.; Caballol, R.
“Theoretical study of the magnetic exchange interaction in catena-μ-Tris[oxalato(2-)-O1,O2;O3,O4]-dicopper complex with interlocked helical chains”.
Chemical Physics, 2011, in press.

4. Negodaev, I.; de Graaf, C.; Caballol, R.; Lukov. V.
“On the magnetic coupling in asymmetrically bridged Cu(II) dinuclear complexes: the influence of substitutions on the carboxylato-group”.
In preparation.

UNIVERSITAT ROVIRA I VIRGILI
THE CALCULATION OF THE THERMAL DEPENDENCY OF THE MAGNETIC SUSCEPTIBILITY
IN EXTENDED SYSTEMS WITH AB INITIO ELECTRONIC STRUCTURE PARAMETERS
Igor Negodaev
ISBN:978-84-694-2171-0/DL:T. 1032-2011